UNIVERSITÀ
DI SIENA
1240

UNIVERSITA' DEGLI STUDI DI SIENA

DIPARTIMENTO DI BIOTECNOLOGIE, CHIMICA E FARMACIA

DOTTORATO DI RICERCA IN 'SCIENZE CHIMICHE E FARMACEUTICHE'

CICLO XXIX

SETTORE SCIENTIFICO-DISCIPLINARE: CHIM/08

COORDINATORE: Prof. Stefano Mangani

Improvement of pyrazolo[3,4-d]pyrimidines pharmacokinetic properties in cancer therapy: nanosystem and prodrugs approaches

TUTOR: Prof.ssa Elena Dreassi

CO-TUTOR: Prof. Maurizio Botta

DOTTORANDA: Giulia Iovenitti

ANNO ACCADEMICO: 2015-2016

Preface

The aim of this thesis is to describe the work that has been carried out during three years of Ph.D. research with regards to improvement of pyrazolo[3,4-d]pyrimidines pharmacokinetic properties in cancer therapy by three different approaches.

The first section represents a general introduction of protein kinases (molecular targets of our molecules), pyrazolo[3,4-d]pyrimidines (a brief overview on studies carried out in our laboratories in recent years) and available strategies to develop a new drug candidate. Furthermore the first section describes the aim of this thesis.

The second section is dedicated to the first designed approach. Four pyrazolo[3,4-d]pyrimidines were chosen on the basis of their anti-neuroblastoma activity and were encapsulated in albumin nanoparticles and liposomes. Albumin nanoparticles and liposomes were prepared and characterized regarding size and ζ-potential distribution, polidispersity index, entrapment efficiency and activity against SH-SY5Y human neuroblastoma cell line. The most promising nanosystem was chosen to perform further studies: confocal microscopy, stability and drug release in physiological conditions, and biodistribution.

In the third section the prodrugs strategy was applied. To synthesize the full set of pyrazolo[3,4-d]pyrimidines prodrugs, a versatile one-pot two-step procedure was set up. Moreover the plasma half-life, the ability to overcome biological membranes, metabolic stability as well as water solubility were analyzed.
Then the most interesting prodrugs were tested in a cellular assay with human GBM U87 cell line
As in vivo proof of concept, the pharmacokinetics of the most promising pair of drug and prodrug were studied in an orthotopic mouse model of GBM.

The section four presents the last work, focused to the development of a plasmin-activated pyrazolo[3,4-d]pyrimidines prodrugs by the inclusion of a small peptide, selectively recognized by this tumor-associated enzymes.
SI113 was the selected compound to develop this approach that allows to selectively generate active parent drug at the target site, as well as increase the water solubility of our molecules.

Index

‘PLASMIN-ACTIVATED PYRAZOLO[3,4-*d*]PYRIMIDINES PRODRUGS: A NEW STRATEGY OF DRUG DELIVERY’

‘REFERENCES AND ACKNOWLEDGEMENTS’

SECTION 1

'INTRODUCTION AND AIM OF THE WORK'

1.1 PROTEIN KINASES

Over 500 human genes encode protein kinases and more than 500 protein kinases (PKs) comprise the human kinome (**Figure 1**).[1]
In general these can be grouped into a number of subsets based primarily on sequence and structural similarities[1] (**Figure 1**) and can be considered broadly to be serine/threonine kinases or tyrosine kinases, or in some instances dual-specificity kinases when they phosphorylate Ser/Thr as well as Tyr residues.

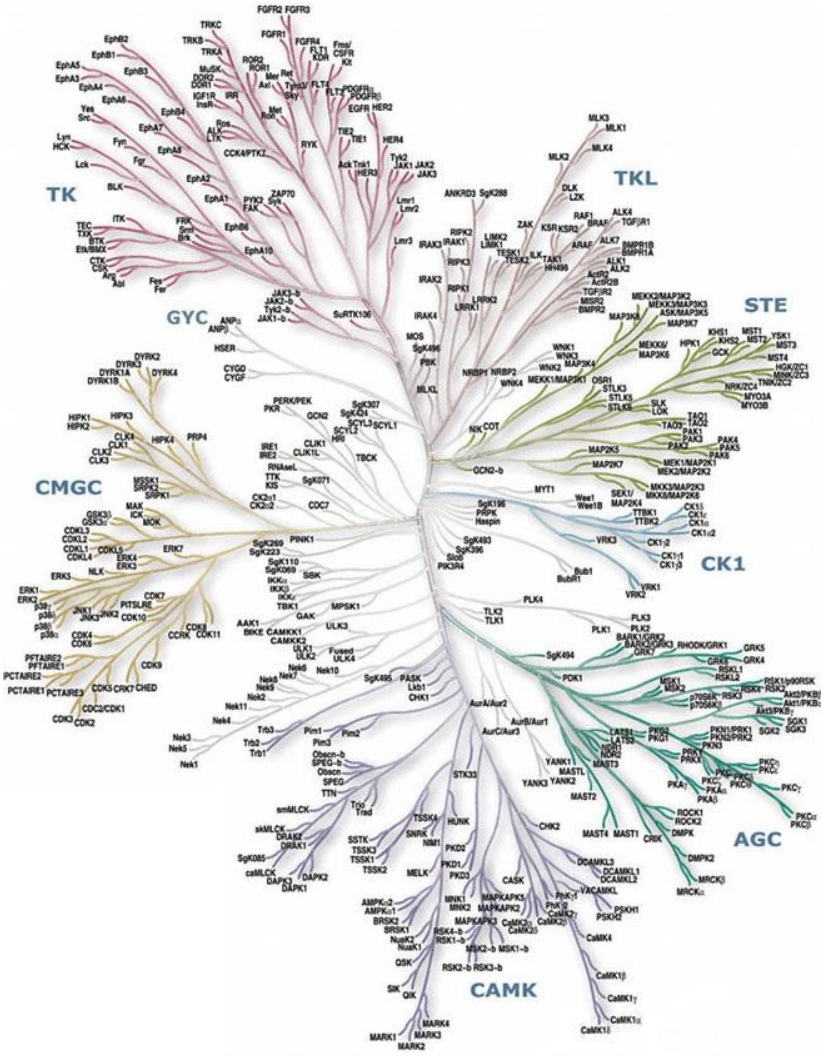

Figure 1: Human kinome

In fact, protein kinases are characterized by their ability to specifically catalyze the transfer of the terminal phosphoryl group of ATP to specific hydroxyl groups of Ser, Thr or Tyr residues of their protein substrates, involved in the growth, differentiation, gene expression, metabolism, cell traffic and apoptosis thereby affecting almost all intracellular signal transduction pathways.
Protein phosphorylation is one of the most significant signal transduction mechanisms by which intercellular signals regulate crucial intracellular processes such as ion transport, cellular proliferation, and hormone responses.

Consistent with the complex role of this post-translational modification in the cell, protein kinases can be regulated by activator proteins, inhibitor proteins, ligand binding to regulatory subunits, cofactors, and phosphorylation by other proteins or by themselves (autophosphorylation).
For discovering reversible protein phosphorylation as a biological regulatory mechanism, Edmond H. Fischer and Edwin G. Krebs were awarded the 1992 Nobel Prize for Physiology and Medicine.
Since protein phosphorylation controls a diverse range of cellular and pathogenic processes, even subtle changes in protein kinase activity can lead to a wide variety of diseases, including cancer, inflammatory disorders, diabetes, neurodegeneration and central nervous system diseases.
Many kinases have been extensively targeted with small molecule inhibitors as therapeutics for the treatment of disease and also for the development of reagents for elucidating the function of a particular kinase in a signaling pathway.[2] The high degree of similarity among kinases often results in off-target inhibition, which can be a significant impediment for correctly interpreting a small molecule's effect on signal transduction[3] as well as resulting in undesirable side-effects in therapeutic applications. Thus there is continued interest in the assessment of the selectivity of small molecule inhibitors to afford appropriately selective biological probes and therapeutics.
Protein kinases are now recognised as an important class of drug targets and recent successful launches of drugs with kinase inhibition as the mode of action demonstrate the ability to deliver kinase inhibitors as drugs with the appropriate selectivity, potency, and pharmacokinetic properties.
The family's key function in signal transduction for all organisms makes it a very attractive target class for therapeutic interventions and represent as much as thirty percent of all protein targets under investigation by pharmaceutical companies.[2,4]

In this work, the involvement of PKs and cancer has been taken into account, in particular the implication of Src, Abl (tyrosine kinase's family) and Sgk1 (AGC kinase's family) since their abnormal activity has been shown to be related to various human tumors including neuroblastoma (NB),[5-9] glioblastoma (GB)[10] and hepatocellular carcinoma (HCC).[11-13]

1.1.1 PROTEIN TYROSINE KINASES

Protein tyrosine kinases (PTKs) modulate a wide variety of cellular events, including differentiation, growth, metabolism and apoptosis.[14-18] Phosphorylation of tyrosine residues in target proteins is essential for maintaining cellular homeostasis, yet this post-translational modification also provides the means by which a number of cellular oncogenes deregulate various signaling pathways and induce transformation. PTKs are therefore important targets for both basic research and drug development.[16]
PTKs represent a diverse superfamily of proteins, including both transmembrane receptor tyrosine kinases (RTKs) and soluble cytoplasmic enzymes also known as non-receptor tyrosine kinases (NRTKs) how Src and Abl. These last have attracted particular interest because their overexpression and hyperactivation is present in many tumors.[19]

1.1.1.1 RTKs

RTKs span the plasma membrane and contain an extracellular portion, which binds ligand, and an intracellular portion, which possesses catalytic activity and regulatory sequences. The RTKs family includes the insulin receptor and the receptors for many growth factors such as epidermal (EGF), platelet-derived (PDGF), fibroblast (FGF), and nerve growth factors.
Upon ligand binding, these receptors commonly undergo dimerisation, resulting in autophosphorylation of tyrosine residues within the cytoplasmic domain.[20,21] These phosphorylation events activate the kinase, thereby increasing its intrinsic PTKs activity, and produce new binding sites for intracellular adapter molecules that bring signal transduction molecules into close proximity.[16,17]

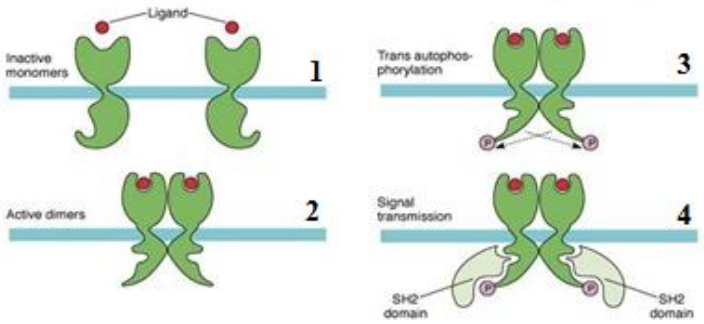

Figure 2: Inactive and active tyrosine-kinase receptor system

RTKs consist of an extracellular portion that binds polypeptide ligands, a trans membrane helix, and a cytoplasmic portion that possesses tyrosine kinase catalytic activity. The vast majority of RTKs exist as a single polypeptide chain and are monomeric in the absence of ligand. Exceptions include Met and its family members, which comprise a short α chain disulfide-linked to a membrane-spanning β chain, and the insulin receptor and its family members, which consist of two extracellular α chains disulfide-linked to two membrane-spanning β chains. The α chains are also disulfide-linked to one another, forming an α2 β2 heterotetramer.
The extracellular portion of RTKs typically contains a diverse array of discrete globular domains such as immunoglobulin (Ig)-like domains, fibronectin type III–like domains, cysteine-rich domains, and EGF-like domains. In contrast, the domain organization in the cytoplasmic portion of RTKs is simpler, consisting of a juxtamembrane region (just after the transmembrane helix), followed by the tyrosine kinase catalytic domain and a carboxy-terminal region. Some receptors, most notably members of the PDGF receptor family, contain a large insertion of ~100
residues in the tyrosine kinase domain. The juxtamembrane and carboxy-terminal regions vary in length among RTKs. Along with the tyrosine kinase insert, these regions contain tyrosine residues that are autophosphorylated upon ligand binding.

1.1.1.2 NRTKs

NRTKs lack receptor-like features such as an extracellular ligand-binding domain and a transmembrane-spanning region, and most NRTKs are localized in the cytoplasm.[21] Some NRTKs are anchored to the cell membrane through amino terminal modification, such as myristoylation or palmitoylation. In addition to a tyrosine kinase domain, NRTKs possess domains that mediate protein-protein, protein-lipid, and protein-DNAinteractions. The most commonly found protein-protein interaction domains in NRTKs are the Src homology 2 (SH2) and 3 (SH3) domains.[22] The SH2 domain is a compact domain of ~100 residues that binds phosphotyrosine residues in a sequence-specific manner. The smaller SH3 domain (~60 residues) binds proline-containing sequences capable of forming a polyproline type II helix.
Some NRTKs lack SH2 and SH3 domains but possess subfamily-specific domains used for protein-protein interactions. For example, members of the Jak family contain specific domains that target them to the cytoplasmic portion of cytokine receptors. The NRTK Fak possesses two domains that mediate protein-protein interactions: an integrin-binding domain and a focal adhesion-binding domain. The NRTK Abl contains a nuclear localization signal and is found in both the nucleus and the cytoplasm. In addition to SH2 and SH3 domains, Abl possesses an F actin–binding domain and a DNA-binding domain.
Another modular domain, present in the Btk/Tec subfamily of NRTKs and in many other signaling proteins, is the pleckstrin homology (PH) domain. PH domains bind to phosphatidylinositol (PtdIns) lipids that have been phosphorylated at particular positions on the head group.

Concentrations of specific PtdIns lipids in the cell membrane, such as PtdIns-3,4,5-P3, increase as a consequence of PI-3K activation. Proteins can be recruited to activated signaling complexes at the membrane through PH domain interactions with phosphorylated PtdIns lipids.
Several cytoplasmic tyrosine kinases have been identified (~35) and classified in different family. among which Src, Abl, Tec, Csk, Syk, Ack, Jak, Fak, Fer.[23]

1.1.1.2-1 c-Src

Much attention has been paid to the understanding of the structure and function of cytoplasmatic type PTKs Src.[14,24-28]
Src tyrosine kinase is a prototypical member of a family of kinases (Src Family Kinases, SFKs) that modulate multiple intracellular signal transduction pathways involved in cell growth, differentiation, migration and survival.[27]
The DNA that encodes the Src protein is known as an oncogene, because it is a gene that is intimately connected with the development of cancer. The Src oncogene was discovered because of this link with cancer: researchers found that the Rous sarcoma virus, which causes tumors in chickens, injects a protein similar to the normal form of Src, called v-Src (for "viral Src"). v-Src, in contrast to the cellular c-Src, is always active. It continually adds phosphate groups to the many proteins serviced by Src, sending a constant, unwavering signal to grow. This leads to cancer, as cells grow without control into tumors. There is evidence that aberrant Src kinase activity is associated with the invasive phenotype in both early and advanced solid tumors.[29,30] Moreover, recent data has demonstrated that Src inhibitors can enhance the antitumor efficacy of hormonal and cytotoxic agents as well as regulate angiogenesis through the control of VEGF expression.[31,32]
Inhibitors of the Src phosphorylation process may halt uncontrolled tumor cell growth and play an important role as new therapeutic agents for the treatment of cancer.[33]
The kinase activity is regulated at the cellular level by the phosphorylation of two key tyrosine residues and interactions with specific ligands. Furthermore, the active or inactive conformation, is mediated by its regulatory domains, which stabilize the kinase active.
All the members retain a structural organization in domains (**Figure 3**) which include, starting from the N-terminal:

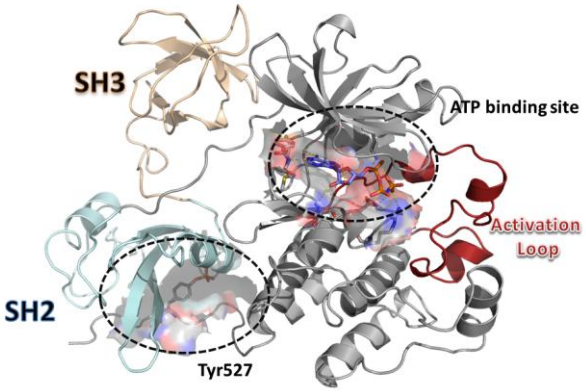

Figure 3: Structural domains of Src

-SH4 domain (Src Homology 4), which includes the first 16 amino acid residues and is responsible for the interaction of SFKs with the plasma membranes. It is known that the SFKs are located in the cytosolic side of the cell membranes, although recent data have shown that can also bind to other structures such as the apparatus of the golgi, secretory vesicles, endosomes, and the perinuclear membrane mitocondri.[34-38] The acylation of two specific amino acid residues present in the Met-

Gly-Cys consensus sequence of the N-terminal region favors the anchoring of SFKs to membranes. All the tyrosine kinase Src are miristoylated at the level of Gly in position +2, despite this reaction is irreversible has proved in some cases not sufficient for a correct localization of SFKs.

-SH3 domain (Src Homology 3), it consists of 50-60 amino acid residues. This domain does not carry out catalytic function but media the protein-protein interactions (both inter- and intra-molecular) involved in the control of enzymatic activity, the sub-cellular localization and interaction with substrates.

-SH2 domain (Src Homology 2) that consists of about 100 amino acid residues, even this domain, as the previous one, has no catalytic function but has the ability to modulate the recognition of the substrates or the catalytic activity by means of protein-protein interactions. The domain has a central β sheet structure and 2 single α helices on the sides of the latter. Both the secondary structure elements and the loops that connect them represent the consensus pattern recognition sites of the partner protein: one for the tyrosine phosphorylated (pTyr) and the other for the amino acids that are located on the C-terminal portion (respect to the pTyr). Crystallographic studies have shown that an Arg residue (Arg175 in c-Src) is highly conserved and located in the pTyr recognition pocket. This Arg residue is essential for the electrostatic interactions with pTyr.

-SH1 domain (Src Homology 1) or catalytic, consists of about 260 amino acids and is responsible of the enzymatic activity. It has, like all Ser / Thr and Tyr kinase, a characteristic bilobate structure. This domain presents: the N-terminal lobe (also called small lobe) consists of 5 sheets and a single β α helix (or helix C); the C-terminal lobe (also called major lobe) is mainly composed of α helices. The primary role of the small lobe is anchoring and orientation of the ATP; the bond with the nucleotide phosphate is coordinated by G-loop (area rich in glycine, also called P-loop, where the P indicates the ATP phosphate group). The large lobe, involved in substrate binding, contains the activation site where is situated the Tyr416; phosphorylation of the latter involves the complete activation of the enzyme. The catalytic site is located in the cleft between the two lobes; in this site occur the transfer of a phosphate group from ATP to the substrate. Structural deformations of the catalytic site determine variations such as to allow the input of ATP and ADP release. Therefore the two lobes assumed different conformations that generate a different accessibility to the catalytic core, such as to promote or inhibit the enzyme activity.

-C-terminal region, consisting of about 15-17 amino acids, it contains a Tyr527 (in c-Src) highly conserved in all SFKs. That tyrosine is an important regulatory site: its phosphorylation involves conformational changes due to the interaction of intramolecular pTyr527 with SH2 domain such as to inactivate the kinase activity. Phosphorylation of this amino acid residue is due to the action of two tyrosine kinase: Csk (C-terminal Src Kinase) and the homologue Chk[39] (Csk-Homologous kinase). *In vivo* under basal conditions, about 90-95% of Src is phosphorylated at Tyr527 and therefore is in an inactive state. The phosphorylation of this tyrosine residue in the inhibition mechanism of c-Src kinase activity was demonstrated. The experimental evidence have shown that mutant c-Src Tyr527Phe have basal constitutive activity associated with cell transformation, even carcinogenic nature.[40]

1.1.1.2-2 c-Abl

c-Abl is another important protein kinases involved in the pathogenesis of cancer.
The hyperactivation of Abl is mainly due to its merger with Bcr, thus leading to the oncoprotein Bcr-Abl, which is constitutively activated.
Abl shares significant sequence homology with Src and, in its active conformation, bears remarkable structural resemblance with most SFKs. (**Figure 4**)

As a result, ATP-competitive compounds originally developed as Src inhibitors frequently exhibit potent inhibition of Abl kinase.[41,42]

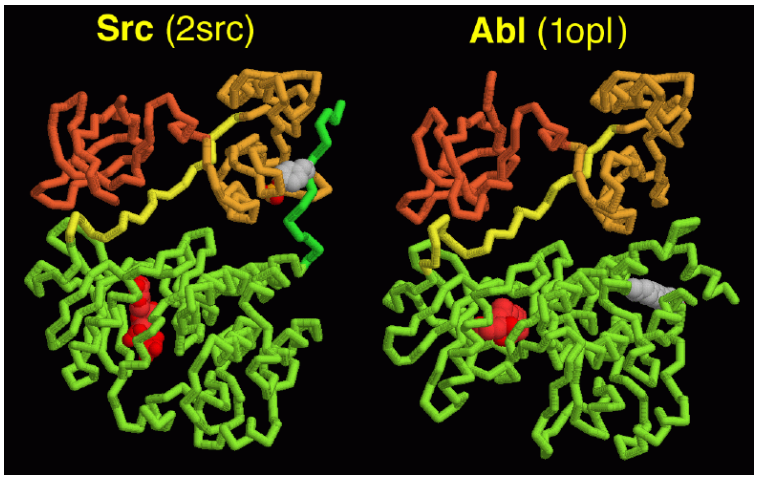

Figure 4: Homology between Src and Abl. Different colours show the 4 domains. In red: nucleotide bound. In white: phosphate group.

Abl is a non-receptor tyrosine kinase that is expressed in most tissues. In cells, the Abl protein could be localized in both the nucleus and cytoplasm of cells and can shuttle between the two compartments, in fact it contains three Nuclear Localization Signals (NLS) and Nuclear Export Signal (NES).[43,44]
It interacts with a wide range of cellular proteins, including cell-cycle regulators, other kinases, signaling adaptor molecules, transcription factors and phosphatases.[45,46]
Several structural domains can be defined within the protein (**Figure 5**). The N-terminus of the 1b variant of c-Abl is myristoylated, whereas the 1a variant is 19 amino acids shorter and does not undergo this modification. Following the myristate signal are the SH3 and SH2 domains, which like Src family kinases play a role in substrate interaction and autoregulation.[47,48]

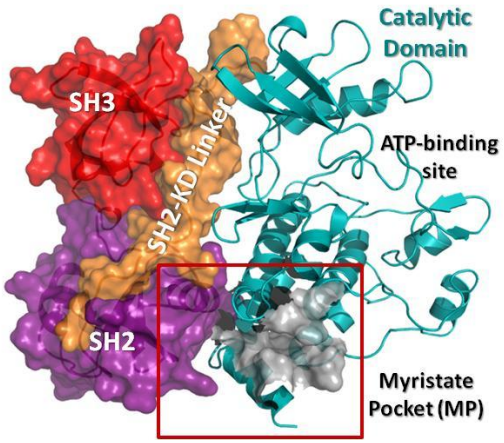

Figure 5: c-Abl structure

Following the SH2 domain is a short linker region, followed by the bi-lobal tyrosine kinase domain. Although the SH3, SH2, and kinase region of c-Abl is homologous in structure and function to the Src family kinases, the N-terminal and C-terminal tail regions of c-Abl are distinct. In fact, the N-terminus consists of a ~80kDa negative regulatory "cap" region, which contains part of the SH3 domain. The C-terminus of Abl comprises a long extension, which contains various

protein-protein interaction motifs and localization signals, such as the NLS and NES mentioned above .
In contrast to the cap region the C-terminal tail does not appear to be required for autoregulation of the kinase.[49]
Similar to Src, c-Abl is regulated by intramolecular interactions that keep the kinase domain in a closed and inactive conformation.
The c-Abl closed conformation involves the interaction between the SH3 domain and the proline-rich sequence localized in the linker between SH2 and kinase domain.[50] This SH3-SH2 clamp, which packs tightly against the distal face of the kinase domain causes a conformation change in the ATP-binding pocket. Furthermore the myristoyl group binds into a deep hydrophobic pocket in the C-lobe of the kinase, causing a conformation "switch" in the αI′ helix. This switch allows the SH2 domain to pack tightly against the C-lobe, inhibiting c-Abl kinase activity. Phosphorylation of Tyr412 in the activation loop and Tyr245 in the SH2 kinase linker are required for full catalytic activity. The function of Tyr245 and Tyr412 has been thoroughly analyzed and mutagenesis has confirmed that these phosphorylation sites are required for c-Abl activation. Opening the close-conformation by any means is predicted to induce catalytic activation. Accordingly, SH2 and SH3 binders can induce c-Abl activation and disruption of these interactions by mutation leads to transforming activity, as observed in oncogenic Abl alleles.[51-55]

1.1.2 PROTEIN AGC KINASES

Although tyrosine kinase inhibitors are the most evaluated kinase inhibitors in clinical trials, a third of kinase inhibitors are targeted against Ser/Thr kinases that belong to the AGC kinase family.
The AGC kinase group comprises 12% of the human kinome and was named after 3 representative families, the cAMP-dependent protein kinase (PKA), the cGMP-dependent protein kinase (PKG) and the protein kinase C (PKC) families. In the human genome, 63 genes encode 61 AGC kinases and 2 pseudokinases, which are classified into 14 families and 21 subfamilies.[1]
In the Sgk family there are three Sgk isoforms that share similar biochemical properties and comparable roles in the regulation of a wide range of physiological and pathophysiological functions. Sgk1 is the most studied member of the family and is involved in cell proliferation and survival as well as tumor growth.[56]

1.1.2.1 Sgk1

The serum- and glucocorticoid-regulated kinase (Sgk) family consists of three members, Sgk1, Sgk2 and Sgk3, all displaying serine/threonine kinase activity and sharing structural and functional similarities with the Akt family of kinases.[56] Sgk1 activity is strictly correlated with its post-translational modifications. It becomes a substrate of the mTOR kinase that phosphorylates its hydrophobic motif (H-motif) at the level of S422. Then, 3-phosphoinositide-dependent kinase-1 (Pdk1) binds to the H-motif of Sgk1, at the level of phospho-S422, and further phosphorylates the protein at T256.[57]
Sgk1 was originally described as a key enzyme in the hormonal regulation of sodium absorption by the amiloride-sensitive sodium channel (ENaC).[58]
Sgk1 is regulated by insulin, IGF-1, cAMP, glucocorticoids[59-62] and IL-2[63] and transduces survival signals in normal and cancer cells. Increased SGK1 expression has been found in several human tumors, including breast,[64] tongue,[65] ovarian,[66] prostate carcinoma,[67] non-small cell lung cancer[68] and HCC.[69-71]
Conversely, SGK1 knock-out models were shown to be resistant to chemically-induced colon carcinogenesis.[72] Sgk1 regulates cell survival, proliferation and differentiation via phosphorylation of Mouse Double Minutes 2 (MDM2), which leads to the ubiquitylation and proteosomal degradation of p53.[73] Sgk1 also activates transcription of RANBP1, a major regulator of the RAN GTPase, thus affecting mitotic stability and paclitaxel sensitivity in colon carcinoma cells (RKO).[74]

Sgk1 interacts with enzymes involved in the metabolism of glycoproteins and lysophospholipids[61,75] suggesting a role in the development of some of the metabolic alterations that may affect colorectal cancer progression.[76-79] Sgk1 specific RNA silencing in cultured RKO colon carcinoma cells has been recently demonstrated to enhance paclitaxel sensitivity, measured as early and late apoptosis.[74] Taken together, these observations suggest an important role for Sgk1 in carcinogenesis and in the mechanisms responsible for resistance to chemotherapy.[80] Sgk1 may thus be considered an interesting molecular target in the therapy of some human tumors.[73,81,82] The expression level of Sgk family of proteins may have a central role in tumors that are resistant to Akt inhibition.[83] Notably Sgk1, as compared with its cognate kinase Akt, is highly regulated by steroids. Glucocorticoid receptor antagonism has been recently proposed as a promising therapy in triple negative breast cancer,[84] and Sgk1 inhibition is thus expected to be at least as effective as glucocorticoid receptor antagonism.

SGK1 gene encodes a protein of 50 kDa, its catalytic domain is 45%–60% homologous to the catalytic domains of other serine/threonine protein kinases such as cAMP-dependent protein kinase (PKA), and the protein kinase C family. Two isoforms (Sgk2 and Sgk3) of Sgk1 have been identified; the biological importance of these isoforms remains unclear.
The crystal structure of the catalytic kinase domain of SGK1 bound to AMP-PNP was determinated by Zhao *et al*.[85] (**Figure 6**)
Sgk1 has the typical bilobal kinase fold, comprised of an N-terminal β-strand domain (residues 60–179) and a C-terminal α-helical domain (residues 180–431). The two domains are linked together by a hinge region that forms an important part of the catalytic active site.

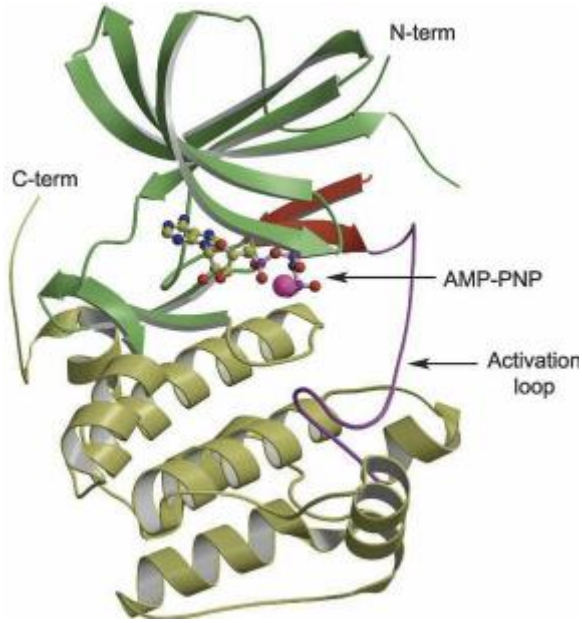

Figure 6: Structure of SGK1 bound to AMP-PNP

1.2 PYRAZOLO[3,4-*d*]PYRIMIDINES COMPOUNDS

The protein kinases overexpression and iperactivation are present in several kind of tumor.
Pyrazolo[3,4-*d*]pyrimidines represent a promising class of compounds capable of inhibiting several oncogenic tyrosine kinases, which represent an attractive target for the development of new therapeutic agents against cancer.[86] In this context, 4-amino-substituted pyrazolo[3,4-*d*]pyrimidines, are extensively studied and regularly synthesized in our laboratories.
Their activity may be due to isosterism with purines, in particular the pyrazolo[3,4-*d*]pyrimidines structure is an isostere of ATP, the natural phosphorylating agent that binds PTKs (**Figure 7,8**).

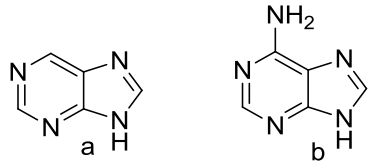

Figure 7: a) general structure of purines b) adenine

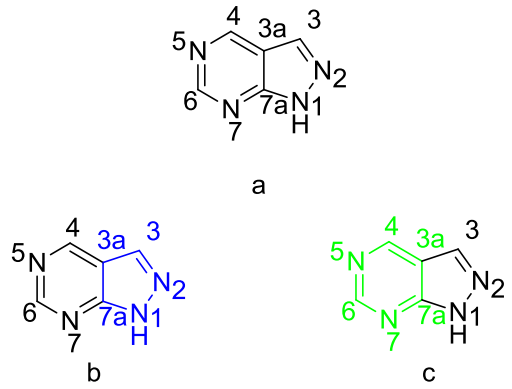

Figure 8: a) pyrazolo[3,4-*d*]pyrimidine b) pyrazolo portion c) pyrimidine portion

The first pyrazolo[3,4-*d*]pyrimidines compounds synthesized by our group, have been tested on a epidermoid carcinoma of the vulva cells line, giving good results.[87]
The biological assays results showed that they were able to stop the proliferation of cancer cells by inhibiting the phosphorylation of tyrosine kinase Src and promoting an apoptotic mechanism.
Given the significant biological activity, our research group decided to synthesize a small library of derivatives, variously substituted.
Therefore, it was decided to substitute the pyrazolo[3,4-*d*]pyrimidines core in N-1, C-4 and C-6 positions (**Figure 9**).

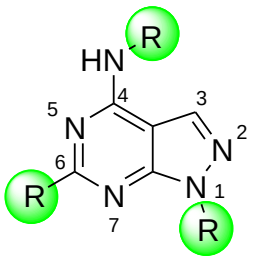

Figure 9: Pyrazolo[3,4-*d*]pyrimidines substituted positions: N-1, C-4 and C-6

Src is overexpressed in several types of tumors, therefore the 1,4,6 trisubstituted compounds were also tested on breast carcinoma cells.
Even for this tumor, phosphorylation on Tyr 416 results in uncontrolled activation of Src.
The micromolar activities values are identified in the cell line (8701-BC).[88]
After, our research group, focused its attention on the synthesis of compounds that inhibit Src activity in osteosarcoma tumor cells. This is a primary malignant tumor of the skeletal system that affects more frequently young people between 10 and 20 years. Among the new derivatives tested, the compound SI83 (**Figure 10**) showed the greatest inhibition of cell proliferation (approximately 85% compared to 63% of the reference compound PP2)[89] on SaOS-2 cells (osteogenic sarcoma: non-trasformed cell line derived from primary osteosarcoma).

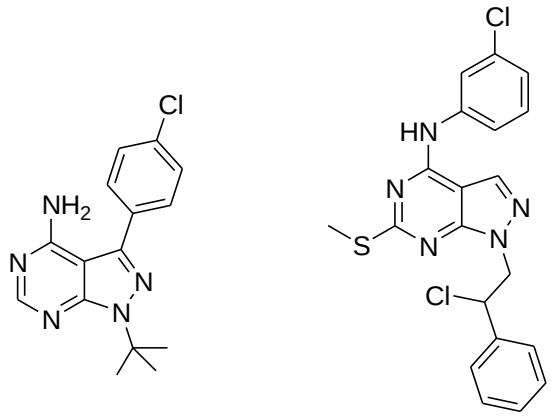

Figure 10: Structures of PP2 and SI83

Than PP2, SI83 displayed more potent and selective proapoptotic activity against cancer cells,
the administration of SI83 in the *in vivo* experiments leads to a decrease of the tumor size.
The effectiveness of these bicyclic compounds has been confirmed also on the other four osteosarcoma cell lines (TE-85, U-2 OS, MG63, MNNG), in more highlighted the very low toxicity to non-neoplastic cells.[90,91]
Some derivatives already tested as Src inhibitors have also shown active against the kinases Bcr/Abl. The dual activity was mainly observed for the compounds having the thiomethyl group at C-6.[92,93]
Over expression of the tyrosine kinase Bcr/Abl, in hyperactivated form, was also observed in chronic myeloid leukemia (CML) This disease is characterized by the presence of the Philadelphia chromosome (discovered in 1960 by Nowell and Hungerford)[94] and results from a reciprocal translocation between chromosomes 9 and 22.[95] This translocation fuses the breakpoint cluster region (Bcr) and the Abelson kinase (Abl) genes, forming the Bcr-Abl oncogene[96] that encodes the constitutively active cytoplasmatic tyrosine kinase (TK) Bcr-Abl, present in >90% of CML.[97]
SI223 and SI278 (**Figure 11**) demonstrated antiproliferative activity and apoptosi induction more interesting. on three different myeloid leukemia cell lines: K-562, KU-812, MEG-01.

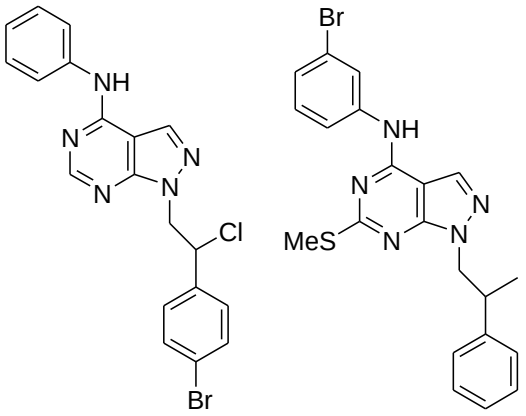

SI223
K_i Src (mM)= 0.064
K_i Abl (mM)= 0.610

SI278
K_i Src (mM)= 0.018
K_i Abl (mM)= 1.07

Figure 11: Structures and enzymatic activity of S223 and SI278

The clinical use of *Imatinib* (Bcr/Abl inhibitor) has changed the landscape of prognostic patient with CML. Subsequently, resistance to this drug have occurred; these have been overcome with the introduction of second generation antitumor as the Nilotinib and Dasatinib.
The recent problem is the appearance of the T315I mutation, which also confers resistance to second generation drugs.
The pyrazolo[3,4-*d*]pyrimidines compounds such as S13 (**Figure 12**) have proved to be an excellent T315I[98] mutants inhibitor.

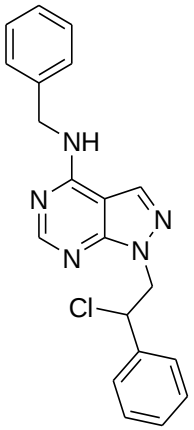

S13

K_i Abl (µM)= 0.37, T315I mutants (µM)= 3.0

Figure 12: Structure, enzymatic activity and cellular activity of S13

The development of these molecules led to the synthesis of a small library with increased activity towards SH-SY5Y neuroblastoma (NB)[99,100] cell line; furthermore the selected lead compound

SI306 (Figure X) was able to induce a tumor volume reduction greater than 50% in a NB subcutaneous xenograft mouse model.[101]
The anticancer activity of pyrazolo[3,4-*d*]pyrimidines was also confirmed in U87 glioblastoma (GBM) cell line,[102] also in this case SI306 (**Figure 13**) was chosen for the *in vivo* experiments. These studies highlighted that SI306 was able to increase survival time of treated mice in a GBM (U87 cells) orthotopic model by 30%, with respect to the vehicle treated mice.[103]

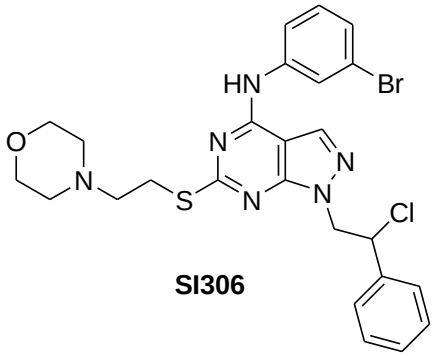

SI306

K_i Src (μM)= 0.13, K_i Abl (μM)= 0.12,
IC_{50} SH-SY5Y (μM)= 0.34, IC_{50} U87 (μM)= 1.98

Figure 13: Structure, enzymatic activity and cellular activity of SI306

Furthermore, the recent screen of a family of dual Src/Abl inhibitors characterized by a substituted pyrazolo[3,4-*d*]pyrimidines scaffold has showed their ability to inhibit Sgk1 and Akt kinase activity, competing with ATP for its binding domain. One of these molecules, SI113 (**Figure 14**), was particularly effective in inhibiting Sgk1 kinase activity (IC_{50} value of 600 nmol/L, 0% of kinase residual activity), being much less effective on Akt1 activity, probably because it fits better with the lipophilic area of the ATP binding domain, that in Sgk1 is larger than in Akt1.[104]

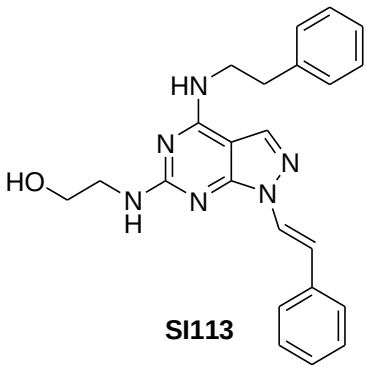

SI113

Figure 14: Structure of SI113

Afterwards was demonstrated an interesting activity profile of this compound. SI113 induced cell death in various malignant cell lines (MCF7 breast carcinoma, A172 glioma and RKO colon carcinoma) and had a synergic apoptotic effect in combination with paclitaxel.[105]
Subsequent studies have also shown the ability of SI113 to inhibits liver cancer cells proliferation (*in vitro* in HepG2 and HUH-7 cells and *in vivo* in NOD/SCID hepatocellular carcinoma (HCC) xenografts mice) and potentiates the effects of radiotherapy.[106]

On the other hand, the good biological activity exhibited by this family of compounds, as for other protein kinases inhibitors, is associated with low water solubility; this could influence the pharmacokinetic parameters and cause issues in the future development of these putative drug candidates. Early assessment of pharmaceutical properties such as solubility, metabolic stability, and permeability has become a key step in the drug discovery process since it is estimated that 40% of potential drug candidates fail to reach the market due to poor physicochemical properties.
In this context, the determination of solubility represents an important and crucial aspect, indeed a low water solubility could possibly be responsible for irreproducible and inaccurate *in vitro* results. This is why a coordinated and in-parallel optimization of biological activity and pharmaceutical properties, such as water solubility, likely represents a valid tactic to develop a new potential drug candidate.

1.3 STRATEGIES TO DEVELOP A NEW DRUG CANDIDATE

Some strategies can be used by medicinal chemists to improve solubility through structure modification:

-Add ionisable group

-Add hydrogen bonding

-Add polar group

-Cyclodextrins complexation

-Nanosystem delivery (like liposomes and nanoparticles)

-Construct a prodrug

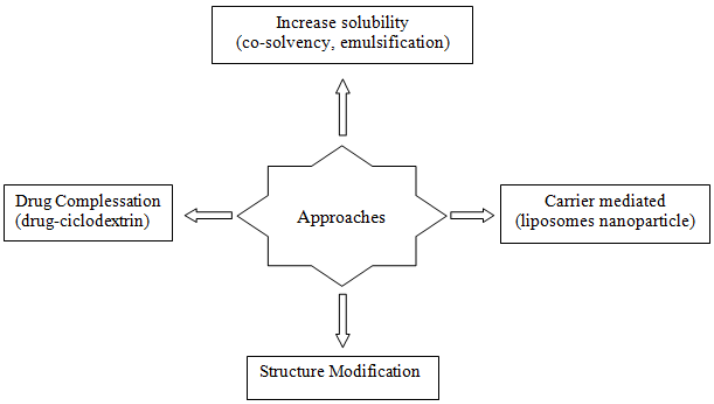

Figure 15: Approaches to improve solubility: structure modification and formulation

Herein, the nanosystem delivery (liposomes and albumin nanoparticles) and use of prodrugs (chemically modified versions of the pharmaceutically active drug, which after undergoing *in vivo* transformations release the active drug), are reported. These approaches represent well established strategies to improve the physicochemical, biopharmaceutical, or pharmacokinetic properties of potential drug candidates.

1.3.1 LIPOSOMES

1.3.1.1 LIPID-BASED FORMULATION

There are four different types of lipid-based formulations depending on the percentage of oil, water-soluble and water-insoluble surfactants, and co-solvents. Lipid-based formulation can increase the solubility of lipophilic compounds. The simplest lipid delivery system is to dissolve a drug into pure oil (e.g., vegetable oil). For example, oil solution is the standard method for administration of lipid-soluble vitamins, such as vitamins A and D. For more complex systems, compounds are dissolved in oil or lipids and then dispersed into aqueous buffers in the presence of surfactants, with or without co-solvents. They can form emulsions, micelles, or liposomes.

An emulsion is a dispersion of two immiscible liquids (e.g., oil and water) with a surfactant or emulsifier. Emulsifier coats the droplets to stabilize the emulsion by creating repulsion between the droplets. There are two common types of emulsions. Water-in-oil (W/O) emulsions typically are used in sustained release of steroids and vaccines by IM delivery. Oil-in-water (O/W) emulsions are one of the most commonly used lipid formulations for various routes of administration, such as SC, IM, and IV. Excipients for emulsion formulation are various oils of polar triglycerides (e.g., soybean oil, sesame oil, corn oil, safflower oil), an aqueous phase (saline, D5W and buffers), and an emulsifier (egg lecithin and Tween 80). Drug emulsions are normally formulated to isotonic concentration at pH 7 to 8, which reduces pain upon injection compared to solvent-based or solubilized formulations.[107]

Micelles are aggregates that self-associate to form a hydrophobic core and hydrophilic outer sphere. Lipophilic drugs can be incorporated into the core and thus dissolved in aqueous media. The sizes of the micelles are approximately 5 to 50 nm.[108] Micelles typically consist of low–molecular-weight amphiphilic molecules, such as bile salts and phospholipids.

The limitations of small molecular micelles are low capacity for drug loading, possible toxicity due to disruption of lipid bilayers and possible precipitation after injection due to breakdown of the micelles. Block copolymer micelles offer many advantages over traditional micellar formulations, with less toxicity, better stability, higher loading, controlled-release properties, and targeted delivery. Liposomes are microscopic spheres, typically made of bilayers of natural or semisynthetic phospholipids and/or cholesterol. Insoluble compounds can be solubilized in the hydrophobic space of liposomes. They vary in size (30 nm to 30 μM), bilayer rigidity, geometry, and charge. Beside the hydrophobic bilayer, the encapsulated aqueous compartment and the polar interface can be used to capture sparingly soluble compounds The versatility makes liposome delivery systems amenable to formulate a wide range of drug classes. Liposome technology is currently focused on applications in oncology, but it can also be used to formulate drugs to treat fungal, bacterial, and viral infections, alleviate pain, reduce inflammation, treat blood disorders, and for medical imaging and vaccines.[109]

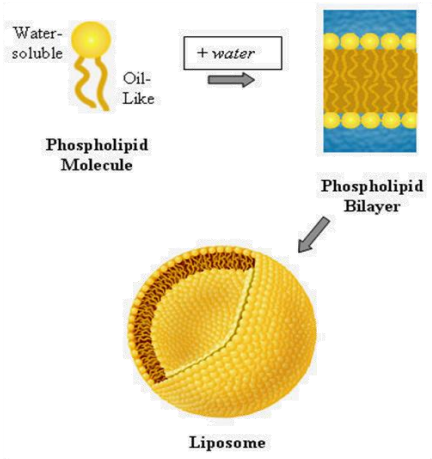

Figure 16: Structure of a lipid-based formulations

Liposomes can be destabilized if overloaded with drug molecules. Drug loading of lipophilic drugs normally is substantially lower for liposomes than for emulsions. It is typically limited to high-potency compounds. Liposome formulations are normally lyophilized because of stability issues and require reconstitution before use.

1.3.1.2 LIPOSOMES DRUG-DELIVERY SISTEM

Liposomes are extensively used as carriers for numerous molecules in cosmetic and pharmaceutical industries. Additionally, food and farming industries have extensively studied the use of liposome encapsulation to grow delivery systems that can entrap unstable compounds (for example, antimicrobials, antioxidants, flavours and bioactive elements) and shield their functionality.

Liposomes can trap both hydrophobic and hydrophilic compounds, avoid decomposition of the entrapped combinations, and release the entrapped at designated targets.[110-112] Because of their biocompatibility, biodegradability, low toxicity, and aptitude to trap both hydrophilic and Lipophilic drugs[113] and simplify site-specific drug delivery to tumor tissues,[114] liposomes have increased rate both as an investigational system and commercially as a drug delivery system. Many studies have been conducted on liposomes with the goal of decreasing drug toxicity and/or targeting specific cells.[115,116]

Liposomal encapsulation technology (LET) is the newest delivery technique used by medical investigators to transmit drugs that act as curative promoters to the assured body organs. This form of delivery system proposal targeted the delivery of vital combinations to the body. LET is a method of generating sub-microscopic foams called liposomes, which encapsulate numerous materials.

These 'liposomes' form a barrier around their contents, which is resistant to enzymes in the mouth and stomach, alkaline solutions, digestive juices, bile salts, and intestinal flora that are generated in the human body, as well as free radicals. The contents of the liposomes are, therefore, protected from oxidation and degradation. This protective phospholipid shield or barrier remains undamaged until the contents of the liposome are delivered to the exact target gland, organ, or system where the contents will be utilized.[117,118]

Clinical medication keeps an enormously broad range of drug molecules at this time in use, and new drugs are added to the list every year. One of the main aims of any cure employing drug is to increase the therapeutic index of the drug while minimizing its side effects. The clinical usefulness of most conservative chemotherapeutics is restricted either by the incapability to deliver therapeutic drug concentrations to the target soft tissue or by Spartan and harmful toxic side effects on normal organs and tissues. Different approaches have been made to overcome these difficulties by providing the 'selective' delivery to the target area; the ideal solution would be to target the drug alone to those cells, tissues, organs that are affected by the disease. Selected carriers, for instance colloidal particulates and molecular conjugates, can be appropriate for this determination. Colloidal particulates result from the physical incorporation of the drug into a particulate colloidal system, for instance reverse micelles, noisome, micro- and nano-spheres, erythrocytes, and polymers and liposomes. Among these carriers, liposomes have been most studied. Their attractiveness lies in their composition, which makes them biodegradable and biocompatible. Liposome involves an aqueous core entrapped by one or more bilayers composed of natural or synthetic lipids. They are composed of natural phospholipids that are biologically inert and feebly immunogenic, and they have low inherent toxicity. Furthermore, drugs with different lipophilicities can be encapsulated into liposomes: strongly lipophilic drugs are entrapped almost totally in the lipid bilayer, intensely hydrophilic drugs are located entirely in the aqueous compartment, and drugs with intermediary logP effortlessly partition between the lipid and aqueous phases, both in the bilayer and in the aqueous core.[119]

1.3.1.3 CLASSIFICATION OF LIPOSOMES

The liposome size can vary from very small (0.025 μm) to large (2.5 μm) vesicles. Moreover, liposomes may have one or bilayer membranes. The vesicle size is an acute parameter in

determining the circulation half-life of liposomes, and both size and number of bilayers affect the amount of drug encapsulation in the liposomes. On the basis of their size and number of bilayers, liposomes can also be classified into one of two categories: multilamellar vesicles (MLV) and unilamellar vesicles.
Unilamellar vesicles can also be classified into two categories: large unilamellar vesicles (LUV) and small unilamellar vesicles (SUV). In unilamellar liposomes, the vesicle has a single phospholipid bilayer sphere enclosing the aqueous solution. In multilamellar liposomes, vesicles have an onion structure.
Classically, several unilamellar vesicles will form on the inside of the other with smaller size, making a multilamellar structure of concentric phospholipids spheres separated by layers of water.[120]

1.3.1.4 METHODS OF LIPOSOME PREPARATION

General methods of preparation

All the methods of preparing the liposomes involve four basic stages:

1. Drying down lipids from organic solvent.
2. Dispersing the lipid in aqueous media.
3. Purifying the resultant liposome.
4. Analyzing the final product.

Method of liposome preparation and drug loading

The following methods are used for the loading of liposome:

1. Passive loading techniques.
2. Active loading technique.

Passive loading techniques include three different methods:

1. Mechanical dispersion method.
2. Solvent dispersion method.
3. Detergent removal method (removal of nonencapsulated material)

1.3.1.5 MECHANISM OF TRANSPORTATION THROUGH LIPOSOMES

The limitations and benefits of liposome drug carrier lie critically on the interaction of liposomes with cells and their destiny *in vivo* after administration. *In vivo* and *in vitro* studies of the contacts with cells have shown that the main interaction of liposomes with cells is either simple adsorption (by specific interactions with cell-surface components, electrostatic forces, or by nonspecific weak hydrophobic) or following endocytosis (by phagocytic cells of the reticulo endothelial system, for example macrophages and neutrophils).
Fusion with the plasma cell membrane by insertion of the lipid bilayer of the liposome into the plasma membrane, with simultaneous release of liposomal content into the cytoplasm, is much rare. The fourth possible interaction is the exchange of bilayer components, for instance cholesterol,

lipids, and membrane-bound molecules with components of cell membranes. It is often difficult to determine what mechanism is functioning, and more than one may function at the same time.

1.3.2 ALBUMIN NANOPARTICLES

1.3.2.1 ALBUMIN

Albumin is emerging as a versatile protein carrier for drug targeting and for improving the pharmacokinetic profile of peptide- or protein-based drugs. Albumin is the most abundant plasma protein (35–50 g/L human serum) with a molecular weight of 66.5 kDa. Like most of the plasma proteins, albumin is synthesized in the liver where it is produced at a rate of approximately 0.7 mg/h for every gram of liver (i.e. 10–15 g daily); human serum albumin (HSA) exhibits an average half-life of 19 days. The functions and binding properties of HSA are multifold:[121] a) it acts as the solubilizing agent for long chain fatty acids and is therefore essential for the metabolism of lipids; b) it binds bilirubin, the breakdown product of heme; c) it binds a great number of therapeutic drugs such as penicillins, sulfonamides, indole compounds, and benzodiazepines to name just a few; d) it binds copper(II) and nickel(II) in a specific and calcium(II) and zinc(II) in a relatively nonspecific manner and acts as the transport vehicle for these metal ions in the blood; e) it is the major protein responsible for the colloid osmotic pressure of the blood; f) when HSA is broken down, the amino acids provide nutrition to peripheral tissue.

The three-dimensional structure of HSA has been elucidated by X-ray structure analysis.[122,123] The approximate three-dimensional shape of HSA can be described as an ellipsoid consisting of three flexible spheres in a row (domains I, II, III) and is illustrated schematically in **Figure 17**.

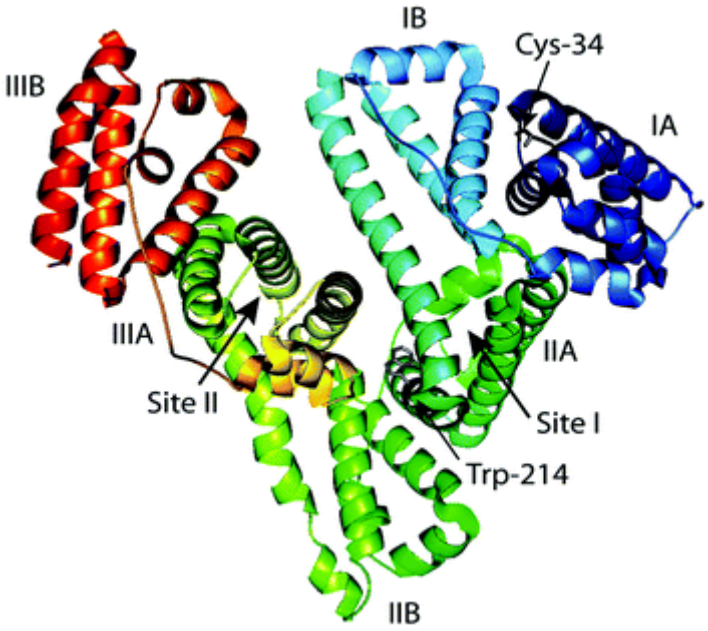

Figure 17: X-ray structure of human serum albumin

HSA is one of the smallest proteins present in blood plasma. Both size and abundance explain the fact that so many metabolic compounds and therapeutic drugs are transported by this protein. The binding sites for metabolic substrates and diagnostic as well as therapeutic drugs have been extensively studied and reviewed.[124,125]

Albumin is an acidic, very soluble protein that is extremely robust: it is stable in the pH range of 4–9, soluble in 40% ethanol, and can be heated at 60°C for up to 10 h without deleterious effects. These properties as well as its preferential uptake in tumor and inflamed tissue, its ready

availability, its biodegradability, and its lack of toxicity and immunogenicity make it an ideal candidate for drug delivery.

1.3.2.2 ALBUMIN AS A DRUG CARRIER

Albumin-based nanoparticle carrier systems represent an attractive strategy, since a significant amount of drug can be incorporated into the particle matrix because of the different drug binding sites present in the albumin molecule.[126] Due to the defined albumin primary structure and high content of charged amino acids (e.g. lysine), albumin-based nanoparticles could allow the electrostatic adsorption of positively (e.g. ganciclovir) or negatively charged (e.g. oligonucleotide) molecules. In addition, albumin nanoparticles offer several specific advantages: they are biodegradable, easy to prepare and they show a smaller size (50 to 300 nm). Commercially, albumins are obtained with significant quantities from egg white (ovalbumin), bovine serum (bovine serum albumin, BSA), and human serum (human serum albumin, HSA) and also available from soybeans, milk, and grains.[127]

1.3.2.3 PREPARATION TECHNIQUES

The protocols to prepare albumin nanoparticles can be classified into three principal techniques:
1. desolvation.

2. emulsification.

3. thermal gelation.

Recently techniques were also used:
-nano spray drying.

-nab-technology.

-self-assembly.

1.3.3 PRODRUGS

The prodrug concept, as first introduced by Adrian Albert in the 1950s, defines a pro-drug as a pharmacologically inactive agent that undergoes an enzymatic and/or chemical transformation in vivo to a therapeutically active drug . Prodrugs are considered to be inactive or at least significantly less active than the released drugs; therefore, salts of active agents and drugs, whose metabolites contribute to the overall pharmacological response, are not included in this definition. The rationale behind the use of prodrugs is generally to optimize the “drug-like” properties [i.e., absorption, distribution, metabolism, and excretion (ADME) properties] because they can cause considerable problems in subsequent drug development, if unfavourable. There are many benefits to using the prodrug approach. It can be applied to improve solubility and passive permeability for absorption improvement. Prodrugs can be prepared to enhance transporter-mediated absorption and to improve metabolic stability. In addition, the prodrug strategy has been used to increase the selectivity of drugs for their intended target. This can not only improve the efficacy of the drug but also decrease systemic and/or unwanted tissue/organspecific toxicity (T). Development of a prodrug with improved properties may also represent a life-cycle management opportunity. The design of an appropriate prodrug should never be viewed as a last resort. If anything, this alternative should be considered in the early stages of preclinical development, bearing in mind that prodrugs may alter the tissue distribution, efficacy, and even toxicity of the parent drug. Therefore, modifying the ADMET properties of the parent drug requires a comprehensive understanding of the physicochemical and biological behaviour of the drug candidate.

Although prodrug design is very challenging, it can still be more feasible and faster than searching for an entirely new therapeutically active agent with suitable ADMET properties. A very good indication of the success of the prodrug approach can be obtained by examining the prevalence of prodrugs on the market: currently approximately 10% of all globally marketed medicines can be classified as prodrugs.

1.3.3.1 USE OF PRODRUGS

Using prodrugs to improve solubility

Prodrug strategies can be applied to improve solubility.[128] **Table 1** shows commercially available prodrugs with improved solubility. The structures of some prodrugs are illustrated in **Figure 18**.

Name	Solubility in water (mg/mL)
Clindamycin	0.2
Clindamycin-2-PO_4	150
Chloramphenicol	2.5
Succinate sodium	500
Metronidazole	10
N,N-dimethylglycinate	200
Phenytoin	0.02
Phosphate	142
Celexicoxib	0.05
Parecoxib sodium	15

Table 1: Commercially available prodrugs and their improved solubility

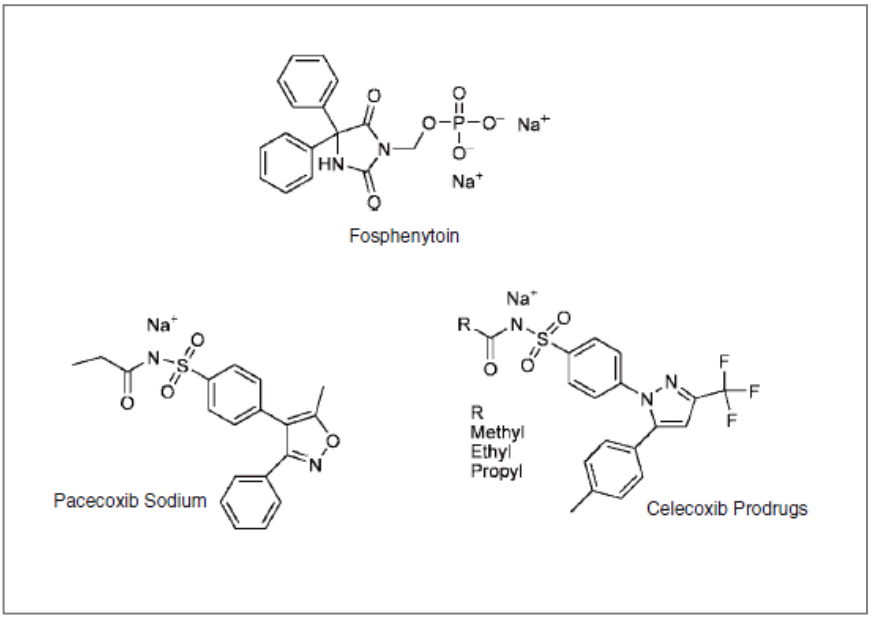

Figure 18: Structures of prodrugs with improved solubility

Prodrugs with a non-ionizable promoiety (e.g., glycol, polyethylene glycol [PEG], sugars) typically can improve solubility by two- to three-fold. Prodrugs with ionizable promoieties (e.g., phosphate) can increase solubility by orders of magnitude. There are three types of ionizable promoieties. Succinate-like derivatives were used early as prodrugs but are chemically unstable. Amino acid type, attached to hydroxyls (e.g., glucocorticoids) and phosphate type, attached to hydroxyls or amines (e.g., fosphenytoin) are common approaches used in the industry to increase solubility.

Prodrugs to increase passive permeability

Prodrug strategies are most commonly used to increase permeability of compounds by masking the polar functional groups and hydrogen bonds with ester or amide linkers and increasing lipophilicity. Oral delivery of ester/amide prodrugs to the therapeutic target is confronted with many physiological, chemical, and biochemical barriers. In general, the highest oral bioavailability values that ester prodrugs can achieve clinically are 40% to 60%. This is due to incomplete membrane permeation, P-glycoprotein efflux, hydrolysis in the GI lumen and intestinal cells, nonesterase metabolism in the liver, biliary excretion, and metabolism of the parent.[129]

Prodrugs to reduce metabolism

A prodrug approach can be used to prolong the half-life of the parent drug by masking the labile functional groups, such as phenolic alcohols, which are susceptible to phase II metabolism. They are essentially slow-release drugs. **Figure 19** shows examples of prodrugs with increased metabolic stability. Bambuterol is a dicarbamate prodrug of terbutaline. The phenolic alcohols are protected from phase II metabolism, and the carbamates are slowly hydrolyzed by nonspecific cholinesterases to release the parent terbutaline. The slow metabolism results in a longer half-life. Bambuterol is dosed once per day versus three times per day for terbutaline.

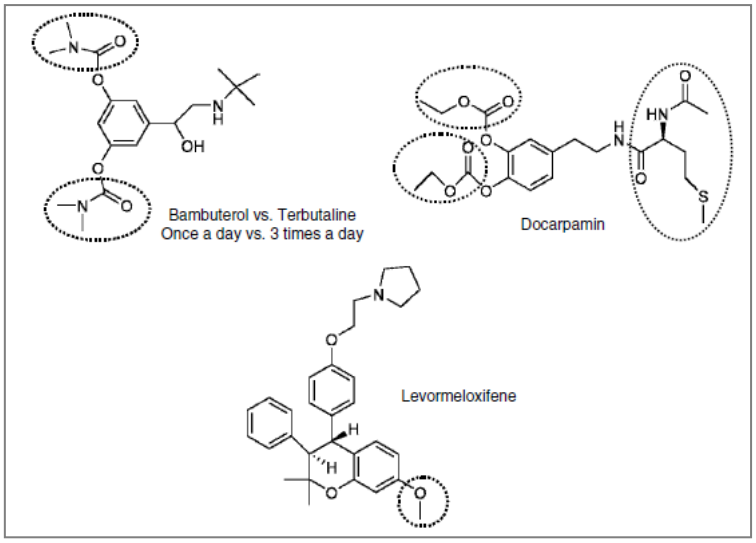

Figure 19. Examples of prodrugs used to reduce metabolism

Prodrugs to Target Specific Tissues

Selective tissue delivery can increase therapeutic activity and reduce side effects. For example, PEG-conjugated anticancer prodrugs (e.g. PEG-paclitaxel) are found to selectively accumulate in tumor cells, prolong half-life, and improve efficacy. Prodrugs can also be used to target brain, bone, colon, and other specific tissues. Organ- or tissue-specific delivery is also known as the magic bullet.

Capecitabine is an orally active prodrug of 5-fluorouracil (5-FU) Bioactivation of capecitabine is shown in **Figure 20**. It is first hydrolyzed in the liver by carboxylesterase and decarboxylated to 5-deoxy-5-fluorocytidine, which is further converted to 5-deoxy-5-fluorouridine by cytidine deaminase. Transformation of 5-deoxy-5-fluorouridine to 5-FU occurs selectively in tumor cells by thymidine phosphorylase. Distribution of 5-FU to tumor is impressive: six times higher than GI and 15 times higher than blood after oral administration of capecitabine.

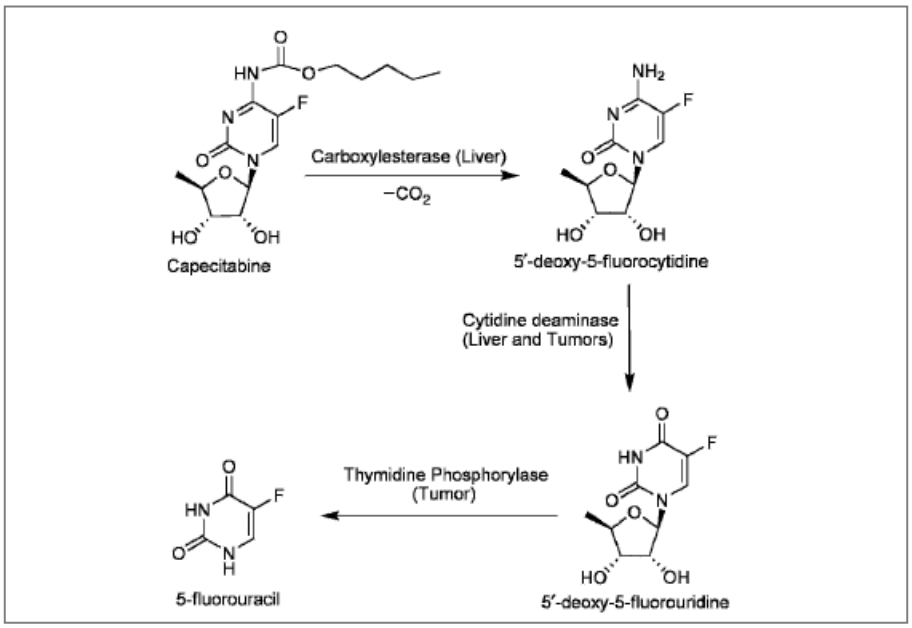

Figure 20: Activation of the tumor-specific prodrug capecitabine to 5-fluorouracil

1.4 AIM OF THE WORK

In the last few years, our research group developed a series of pyrazolo[3,4-*d*]pyrimidines as anticancer agents. To date, our pyrazolo[3,4-*d*]pyrimidines library consists of more than 400 members, developed mostly as ATP-competitive protein kinase inhibitors (Src, Abl and Sgk1).[104,130]
The anticancer activity of these molecules was confirmed in several cancer cell lines, both from solid tumors (i.e. osteosarcoma SaOS-2,[91] prostate PC3,[131] neuroblastoma SH-SY5Y,[99,101] glioblastoma U87,[102,103] rabdomyosarcoma,[132] mesothelioma,[133] medulloblastoma,[134] medullary thyroid carcinoma,[135] hepatocellular carcinoma (HepG2 and HUH-7)[106] and leukemia (i.e. 32D-p210 and 32D-T315I)[136] and Burkitt lymphomas.[137]
In vivo data, generated in xenograft mouse models further supported the antitumor activities of several pyrazolo[3,4-*d*]pyrimidines against leukemia (32D-p210 and 32D-T315I),[136] neuroblastoma (SH-SY5Y),[99] glioblastoma (U87),\03 and hepatocellular carcinoma (HUH-7).[106]
Despite their promising biological activity, pyrazolo[3,4-*d*]pyrimidines have low water solubility, a property that could interfere with the development of these compounds to become drug candidates.
In this view, the purpose of this work was, together with the optimization of the biological activity of these compounds, studying different strategies to improve their water solubility and pharmacokinetic properties.

As a first strategy, four pyrazolo[3,4-d]pyrimidines were chosen on the basis of their activity against **neuroblastoma (NB)**. The compounds were synthesized and encapsulated in **albumin nanoparticles** and **liposomes**. Albumin nanoparticles and liposomes were prepared and characterized regarding size and ζ-potential distribution, polidispersity index, entrapment efficiency and activity against SH-SY5Y human neuroblastoma cell line. The most promising nanosystem was chosen to perform further studies: confocal microscopy, stability and drug release in physiological conditions, and biodistribution.[138]
This strategy is described in the section 2.

In the second approach the **prodrugs strategy** was applied. To synthesize the full set of pyrazolo[3,4-*d*]pyrimidines prodrugs, a versatile one-pot two-step procedure was set up. Moreover, the plasma half-life, the ability to overcome biological membranes, metabolic stability as well as water solubility were analyzed.
Then the most interesting prodrugs were tested in a cellular assay with human **glioblastoma (GBM)** U87 cell line.
As *in vivo* proof of concept, the pharmacokinetics of the most promising pair of drug and prodrug were studied in an orthotopic mouse model of GBM.
This strategy is described in the section 3.

Finally, selectively activated prodrugs by a tumor-associated enzymes were developed.
This approach allows to generate active parent drug at the target site, as well as increase the water solubility of our molecules.
Tumor-associated enzymes, overexpressed in the tumoral environment, can be used as a trigger for specific prodrugs activation.
Therefore we synthesized a **plasmin-activated pyrazolo[3,4-*d*]pyrimidines prodrugs** by the inclusion of a small peptide, selectively recognized by this tumor-associated enzymes.
SI113 was the selected compound to develop this approach.
Indeed, SI113 showed an interesting activity profile against hepatocellular carcinoma (HCC), where the enzyme plasmin is overexpressed.[139]

Also in this case the plasma half-life, the ability to overcome biological membranes, metabolic stability as well as water solubility were analyzed. In addition the hydrolysis ability of prodrugs in the presence of the enzyme plasmin was evaluated.
Afterwards the synthesized compounds were tested in a cellular assay with hepatocellular carcinoma HepG2 cell line. *In vitro* cytotoxicity was also determinated by pre-incubation of the cell with the plasmin.
Given the obtained results, *in vivo* experiments in xenograft mouse models of hepatocellular carcinoma and in *vivo* studies of pharmacokinetics are ongoing.
This strategy is described in the section 4.

SECTION 2

‘IMPROVEMENT OF PYRAZOLO[3,4-*d*]PYRIMIDINES PHARMACOKINETIC PROPERTIES: NANOSYSTEM APPROACHES FOR DRUG DELIVERY’[138]

SCIENTIFIC REPORTS

OPEN

Improvement of pyrazolo[3,4-*d*] pyrimidines pharmacokinetic properties: nanosystem approaches for drug delivery

Received: 07 October 2015
Accepted: 26 January 2016
Published: 22 February 2016

Giulia Vignaroli[1,2,*], Pierpaolo Calandro[1,*], Claudio Zamperini[1,2], Federica Coniglio[1,2], Giulia Iovenitti[1,2], Matteo Tavanti[1], David Colecchia[3], Elena Dreassi[1], Massimo Valoti[4], Silvia Schenone[5], Mario Chiariello[3] & Maurizio Botta[1,2,6]

Pyrazolo[3,4-*d*]pyrimidines are a class of compounds with a good activity against several cancer cell lines. Despite the promising anticancer activity, these molecules showed a poor aqueous solubility. This issue could threat the future development of pyrazolo[3,4-*d*]pyrimidines as clinical drug candidates. With the aim of improving their solubility profile and consequently their pharmacokinetic properties, we have chosen four compounds (1–4) on the base of their anti-neuroblastoma activity and we have developed albumin nanoparticles and liposomes for the selected candidates. Albumin nanoparticles and liposomes were prepared and characterized regarding size and ζ-potential distribution, polidispersity index, entrapment efficiency and activity against SH-SY5Y human neuroblastoma cell line. The most promising nanosystem, namely LP-2, was chosen to perform further studies: confocal microscopy, stability and drug release in physiological conditions, and biodistribution. Altogether, the obtained data strongly indicate that the encapsulation of pyrazolo[3,4-*d*]pyrimidines in liposomes represent an effective method to overcome the poor water solubility.

Neuroblastoma (NB) is the most common extracranial solid tumor in early childhood (the median age at diagnosis is 17 months). This tumor arises in the sympathetic nervous system as a result of genetic alterations occurring in neural crest cells[1]. Although NB is characterized by clinical and biological heterogeneity, on the base of age, tumor stage and genomic rearrangements (MYCN amplification and aneuploidy), the International Neuroblastoma Risk Group Staging System (INRGSS) classification divides patients in four groups, ranging from very low- to high-risk[2]. Up to 50% of NB patients have very aggressive tumors, associated with high risk of relapse and very poor prognosis with a 5-year event-free survival rate around 40%. Treatment strategies for high-risk patients are still far from satisfaction, especially considering the severe side effects of the most used drugs (i.e. cisplatin, etoposide, vincristine, doxorubicin and cyclophosphamide)[1]. Consequently, the search for novel drugs to improve NB treatment options still represents an outstanding pharmaceutical issue[3].

In this context, Tyrosine Kinases (TKs) represent an interesting target for cancer treatment because of their involvement in several altered cellular pathways[4]. Molecular targeted therapies with Tyrosine Kinase Inhibitors (TKIs) are designed to disrupt signalling pathways responsible for the abnormal proliferation of cancer cells. Given the importance of this mechanism, several TKIs are currently under preclinical or clinical development[5]. A subclass of TKIs is represented by inhibitors of c-Src kinase, which is involved in cell proliferation, migration, invasion and angiogenesis as well as drug resistance development[6,7]. Since c-Src kinase has a strong connection with cancer development, several classes of small molecules (i.e. purines[8], anilinoquinazolines[9],

[1]Dipartimento di Biotecnologie, Chimica e Farmacia, Università degli Studi di Siena, via Aldo Moro 2, 53100, Siena, Italy. [2]Lead Discovery Siena S.r.l., via Vittorio Alfieri 31, 53019, Castelnuovo Berardenga, Siena, Italy. [3]Consiglio Nazionale delle Ricerche, Istituto di Fisiologia Clinica and Istituto Toscano Tumori, Core Research Laboratory, Via Fiorentina 1, 53100, Siena, Italy. [4]Dipartimento di Scienze della Vita, Università degli Studi di Siena, via Aldo Moro 2, 53100, Siena, Italy. [5]Dipartimento di Farmacia, Università di Genova, Viale Benedetto VX 3, 16132, Genova, Italy. [6]Biotechnology College of Science and Technology, Temple University, Biolife Science Building, Suite 333, 1900 N 12th Street, Philadelphia, Pennsylvania 19122, USA. *These authors contributed equally to this work. Correspondence and requests for materials should be addressed to M.B. (email: botta@unisi.it)

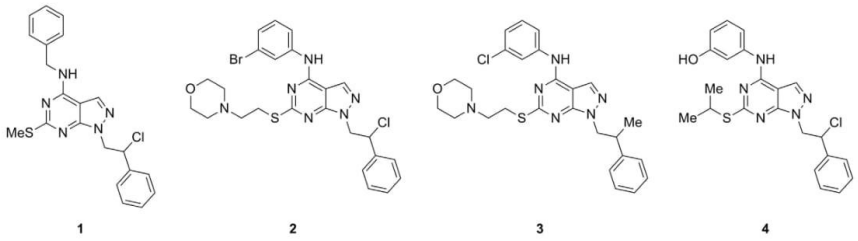

Figure 1. Structures of pyrazolo[3,4-*d*]pyrimidines 1–4.

quinolinecarbonitriles[10], benzotriazines[11], and thiazole-carboxamides[12]) have been developed to target this enzyme. Some outstanding c-Src inhibitors are: (I) Dasatinib, a dual Src/Abl TKI, FDA approved for chronic myeloid leukemia (CML) treatment, (II) Saracatinib[13], currently in phase II clinical trials for the treatment of solid tumors, such as melanoma, prostate and gastric cancer, (III) Bosutinib[14], a dual Src/Abl TKI, FDA approved for CML treatment[15]. Several studies confirmed that hyperactivated c-Src plays a key role in NB cell differentiation, adhesion and survival[16–20]. This TK was also associated to the progression of aggressive NB forms[21,22]. As a proof of concept of the effectiveness of inhibiting c-Src for NB treatment, recent studies demonstrated that the well-known c-Src inhibitor PP2 was able to inhibit cellular growth and to induce aggregation in NB cell lines[23]. Additionally the dual Src/Abl inhibitor Dasatinib was proved to be effective in reducing NB tumor growth *in vitro* and *in vivo*[24].

The development of pyrazolo[3,4-*d*]pyrimidines as potential anticancer drugs, represents a major research focus of our group. This family of compounds showed a good cytotoxicity profile against several cancer cell lines: NB[25–27], CML[28], glioblastoma (GB)[29], rhabdomyosarcoma (RMS)[30], osteosarcoma (OS)[31], prostate cancer (PC)[32]. The activity of pyrazolo[3,4-*d*]pyrimidines has been related to the inhibition of TKs such as Abl and Src-family proteins[33]. Recently, remarkable results have been obtained in several mouse models of cancer[25,28,30]. For instance, a small library of compounds with increased activity towards SH-SY5Y NB cell line was synthesized. The synthesis was driven by molecular modelling studies based on the X-ray crystal structure of c-Src in complex with one of our pyrazolo[3,4-*d*]pyrimidines. The selected lead compound was able to induce a tumor volume reduction greater than 50% in a NB subcutaneous xenograft mouse model[25].

Given their unique physicochemical features, albumin nanoparticles and liposomes have showed a great potential as drug-carriers able to modify pharmacokinetic and pharmacodynamic properties of compounds. Encapsulation of a drug might result in an improved biodistribution, a higher stability, a controlled release, an ability to target sites otherwise not accessible, a decreased toxicity, and an enhanced bioavailability[34]. Oligomers built with albumin are widely used as nanoparticles for drug delivery[35]. This small protein, the most abundant in human plasma, presents very interesting features (i.e. biocompatibility, half-life of 19 days, water solubility and ability to bind a variety of different entities) and accumulates in malignant and inflamed tissues[36]. A breakthrough for albumin-based nanotechnology was the commercialization of Abraxane©, a solvent-free formulation of paclitaxel, where albumin binds paclitaxel to carry it through the endothelial cells to the tumor area[37].

Liposomes are small vesicles characterized by a hydrophilic core surrounded by a phospholipid bilayer membrane whose composition can be adjusted to increase the therapeutic index of the encapsulated drug while minimizing its side effects. Liposomes are biodegradable and the Mononuclear Phagocyte System (MPS) uptake is strongly reduced when polyethylene glycol (PEG) is included in the membrane composition (Stealth Liposomes). Moreover, liposomes can be selectively trapped by the tumor due to enhanced permeation and retention[38]. Doxil, a PEGylated liposome-encapsulated form of doxorubicin, was the first FDA-approved nano-drug. It ensures prolonged blood circulation and lower cardiotoxicity when compared to free doxorubicin[39].

Although the promising anticancer activity, pyrazolo[3,4-*d*]pyrimidines are usually characterized by a low water solubility profile[40,41]. Consequently, in this study we have further developed four pyrazolo[3,4-*d*]pyrimidines (1–4, Fig. 1) previously characterized for their activity against NB by enzymatic, cellular and *in vivo* assays (Table 1)[25–27]. Several strategies were applied to overcome this issue in recent years (i.e. introduction of hydrophilic moieties in solvent-exposed positions[42], synthesis of prodrugs[43] and inclusion in cyclodextrins)[40,41].

With the aim of increasing the low water solubility of this class of compounds, in this study we have explored albumin nanoparticles and stealth liposomes as possible nanotechnologies.

Results

Pyrazolo[3,4-*d*]pyrimidines 1–4. The 4-amino substituted pyrazolo[3,4-*d*]pyrimidine ring represents a very interesting scaffold for the synthesis of molecules with antitumor activity. This structure is an isostere of ATP, the natural phosphorylating agent that binds TK. In our series of derivatives, the C4 amino function, essential for the interaction with the ATP-binding site, is attached to a *m*-substituted phenyl ring in derivatives 2–4 and a benzyl ring in derivative 1. Among the compounds previously characterized, pyrazolo[3,4-*d*]pyrimidine 1–4 were chosen for their ability to inhibit c-Src (with K_i values in the submicromolar range) and for their activity against NB cells[25–27]. Chemical structures of compounds 1–4 are shown in Fig. 1. *In vitro* ADME properties were also taken into account. In fact, the selected compounds demonstrated a very good metabolic stability (greater than 93% after incubation with human liver microsomes). Unfortunately, this favourable property was also associated

Cpd	Aqueous Solubility (μg/mL)	LogP[b]	Src (K_i μM)	PAMPA (10^{-6} cm^2/sec)	MR[c] (%)	Metabolic Stability[d] (%)
1	0,21	6,555	3.7	3.98	46.8	95.8
2	3,71	5,813	0.13	5.27	46.1	96.0
3	0,22	5,678	0.4	5.51	48.9	97.9
4	0,90	5,992	0.01	4.53	49.6	93.5

Table 1. Compounds 1–4: Activity against Src and ADME properties[a]. [a]All the data were previously reported, see supporting material for experimental details[25–27]. [b]Calculated by Qikprop. [c]Membrane Retention (MR) expressed as percentage of compound unable to reach the acceptor compartment. [d]Expressed as percentage of unmodified drug.

Formulation	Size[a] (nm)	Polydispersity index[a] (PDI)	Entrapment Efficiency[b] (%)	ζ-potential[a] (mV)
Liposomes	135.2 ± 9.45	0.23 ± 0.01	–	−27.4 ± 1.79
LP-1	151.3 ± 2.06	0.40 ± 0.04	65.0 ± 6.36	−41.9 ± 5.75
LP-2	105.1 ± 6.39	0.21 ± 0.01	99.1 ± 0.71	−39.9 ± 0.55
LP-3	131.3 ± 5.14	0.21 ± 0.03	85.2 ± 9.84	−28.8 ± 0.15
LP-4	232.4 ± 7.35	0.13 ± 0.01	96.3 ± 2.83	−47.6 ± 0.38
Albumin	9.30 ± 0.15	0.26 ± 0.01	–	−10.3 ± 1.41
AL-1	165.6 ± 6.11	0.97 ± 0.01	6.7 ± 0.91	−15.2 ± 1.17
AL-2	125.3 ± 3.76	0.68 ± 0.01	51.0 ± 2.88	−4.47 ± 1.93
AL-3	118.8 ± 3.00	0.58 ± 0.06	24.8 ± 1.23	−13.4 ± 2.90
AL-4	135.4 ± 15.9	0.55 ± 0.01	52.3 ± 1.82	−14.9 ± 1.46

Table 2. Properties of liposomes and albumin nanoparticles. [a]Determined by DLS (Nano-Zeta Sizer, Malvern Instruments Ltd, Malvern, UK). [b]For experimental details, see supporting material.

with a low aqueous solubility and a medium-low passive permeability through membrane. Enzymatic assays and ADME properties of compounds 1–4, as previously described[25–27], are reported in Table 1. Characterization of compounds 1–4 and assay methods can be found in the supporting material.

Characterization of albumin and liposome nanoparticles. To improve the poor solubility in aqueous solution and the biodistribution of this family of compounds, albumin nanoparticles (AL-1, AL-2, AL-3 and AL-4) and liposomes (LP-1, LP-2, LP-3 and LP-4) were prepared. The albumin-drug nanoparticles, prepared by disulphide-bond induced self-assembly, were analyzed by Dynamic Light Scattering (DLS) and results are reported in Table 2. The mean diameter ranged between 118.8 nm (AL-3) and 165.6 nm (AL-1). This size parameter was associated with high polidispersity indexes (close to 1), which indicated broad size distributions. Indeed, morphological analysis by Field Emission Scanning Electron Microscope (FESEM), confirmed the presence of aggregates (Figure S1). The tendency to form aggregates was also suggested by ζ-potential values belonging to the instability range[44]. The drug loading was around 6% when a very lipophilic compound, namely 1, was encapsulated. However, it rose up to 50% with compounds 2 and 4, both characterized by a better aqueous solubility than compound 1 (Table S1).

Lipid ratio and drug concentration represent two important factors for the encapsulation of drugs in liposomes. Liposomes were prepared by the thin layer evaporation method, using the widely used lipids DPPC:Chol:MPEG-2000-DPPE Na (molar ratio of 20:10:1). The multilamellar vesicles (MLV) were converted by sonication to small unilamellar vesicles (SUV)[45,46] to reduce *in vivo* potential opsonization[47,48]. The suspension was filtered through 200 nm filters, to obtain liposomes with a suitable diameter in order to avoid possible occlusion of capillaries *in vivo*[49]. The mean diameter and ζ-potential were measured by DLS (Table 2). The size of nanoparticles ranged between 105 nm and 232 nm (LP-2 and LP-4, respectively), with LP-1 and LP-3 being around 151 nm and 131 nm, respectively. The whole set of liposomes presented good values of ζ-potential (from −27.4 mV to −47.6 mV) and polidispersity index (from 0.2 to 0.4). These data suggested the stability of the final suspension. The concentration of drug (1–4) in each liposomal sample was determined by HPLC-UV-MS analysis, after the disruption of the liposomes. The entrapment efficacy was excellent: above 85% for LP-2, LP-3 and LP-4 and 65% for LP-1. The effects of sonication, temperature and lipid composition were analyzed to maximize the entrapment efficacy and to reduce the variability associated to the solubility of different compounds (Table S2).

Antiproliferative activity on human cell line SH-SY5Y. The cytotoxicity of nanoparticles (liposomes: LP-1, LP-2, LP-3, LP-4 and albumin: AL-4) was evaluated in SH-SY5Y NB cell line. Taking into account the data regarding albumin nanoparticles previously evaluated, the only sample with satisfactory values of ζ-potential, PDI and EE% values was AL-4. Consequently, it was selected to perform cellular assays in the human NB cell line SH-SY5Y. Pure compounds (DMSO solution), empty liposomes (0.9% NaCl solution, pH 7.4) and albumin (PBS solution, pH 7.4) were included as controls. IC_{50}s of these compounds were evaluated at 24, 48 and 72 h, for

Cpd/Formulation	IC_{50} 24 h (μM)	IC_{50} 48 h (μM)	IC_{50} 72 h (μM)
1	21.84 ± 1.70	16.5 ± 1.67	13.54 ± 2.00
LP-1	8.03 ± 0.59	7.14 ± 1.90	6.35 ± 1.44
2	12.6 ± 1.6	2.66 ± 0.015	2.28 ± 0.29
LP-2	6.80 ± 0.98	1.74 ± 0.31	0.94 ± 0.68
3	3.04 ± 0.09	2.65 ± 0.08	1.54 ± 1.07
LP-3	3.50 ± 0.17	1.52 ± 0.94	1.54 ± 0.79
4	13.64 ± 0.94	10.06 ± 0.50	8.63 ± 0.75
LP-4	3.87 ± 0.51	1.91 ± 1.46	1.90 ± 0.46
AL-4	20.04 ± 1.04	12.02 ± 0.97	12.03 ± 0.30

Table 3. Cytotoxicity in SH-SY5Y NB cells. SH-SY5Y cells were seeded at 10^5 cells/well density. The cultures were maintained at 37 °C in 5% v/v CO_2 for 24, 48 and 72 h. IC_{50}s were evaluated by Trypan blue assay and calculated by GraphPad Prism 6.0 software using the best fitting sigmoid curve.

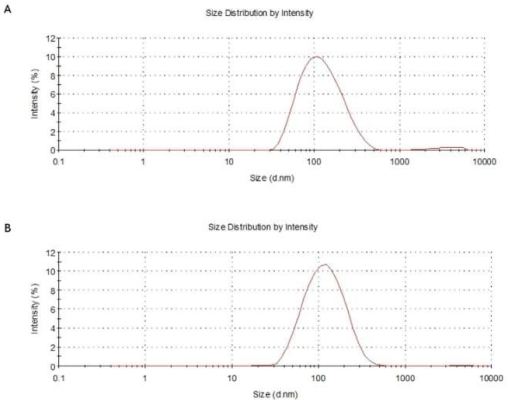

Figure 2. Characterization of size distribution by dynamic light scattering. (**A**) Empty liposomes; (**B**) LP-2.

different concentrations (0.1, 1.0, 10, 50 μM) (Table 3). A greater 24 h-activity was obtained for liposomal samples in comparison with their corresponding drugs. The only exception was pair 3/LP-3 (drug/LP-drug), whose analysis revealed a comparable cytotoxicity. Data collected after 48 h showed a reduced difference in cytotoxicity within each pair. The activity at 72 h was higher for liposomal samples (LP-1 and LP-4) in comparison with the respective free drug (1 and 4). Within the pairs 2/LP-2 and 3/LP-3, a comparable IC_{50} value between each drug and its respective liposomal formulation was found. IC_{50} (72 h) of AL-4 was 12.03 μM, further demonstrating the lower activity of albumin nanoparticles in comparison with the free drug 4 (IC_{50} = 8.63 μM) and the liposome LP-4 (IC_{50} = 1.90 μM).

Characterization of LP-2. As all the other liposomal nanoparticles, LP-2, was characterized by DLS to assess size and ζ-potential and by cellular assays (SH-SY5Y NB) to determine cytotoxicity (Tables 2 and 3). More in detail, Fig. 2 shows the different size distribution by intensity of unloaded liposomes (Fig. 2A) and liposomes loaded with 2 (Fig. 2B). The average size resulted smaller for the sample with encapsulated drug, 105.1 ± 6.39 nm (LP-2) versus 135.2 ± 9.45 nm (Empty LP). Empty liposomes were tested in SH-SY5Y NB cell line in order to exclude any possible cytotoxic activity (Fig. 3A). This was particularly important because, although DPPC and DPPE are widely used to produce liposomes, recent studies[50] demonstrated that saturated fatty acids might have a toxic effect in NB cells. In our assays, however, the obtained curve confirmed that liposomes do not influence significantly cell viability, indicating that the amount of saturated fatty acids derived from the liposomal preparation is not enough to determine a cytotoxic effect. LP-2 demonstrated an activity comparable with the one of compound 2 at 48 h (Fig. 3B). Additionally, the liposomal formulation at 72 h showed an enhanced cytotoxic effect (Fig. 3C). Subsequently, liposomal preparation LP-2 was morphologically analyzed by cryo-Electron Microscopy (cryo-EM) (Fig. 4). The result confirmed the presence of a homogeneous population of unilamellar nanoparticles with size around 100 nm. Liposomes were round, smooth and free from drug crystals; while bilamellar, multilamellar or giant-liposomes were not observed in the image from cryo-EM. The average thickness of the phospholipidic bilayer corresponded to 5.77 ± 1.05 nm (12 measurements performed by ImageJ Software, 1.46r).

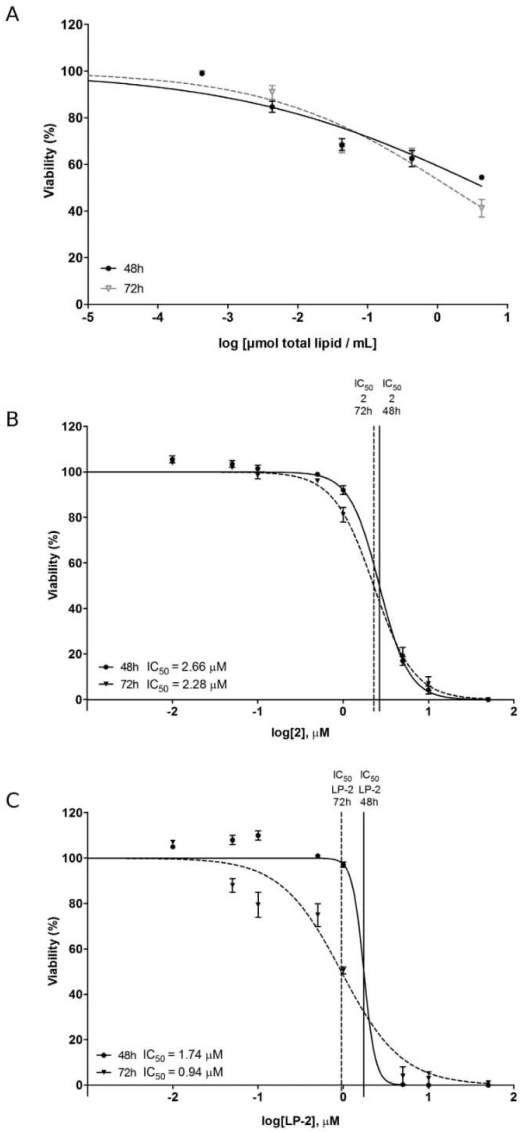

Figure 3. Viability of SH-SY5Y human NB cells evaluated at 48 and 72 h. (**A**) Empty liposomes, (**B**) Free compound 2 and (**C**) LP-2. Compound 2 and LP-2 were tested at the following concentrations: 0.01, 0.05, 0.1, 0.5, 1.0, 10 and 50 μM.

Delivery of liposomes in neuroblastoma cells. Neuroblastoma cells were incubated with normal and fluorescent liposomes to evaluate their possible uptake. Fluorescent liposomes were prepared incorporating a fluorescent phospholipid (NBD-DOPE) in the lipid mixture. After 4 h of incubation, fluorescent liposomes were internalized into neuroblastoma cells (Fig. 5A,B). Z-stack image confirmed the localization of NBD-labelled liposome inside SH-SY5Y cells (Figure S2).

***In vitro* release.** To determine the stability in physiological settings and to confirm the release of the drug 2 from its liposomal formulation LP-2, the release kinetics of 2 was analysed *in vitro* by measuring the concentration of drug released from liposomes into a physiological medium (BSA 50 mg/mL) at 37 °C (Fig. 6A). The cumulative percentage of drug release was determined over a 96 h-period. The results demonstrated the stability

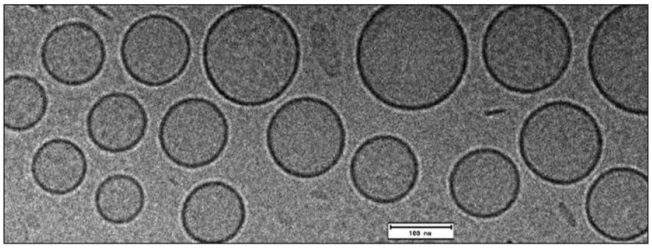

Figure 4. Characterization of LP-2: morphological analysis by Cryo-EM.

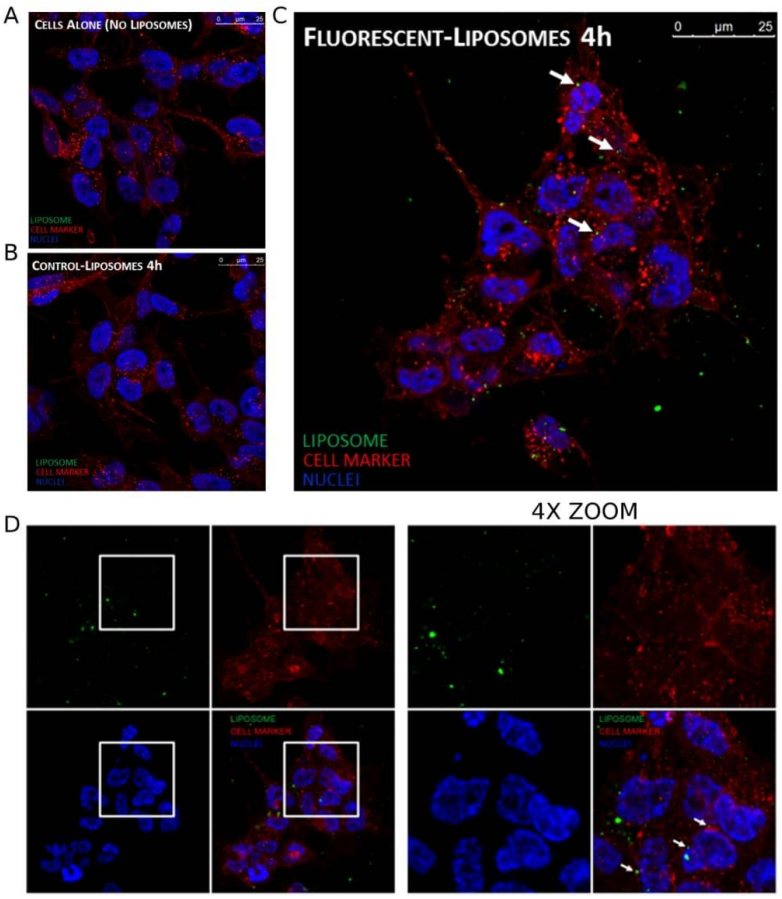

Figure 5. Confocal microscopy experiments. Neuroblastoma cells (SH-SY5Y) were seeded on glass coverslip and then incubated for 4 h with: (**A**) control, (**B**) normal liposomes, (**C**) fluorescent liposomes. Liposomes are visualized in green, cellular membranes in red and nuclei in blue. (**D**) Z-stack projection, on the right 4X zoom of the highlighted regions of the left panel.

of the sample in physiological conditions at 37 °C. In fact, the percentage of 2 released from LP-2 resulted below 28% after 24 h and 49% over a 72 h-period. The final percentage of drug released was of 50.5%. In addition, the rate of drug release was evaluated during the 24 h (0.96 µg/h).

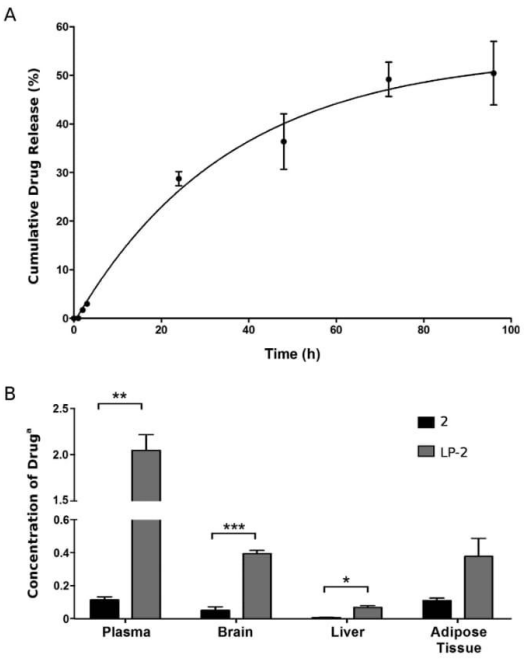

Figure 6. *In vitro* release and biodistribution at 24 h. (**A**) Release of compound 2 from liposomal system LP-2 in physiological conditions, with 50 mg/mL of BSA, at 37 °C. (**B**) Concentration of compound 2 determined in plasma, brain, liver and adipose tissue, after the administration of the free drug 2 (black) and the liposomal formulation LP-2 (grey). [a]The concentration is expressed as μg/mL for plasma and as μg/g for brain, liver and adipose tissue.

Biodistribution at 24 h. Biodistribution of LP-2 and free drug 2 were evaluated in male Sprague-Dawley rats. The concentration of compound 2 was determined after 24 h in the following tissues: plasma, brain, liver and adipose tissue (Fig. 6B). The concentration of the active compound was one order of magnitude higher in the plasma of rats treated with LP-2, validating the use of liposomes to enhance the plasma-exposure of a drug. In fact, the concentration of the free compound 2 was 0.11 μg/mL and 2.05 μg/mL in the groups treated with 2 and LP-2 respectively. The concentration of compound recovered in the brain was 0.05 μg/g (group treated with 2) versus 0.39 μg/g (group treated with LP-2). Again, the increase of quantity of compound 2 indicated the improved biodistribution of 2 when liposomes are used as drug delivery systems.

Discussion

With the aim determining if the use of albumin nanoparticles and liposomes could represent a possible strategy to improve pharmacokinetic properties of our compounds, four pyrazolo[3,4-*d*]pyrimidines (1–4), selected from our library of compounds, were encapsulate in these nanosystems. Pyrazolo[3,4-*d*]pyrimidines have demonstrated a high anticancer activity associated to the inhibition of tyrosine kinases c-Src and Bcr-Abl and we have recently demonstrated that pyrazolo[3,4-*d*]pyrimidines were able to reduce tumor growth in NB xenograft mouse model[25]. Thus, we have decided to focus on NB for this study. Compounds 1–4 were selected on the basis of previously reported data regarding activity and *in vitro* ADME properties[25–27]. Nanoparticles were characterized by DLS regarding their size, polydispersity index and ζ-potential. Particle size has a significant impact on the circulation time[51]. Furthermore, the dimensions of the smallest capillaries need to be taken into account to avoid a possible obstruction. Particle size also affects cellular uptake, influencing phagocytosis and endocytosis. In general, the larger is the nanoparticle, the faster is the clearance by the MPS. Optimal size to facilitate extravasation is about 150 nm or less, i.e. Doxil© has size between 80–100 nm and Myocet© is around 150 nm. In this context, this study demonstrated that our liposomes are suitable drug-delivery systems with a diameter that ranges from 105 nm to 232 nm. Another important feature for nanoparticle dispersion stability is the ζ-potential that indicates the degree of electrostatic repulsion between particles. In detail, nanoparticles with ζ-potential values greater than + 25 mV or less than −25 mV typically have high degrees of stability[44]. Showing a ζ-potential value between −28.65 mV and −48.00 mV, our liposome systems were confirmed to be stable.

On the other side, albumin systems were characterized by ζ-potentials and PDIs into the range of instability (values around −10 mV and close to 1, respectively). These data suggested that these nanoparticles might form

aggregates (hypothesis confirmed by DLS analysis and FESEM study). However, we decided to proceed with the evaluation of the cytotoxicity of the most promising albumin sample, namely AL-4.

Liposomes demonstrated greater 24 h-activity when compared with the appropriate free drug (comparable IC_{50}s of LP-3 and 3, represented the only exception). This difference in cytotoxicity might be related to different internalization processes. In fact, while the free drug can enter into cells by passive membrane transport, liposomes need to be taken up by different processes (i.e. endocytosis, fusion). At 48 h and 72 h, pairs LP-2/2 and LP-3/3 showed similar IC_{50}s. However, LP-1 and LP-4 demonstrated higher cytotoxicity than the respective free drug both, in 48 h and 72 h measurements. Cellular assays further demonstrated the unfavourable properties of albumin nanoparticles, as the IC_{50} value was higher than the ones obtained by testing free drug 4 and liposomes LP-4. Given their poor properties (PDI, ζ-potential, EE% and IC_{50}) albumin nanoparticles were not further characterized.

LP-2 resulted our most promising liposomal candidate because of the following: (I) IC_{50} value of 0.97 μM against NB cells, (II) 99% of entrapment efficiency, (III) ζ-potential value of -39.9 ± 0.55 mV and (IV) size of 105.1 ± 6.39 nm. Additionally, 2 was the compound previously tested in NB xenograft mouse model[25]. Thus, LP-2 was further characterized by cryo-EM, confirming the data obtained by DLS analysis. The sample was indeed characterized by a homogenous population of unilamellar liposomes with size around 100 nm. Furthermore, a confocal microscopy-based study was performed to elucidate whether the drug is released from liposomes outside the cells or inside the cytoplasm, after an internalization of the whole liposomal system. The analysis showed the presence of fluorescent liposomes into the cytoplasm of NB cells, suggesting a delivery of the free drug after cellular uptake of liposomes.

The release of compound 2 from the liposomal system LP-2 was evaluated with an *in vitro* assay that allowed the quantification of compound 2 likely to be released from liposomes into physiological conditions. The resulting monophasic release curve was a typical feature of unilamellar liposomes, accordingly with DLS and cryo-EM results. A proof of concept *in vivo* experiment was then performed to evaluate and compare the biodistribution of free compound 2 and liposomes LP-2 in several tissues, at 24 h. Additionally, this study was important to determine the *in vivo* stability of our liposomal systems. Data showed a generally improved biodistribution - higher concentration - of the drug 2 when liposomes were used as drug-delivery system. Considerably, when LP-2 was administered a 20-fold increase in plasma-concentration of free compound 2 was observed. In addition, the quantity of compound 2 recovered from the brain tissue after injection of LP-2 was significantly higher than the concentration obtained after administration of compound 2.

In conclusion, this study validated the use of stealth liposomes to improve the biodistribution of pyrazolo[3,4-*d*]pyrimidines. Herein we demonstrate that liposomes retain the efficacy of our encapsulated drug against SH-SY5Y NB cells and that this cytotoxic activity is likely to be exerted by the release of the active compound in the cytoplasm after uptake of the nanoparticles. Importantly, the liposomal system resulted stable and able to release the encapsulated drug in physiological conditions and the biodistribution assay finally proved the beneficial properties of LP-2. Further preclinical *in vivo* studies will allow the determination of the full pharmacokinetic profile and the therapeutic efficacy of this novel formulation.

Methods

Materials. Pyrazolo[3,4-*d*]pyrimidine compounds (1–4), were previously synthesized and characterized by our research group[25–27]. 1,2-Dipalmitoyl-*sn*-glycero-3-phosphocholine semisynthetic, ≥99% (DPPC), *N*-(carbonyl methoxypolyethylenglycol 2000)-1,2-dipalmitoyl-*sn*-glycero-3-phosphoethanolamine sodium salt (MPEG-2000-DPPE Na), 1,2-dioleoyl-sn-glycero-3-phosphoethanolamine,7-nitrobenzofurazan-labeled (NBD-DOPE), 4′,6-diamidino-2-phenylindole (DAPI), cholesterol (Chol), human serum albumin (HSA) (lyophilized, 97%), dialysis tubing cellulose membrane (cut-off 14 kDa), L-cysteine and and D,L-glyceraldehyde and all the solvents were purchased from Sigma Aldrich. Nylon syringe filters with pores of 0.2 μm (Acrodisc 13 mm Syringe Filter) and PTFE syringe filters with pores of 0.2 μm (Acrodisc 13 mm Syringe Filter) were from purchased VWR. High purity deionised water was obtained from milli-Q (Millipore, Milford, MA, USA). Wheat germ agglutinin, Alexa Fluor 647 Conjugate (WGA) was purchased from Life Technologies. Fetal Bovine Serum (FBS), Dulbecco's Modified Eagle Medium: Nutrient Mixture F-12 (DMEM/F12), L-glutamine (L-Glu) and Penicillin-Streptomycin (Pen/Strep) were purchased from Euroclone.

Preparation of albumin-drug nanoparticles. The albumin nanoparticles were prepared by mixing 100 μL of compound solution in EtOH (1 mg/mL) with 900 μL of HSA solution in PBS (pH 7.4, 25 mM) (5 mg/mL)[52]. Cysteine was added up to a final concentration of 5 mg/mL, and the resulting solution was kept at 37 °C, for 45 min. The excess of cysteine was eliminated by dialysis using a cellulose membrane (capacity 60 mL/ft, cut-off 14 kDa, diameter 16 mm, width 25mm). D,L-glyceraldehyde was added to this solution, to a final concentration of 5 μM[53]. The sample was then filtered through a nylon syringe filter with pores of 0.2 μm (Acrodisc 25 mm Syringe Filter) to obtain a sterile solution of the drug-albumin nanoparticles. The concentration of the compound in the final sample was determined by HPLC-UV-MS (HPLC-UV-MS method in the supporting material), after denaturation of the protein by acetonitrile and centrifugation (4500 rpm, 15 min, 4 °C).

Preparation of Liposome-drug nanoparticles. The method developed by A.D. Bangham, namely thin layer evaporation, was used for the preparation of LP-1, LP-2, LP-3 and LP-4. Lipids DPPC, Chol and MPEG-2000-DPPE Na (molar ratio 20:10:1) were dissolved in a mixture of $CHCl_3$:MeOH = 3:1 (3 mL, round-bottomed flask). A 1 mM solution of each compound (1, 2, 3, 4) in $CHCl_3$:MeOH = 3:1 was prepared. An aliquot was transferred in the lipid solution to obtain 500 μM as final concentration of compound. The solvent was removed under reduced pressure to obtain a thin layer of lipids (kept under high vacuum overnight). The thin layer was hydrated with a 0.9% NaCl solution and the mixture was stirred for 1 hour at a temperature higher than the Tm of the

lipids. The suspension was mixed (Vortex, 3 min) and SUV liposomes were formed by sonication for 20 min at room temperature. The solution was filtered with PTFE syringe filters with pores of 0.2 μm (Acrodisc 13 mm Syringe Filter), to eliminate liposomes with diameter over 200 nm and potentially precipitated drugs. The drug concentration was determined after disruption of liposomes by treatment with ethanol at 40 °C (1:1 = v/v). The compound was extracted and quantified by HPLC-UV-MS (HPLC-UV-MS method in the supporting material).

Measurements of size and ζ-potential. Size distribution and ζ-potential were determined by Dynamic Light Scattering (DLS) (Zeta Sizer Nano ZS90, Malvern Instruments Ltd, Malvern, UK). Measurements were performed directly after rehydration of the samples with 1 mM NaCl aqueous solution. Samples stability was evaluated by DLS after one week.

Antiproliferative activity on human cell line SH-SY5Y. *In vitro* experiments were carried out using the human NB cell line SH-SY5Y. Cells were purchased from American Type Culture Collection (ATCC, Manassas, VA, USA) and were cultured in DMEM/F12 1:1 medium supplemented with 10% FBS, 2 mM L-glutamine and 10000 units/mL Penicillin/Streptomycin at 37 °C in 5% CO_2 atmosphere. In order to determine the antiproliferative effect of drugs (1–4) and nanosystems, SH-SY5Y cells were seeded at 10^5 cells/well density and treated with albumin (PBS solution, pH 7.4) or empty liposomes (0.9% NaCl solution, pH 7.4), compounds encapsulated with albumin (PBS solution, pH 7.4) or liposomes LP-1, LP-3 and LP-4 (0.9% NaCl solution, pH 7.4) and free compounds 1, 3 and 4 (DMSO solution) at increasing concentrations (0.1 μM, 1.0 μM, 10 μM and 50 μM). IC_{50} determination for LP-2 and compound 2 was performed testing the following concentrations as well: 0.01 μM, 0.05 μM, 0.5 μM and 5 μM. The cultures were maintained at 37 °C in 5% v/v CO_2 for 24, 48 and 72 h. Cell number and viability were evaluated using the Bürker chamber, after treatment with Trypan Blue. IC_{50} was calculated by GraphPad Prism 6.0 software using the best fitting sigmoid curve.

Morphology study. Morphology was observed by Cryo Electron Microscopy. 3 μL of sample were applied on Quantifoil® holey carbon grids (copper Multi A, Quantifoil® Micro Tools GmbH, Jena, Germany). Excess fluid was blotted from the grid for 2 sec with Whatman filter paper and then plunge frozen in liquid ethane, using a plunge freezer, to achieve sample vitrification. Frozen samples were stored in liquid nitrogen until EM imaging. Vitrified samples were imaged using a CM200 FEG transmission EM (FEI, Eindhoven, the Netherlands) operated at 200 keV and equipped with a F224HD 2048 × 2048 CCD camera (TVIPS Gauting, Germany). EM images were acquired at 27,500× magnification (pixel size 0,602 nm) at −12, −18 μm defocus.

Confocal microscopy studies on the cellular uptake. For confocal microscopy experiments, fluorescent liposomes, carrying NBD-DOPE in the lipid bilayer, were used. DPPC, Chol and MPEG-2000-DPPE were dissolved at a molar ratio of 20:10:1, respectively, $CHCl_3$:MeOH = 3:1 v/v. Then, NBD-DOPE was added to the lipid mixture to a final molar ratio of 2% of total lipids. The lipid mixture was dried and placed in a vacuum desiccator for at least 24 h to ensure complete solvent removal. Finally, lipid film was rehydrated with NaCl 0.9% solution to obtain a NBD-DOPE final concentration of 440 μM. SH-SY5Y cells were maintained in DMEM/F12 1:1 medium supplemented with 10% FBS, 2 mM L-glutamine and 10000 units/mL Penicillin/Streptomycin at 37 °C in 5% CO_2 atmosphere. SH-SY5Y cells were plated on glass coverslip at a density of 20000 cells per well in 24-well plates. After 24 h, cells were incubated with liposome formulation, and then fixed in 4% paraformaldehyde in PBS for 20 min. Nuclei and cellular membranes were stained respectively with a 6 μM solution of DAPI and 2 μg/mL WGA Alexa Fluor 647 labelled for 10 min. Coverslips were mounted in fluorescence mounting medium (Dako, S3023). Samples were visualized on a TSC SP5 confocal microscope (Leica, 5100000750) installed on an inverted LEICA DMI 6000CS (10741320) microscope and equipped with an oil immersion Plan Apo 63 × 1.4 NA objective. Images were acquired using the LAS AF acquisition software (Leica, 10210). NBD fluorescence was acquired in 500–560 nm range and excited with 476 nm argon laser, DAPI was acquired in 420–480 nm range and excited with 405 nm UV laser and WGA was acquired in 650–730 nm range and excited with 633 nm laser.

***In vitro* release.** Rates of drug release were studied by dialyzing the nanosystem LP-2 (3.5 mL, 0.4 mM) against PBS (20 mL, pH 7.4, 10 mM) with 50 mg/mL of BSA (physiological plasma concentration). The entire system was stirred at 37 °C and samples (1 mL, from the PBS-BSA) were collected at different time points (0, 1, 2, 3, 24, 48, 72 and 96 h) (1 mL of PBS-BSA was added each time to maintain sink condition). Each sample was treated with 1 mL of ACN and centrifuged at 4000 rpm for 20 min. Then, the supernatant was recovered, concentrated under reduced pressure and analyzed to determine the concentration of compound 2 by HPLC-UV-MS (HPLC-UV-MS method in the supporting material).

***In vivo* plasmatic distribution.** Male Sprague Dawley rats (Charles River, Milan, Italy) were maintained according to ethical EEC regulations for animal research. The animal protocols used were reviewed and approved by the Animal Care and Ethics Committee of the University of Siena, Italy. The animals were anesthetized (*i.p.* xylazine hydrochloride, 10 mg/kg, Xilor, Bayer AG, and ketamine hydrochloride 35 mg/kg, Ketavet, Gellini) and treated by *i.v.* injection through the tail vein. The experiment was performed in triplicate. The two groups received intravenously LP-2 (500 μL, PBS, pH 7.4) or 2 (50 μL in DMSO), corresponding to a bolus of 10 mg/Kg. After 24 h, animals were sacrificed and blood and tissues were treated for the quantitative analysis. The blood, previously heparinized, was centrifuged at 4000 rpm for 20 min to separate the plasma fraction and then, 500 μL were collected in a test tube. Tissues were homogenized using a glass/glass Potter-Elvehjem homogenizer. For each sample 1 mL of ACN (in the presence of the internal standard 1-(2-chloro-2-(4-chlorophenyl)ethyl)-*N*-(3-fluorobenzyl)-1*H*-pyrazolo[3,4-*d*]pyrimidin-4-amine, 10 μM) was added to denature proteins and to extract 2. Samples were

centrifuged at 4000 rpm for 20 min; the supernatant was recovered, evaporated and analyzed by HPLC-UV-MS (HPLC-UV-MS method in the supporting material).

References

1. Hara, J. Development of treatment strategies for advanced neuroblastoma. *Int. J. Clin. Oncol.* **17,** 196–203 (2012).
2. Matthay, K. K. *et al.* Criteria for evaluation of disease extent by (123)I-metaiodobenzylguanidine scans in neuroblastoma: a report for the International Neuroblastoma Risk Group (INRG) task force. *Br. J. Cancer* **102,** 1319–1326 (2010).
3. Maris, J. M., Hogarty, M. D., Bagatell, R. & Cohn, S. L. Neuroblastoma. *Lancet* **369,** 2106–2120 (2007).
4. Arora, A. & Scholar, E. M. Role of tyrosine kinase inhibitors in cancer therapy. *J. Pharmacol. Exp. Ther.* **315,** 971–979 (2005).
5. Pytel, D., Sliwinski, T., Poplawski, T., Ferriola, D. & Majsterek, I. Tyrosine kinase blockers: new hope for successful cancer therapy. *Anticancer Agents Med. Chem.* **9,** 66–76 (2009).
6. Brunton, V. G. & Frame, M. C. Src and focal adhesion kinase as therapeutic targets in cancer. *Curr. Opin.Pharmacol.* **8,** 427–432 (2008).
7. Grant, S. & Dent, P. Kinase inhibitors and cytotoxic drug resistance. *Clin. Cancer Res.* **10,** 2205–2207 (2004).
8. Huang, H. *et al.* Discovery of novel purine derivatives with potent and selective inhibitory activity against c-Src tyrosine kinase. *Bioorg. Med. Chem.* **18,** 4615–4624 (2010).
9. Green, T. P. *et al.* N-(5-Chloro-1,3-benzodioxol-4-yl)-7-[2-(4-methylpiperazin-1-yl)ethoxy]-5-(tetrahydro-2H-pyran-4-yloxy) quinazolin-4-amine, a novel, highly selective, orally available, dual-specific c-Src/Abl kinase inhibitor. *J. Med. Chem.* **49,** 6465–6488 (2006).
10. Cao, X. *et al.* Design and synthesis of 7-alkoxy-4-heteroarylamino-3-quinolinecarbonitriles as dual inhibitors of c-Src kinase and nitric oxide synthase. *Bioorg. Med. Chem.* **16,** 5890–5898 (2008).
11. Palanki, M. S. *et al.* Development of novel benzotriazines for drug discovery. *Expert Opin. Drug Discov.* **4,** 33–49 (2009).
12. Das, J. *et al.* 2-Aminothiazole as a novel kinase inhibitor template. Structure-activity relationship studies toward the discovery of N-(2-chloro-6-methylphenyl)-2-[[6-[4-(2-hydroxyethyl)-1-piperazinyl)]-2-methyl-4-pyrimidinyl]amino)]-1,3 thiazole-5-carboxamide (dasatinib, BMS-354825) as a potent pan-Src kinase inhibitor. *J. Med. Chem.* **49,** 6819–6832 (2006).
13. Nam, H. *et al.* Antitumor activity of saracatinib (AZD0530), a c-Src/Abl Kinase Inhibitor, alone or in combination with chemotherapeutic agents in gastric cancer. *Mol. Cancer Ther.* **12,** 16–26 (2013).
14. Rassi, F. E. & Khoury, H. J. Bosutinib: a SRC-ABL tyrosine kinase inhibitor for treatment of chronic myeloid leukemia. *Pharmacogenomics Pers. Med.* **6,** 57–62 (2013).
15. Puls, L. N., Eadens, M. & Messersmith, W. Current Status of Src Inhibitors in Solid Tumor Malignancies. *The Oncologist* **16,** 566–578 (2011).
16. Bolen, J. B., Rosen, N. & Israel, M. A. Increased pp60c-src tyrosyl kinase activity in human neuroblastoma is associated with amino-terminal tyrosine phosphorylation of the src gene product. *Proc. Natl. Acad. Sci. USA* **82,** 7275–7279 (1985).
17. O'Shaughnessy, J., Deseau, V., Amini, S., Rosen, N. & Bolen, J. B. Analysis of the c-src gene product structure, abundance, and protein kinase activity in human neuroblastoma and glioblastoma cells. *Oncogene Res.* **2,** 1–18 (1987).
18. Bjelfman, C., Hedborg, F., Johansson, I., Nordenskjöld, M. & Påhlman, S. Expression of the neuronal form of pp60c-src in neuroblastoma in relation to clinical stage and prognosis. *Cancer Res.* **50,** 6908–6914 (1990).
19. Matsunaga, T. *et al.* Expression of n-myc and c-src proto-oncogenes correlating to the undifferentiated phenotype and prognosis of primary neuroblastomas. *Cancer Res.* **51,** 3148–3152 (1991).
20. Finlay, D. & Vuori, K. Novel noncatalytic role for caspase-8 in promoting SRC-mediated adhesion and Erk signaling in neuroblastoma cells. *Cancer Res.* **67,** 11704–11711 (2007).
21. Takahashi, H. & Simizu, B. Expression of alternatively spliced src messenger RNAs related to neuronal differentiation in human neuroblastomas. *Cancer Res.* **53,** 3179–3185 (1993).
22. Matsunaga, T. *et al.* Expression of neuronal Src mRNA as a favorable marker and inverse correlation to N-myc gene amplification in human neuroblastomas. *Int. J. Cancer* **58,** 793–798 (1994).
23. Hishiki, T. *et al.* Src kinase family inhibitor PP2 induces aggregation and detachment of neuroblastoma cells and inhibits cell growth in a PI3 kinase/Akt pathway-independent manner. *Pediatr. Surg. Int.* **27,** 225–230 (2011).
24. Vitali, R. *et al.* Activity of tyrosine kinase inhibitor dasatinib in neuroblastoma cells *in vitro* and in orthotopic mouse model. *Int. J. Cancer* **125,** 2547–2555 (2009).
25. Tintori, C. *et al.* Combining X-ray crystallography and molecular modeling toward the optimization of pyrazolo[3,4-*d*]pyrimidines as potent c-Src inhibitors active *in vivo* against neuroblastoma. *J. Med. Chem.* **58,** 347–361 (2015).
26. Navarra, M. *et al.* Antiproliferative and pro-apoptotic effects afforded by novel Src-kinase inhibitors in human neuroblastoma cells. *BMC Cancer* **10,** 602–614 (2010).
27. Radi, M. *et al.* Identification of potent c-Src inhibitors strongly affecting the proliferation of human neuroblastoma cells. *Bioorg. Med. Chem. Lett.* **21,** 5928–5933 (2011).
28. Radi, M. *et al.* Design, synthesis, and biological evaluation of pyrazolo[3,4-*d*]pyrimidines active *in vivo* on the Bcr-Abl T315I mutant. *J. Med. Chem.* **56,** 5382–5394 (2013).
29. Ceccherini, E. *et al.* SRC Family kinase inhibition through a new pyrazolo[3,4-*d*]pyrimidine derivative as a feasible approach for glioblastoma treatment. *J. Cell. Biochem.* **116,** 856–863 (2015).
30. Casini, N. *et al.* SRC family kinase (SFK) inhibition reduces rhabdomyosarcoma cell growth *in vitro* and *in vivo* and triggers p38 MAP kinase-mediated differentiation. *Oncotarget* **20,** 12421–12435 (2015).
31. Spreafico, A. *et al.* Antiproliferative and proapoptotic activities of new pyrazolo[3,4-d]pyrimidine derivative Src kinase inhibitors in human osteosarcoma cells. *FASEB J.* **22,** 1560–1571 (2008).
32. Angelucci, A. *et al.* Pyrazolo[3,4-*d*]pyrimidines c-Src inhibitors reduce epidermal growth factor-induced migration in prostate cancer cells. *Eur. J. Cancer* **42,** 2838–2845 (2006).
33. Schenone, S., Brullo, C., Musumeci, F. & Botta, M. Novel dual Src/Abl inhibitors for hematologic and solid malignancies. *Expert Opin. Invest. Drugs* **19,** 931–945 (2010).
34. Saha, R. N., Vasanthakumar, S., Bende, G. & Snehalatha, M. Nanoparticulate drug delivery systems for cancer chemotherapy. *Mol. Membr. Biol.* **27,** 215–231 (2010).
35. Kratz, F. Albumin as a drug carrier: design of prodrugs, drug conjugates and nanoparticles. *J. Control. Release* **132,** 171–183 (2008).
36. Elzoghby, A. O., Samy, W. M. & Elgindy, N. A. Albumin-based nanoparticles as potential controlled release drug delivery systems. *J. Control. Release* **157,** 168–182 (2012).
37. Kratz, F. A clinical update of using albumin as a drug vehicle - a commentary. *J. Control. Release* **190,** 331–336 (2014).
38. Allen, T. M. & Cullis, P. R. Liposomal drug delivery systems: from concept to clinical applications. *Adv. Drug Deliv. Rev.* **65,** 36–48 (2013).
39. Barenholz, Y. Doxil® –The first FDA-approved nano-drug: Lessons learned. *J. Control. Release* **160,** 117–134 (2012).
40. Dreassi, E. *et al.* 2-Hydroxypropyl-β-cyclodextrin strongly improves water solubility and anti-proliferative activity of pyrazolo[3,4-*d*]pyrimidines Src-Abl dual inhibitors. *Eur. J. Med. Chem.* **45,** 5958–5964 (2010).
41. Radi, M. *et al.* A combined targeted/phenotypic approach for the identification of new antiangiogenics agents active on a zebrafish model: from in silico screening to cyclodextrin formulation. *Bioorg. Med. Chem. Lett.* **22,** 5579–5583 (2012).

42. Vignaroli, G. *et al.* Exploring the chemical space around the privileged pyrazolo[3,4-*d*]pyrimidine scaffold: toward novel allosteric inhibitors of T315I-mutated Abl. *ACS Comb. Sci.* **16,** 168–175 (2014).
43. Vignaroli, G. *et al.* Pyrazolo[3,4-*d*]pyrimidine prodrugs: strategic optimization of the aqueous solubility of dual Src/Abl inhibitors. *ACS Med. Chem. Lett.* **4,** 622–626 (2013).
44. Gregoriadis, G. *et al.* Vaccine entrapment in liposomes. *Methods.* **19,** 156–162 (1999).
45. Lapinski, M. M., Castro-Forero, A., Greiner, A. J., Ofoli, R. Y. & Blanchard, G. J. Comparison of liposomes formed by sonication and extrusion: rotational and translational diffusion of an embedded chromophore. *Langmuir* **23,** 11677–11683 (2007).
46. Cho, N. J., Hwang, L. Y., Solandt, J. J. R. & Frank, C. W. Comparison of extruded and sonicated vesicles for planar bilayer self-assembly. *Materials* **6,** 3294–3308 (2013).
47. Moghimi, S. M. & Szebeni, J. Stealth liposomes and long circulating nanoparticles: critical issues in pharmacokinetics, opsonization and protein-binding properties. *Prog. Lipid Res.* **42,** 463–478 (2003).
48. Yan, X., Scherphof, G. L. & Kamps, J. A. Liposome opsonization. *J. Liposome Res.* **15,** 109–139 (2005).
49. Hallmark, B. *et al.* Observation and modelling of capillary flow occlusion resulting from the capture of superparamagnetic nanoparticles in a magnetic field. *Chem. Eng. Sci.* **63,** 3960–3965 (2008).
50. Bolognesi, A., Chatgilialoglu, A., Polito, L. & Ferreri, C. Membrane lipidome reorganization correlates with the fate of neuroblastoma cells supplemented with fatty acids. *PLoS One* **8,** e55537 (2013).
51. Laverman, P. *et al.* Liposomes for scintigrafic detection of infection and inflammation. *Adv. Drug Deliv. Rev.* **37,** 225–235 (1999).
52. Jiang, L. *et al.* A nontoxic disulfide bond reducing method for lipophilic drug-loaded albumin nanoparticle preparation: formation dynamics, influencing factors and formation mechanisms investigation. *Int. J. Pharm.* **443,** 80–86 (2013).
53. Vandelli, M. A., Rivasi, F., Guerra, P., Forni, F. & Arletti, R. Gelatin microspheres crosslinked with D,L-glyceraldehyde as a potential drug delivery system: preparation, characterisation, *in vitro* and *in vivo* studies. *Int J Pharm.* **215,** 175–184 (2001).

Acknowledgements

The authors would like to thank Prof. Gianni Pozzi and Dr. Francesco Santoro (Dipartimento di Biotecnologie Mediche, Università degli Studi di Siena, Italy) for Dynamic Light Scattering experiments, Prof. Pietro Lupetti (Dipartimento di Scienze della Vita, Università degli Studi di Siena, Italy) for Cryo EM experiments.

Author Contributions

P.C. and D.C. cellular and confocal microscopy studies; C.Z., F.C. and M.T. nanoparticles preparation and characterization; G.I., G.V. and S.S. synthesis and characterization of compounds; G.V., C.Z., D.C., E.D., M.V., S.S., M.C. and M.B. design of methods and experiments, analysis and interpretation of data; G.V., P.C., C.Z., D.C. and M.B. preparation of the manuscript. All authors have approved the final version of manuscript.

Additional Information

Supplementary information accompanies this paper at http://www.nature.com/srep

Competing financial interests: The authors declare no competing financial interests.

How to cite this article: Vignaroli, G. *et al.* Improvement of pyrazolo[3,4-*d*]pyrimidines pharmacokinetic properties: nanosystem approaches for drug delivery. *Sci. Rep.* **6**, 21509; doi: 10.1038/srep21509 (2016).

SECTION 3

‘PRODRUGS OF PYRAZOLO[3,4-*d*]PYRIMIDINES: FROM LIBRARY SYNTHESIS TO EVALUATION AS POTENTIAL ANTICANCER AGENTS IN AN ORTHOTOPIC GLIOBLASTOMA MODEL’

Submitted to ‘Journal of Medicinal Chemistry’ on 01-Dec-2016

PRODRUGS OF PYRAZOLO[3,4-*d*]PYRIMIDINES: FROM LIBRARY SYNTHESIS TO EVALUATION AS POTENTIAL ANTICANCER AGENTS IN AN ORTHOTOPIC GLIOBLASTOMA MODEL

Giulia Vignaroli,[†,‖] Giulia Iovenitti,[†,‖] Federica Coniglio,[†,‖] Claudio Zamperini,[†,‖] Pierpaolo Calandro,[†] Alessio Molinari,[†] Andrea Sartucci,[†] Alessia Calgani,[‡] David Colecchia,[¥] Andrea Mancini,[‡] Claudio Festuccia,[‡] Elena Dreassi,[†] Massimo Valoti,[†] Francesca Musumeci,[§] Silvia Schenone,[§] Mario Chiariello,[¥] Adriano Angelucci,[‡] Maurizio Botta,[†,‖,ᵎ]

[†]Dipartimento di Biotecnologie, Chimica e Farmacia, Università degli Studi di Siena, Via Aldo Moro 2, 53100 Siena, Italy

[‖]Lead Discovery Siena S.r.l., via Vittorio Alfieri 31, 53019, Castelnuovo Berardenga, Siena (IT)

[¥]Consiglio Nazionale delle Ricerche, Istituto di Fisiologia Clinica and Istituto Toscano Tumori, Core Research Laboratory, Via Fiorentina 1, 53100, Siena (IT)

[§]Dipartimento di Scienze Farmaceutiche, Università degli Studi di Genova, Viale Benedetto XV 3, 16132 Genova, Italy

[‡]Dipartimento di Scienze Cliniche Applicate e Biotecnologiche, Università dell'Aquila, Via Vetoio, 67100 Coppito, L'Aquila, Italy.

[ᵎ]Sbarro Institute for Cancer Research and Molecular Medicine, Center for Biotechnology, College of Science and Technology, Temple University, BioLife Science Building, Suite 333, 1900 N 12th Street, Philadelphia, Pennsylvania 19122

Submitted to Journal of Medicinal Chemistry on 30-Nov-2016

ABSTRACT

Pyrazolo[3,4-*d*]pyrimidines have previously shown interesting antitumor activity towards several cancer cells such as leukemia, glioblastoma, neuroblastoma and osteosarcoma cell lines. The efficacy of these compounds has been demonstrated by enzymatic, cellular and *in vivo* assays. To date, The library of pyrazolo[3,4-*d*]pyrimidines synthesized to date by our research group consists of more than 400 members. The good antitumor activities of these compounds are usually

associated with low aqueous solubility, a property that might hinder their further development. Herein, to prove whether the preparation of prodrugs represents a valid approach to enhance aqueous solubility and possibly pharmacokinetic properties, a set of pyrazolo[3,4-*d*]pyrimidine prodrugs was synthesized and characterized. Firstly, to synthesize the full set of prodrugs a versatile one-pot two-step procedure was set up. Next, the plasma half-life, the ability to overcome biological membranes, metabolic stability as well as water solubility were analysed. Further, the ability of inhibiting the tyrosine kinases, which represent the target of the parental drugs, and the cytotoxicity against human glioblastoma U87 cell line were evaluated. As final *in vivo* proof of concept, the pharmacokinetic properties and antitumor efficacy of the most suitable and promising pair of drug and prodrug were studied and compared.

INTRODUCTION

During the last years, several pyrazolo[3,4-*d*]pyrimidine derivatives have been studied and synthesized by our research group. To date, our pyrazolo[3,4-*d*]pyrimidine library consists of more than 400 members, developed mostly as ATP-competitive tyrosine kinase inhibitors.[1] The SRC kinases are key molecular targets in cancer therapy; their family includes the nine non-receptor tyrosine kinases Src, Yes, Fyn, Hck, Lyn, Blk, Fgr, Lck and Frk. These kinases are activated or overexpressed in many cancer types and are involved in the regulation of cell proliferation, survival, invasion and angiogenesis, thus playing a crucial role in tumor development and progression.[2]

The anticancer activity of pyrazolo[3,4-*d*]pyrimidines was confirmed in several cancer cell lines, both from solid tumors (i.e. osteosarcoma SaOS-2,[3] prostate PC3,[4] neuroblastoma SH-SY5Y,[5-6] glioblastoma U87,[7-8] rabdomyosarcoma[9], mesothelioma[10], medulloblastoma[11], medullary thyroid carcinoma[12]) and leukemia (i.e. 32D-p210 and 32D-T315I) [13] and Burkitt lymphomas.[14] *In vivo* data,

generated in subcutaneous xenograft mouse models further supported the antitumor activities of several pyrazolo[3,4-*d*]pyrimidines against leukemia (32D-p210 and 32D-T315I),[13] neuroblastoma (SH-SY5Y),[5] and glioblastoma (U87).[8] With regards to glioblastoma (GBM), targeting of the activated Src might play an important role in reducing the high proliferation and invasion capacity that characterizes this tumor. GBM is the most frequent primary brain tumor in adults and still poses clinical challenges since the available therapeutic choices, including surgical resection, followed by concomitant radiotherapy and temozolomide therapy, do not significantly improve the prognosis.[15] Targeted therapy might offer new opportunities, but to date it is facing two important issues: the selection of the most adequate molecular target and the low drug delivery to the brain.[16] In our recent study, a selected pyrazolo[3,4-*d*]pyrimidine was able to increase the survival time of treated mice in a GBM (U87 cells) orthotopic model by 30%, with respect to the vehicle-treated mice.[8] Despite their promising biological activity, pyrazolo[3,4-*d*]pyrimidines have low aqueous solubility, a property that could interfere with the development of these compounds to become drug candidates.[17-18] In this context, early assessment of pharmaceutical properties such as solubility, metabolic stability and permeability has become a key step in the drug discovery process,[19] as it is estimated that around 40% of potential drug candidates fail to reach the market due to poor physicochemical properties.[20-21] Accordingly, the development of potential alternative strategies to improve properties like solubility, tissue distribution, efficacy and toxicity should be considered in the very early stages of preclinical development.

In this view, together with the optimization of the biological activity of these compounds we are studying several strategies to improve their aqueous solubility and pharmacokinetic properties (i.e. prodrugs,[22] cyclodextrins,[17] albumin nanoparticles,[23] liposomes [23]).

As for the prodrug approach,[24-25] we recently reported that (I) the secondary amino group at C4 of the pyrazolo[3,4-*d*]pyrimidine nucleus was the most suitable position to connect with the prodrug

moiety, (II) the *N*-methylpiperazino group was effective in increasing the water solubility of the resulting prodrugs in comparison to the parent drugs and, (III) the *O*-alkyl carbamate was a suitable *in vivo*-hydrolysable linker to connect the secondary amino group at C4 with the solubilizing entity.[22]

Based on these data, in the current study we advanced the development of pyrazolo[3,4-*d*]pyrimidine prodrugs as a valid approach to overcome the low water solubility of this class of compounds. The study started with the optimization of the previously reported chemical synthesis. The resulting one-pot, two-step procedure was efficiently applied to nine selected pyrazolo[3,4-*d*]pyrimidine parent drugs (**1-9**) presenting different chemical moieties.[5,13,26-29] To further demonstrate the versatility of the chemical approach, a series of prodrugs (**9a-9e**) with increased steric bulk on the prodrug moiety was synthesized. All the synthesized compounds were characterized for their water solubility, stability in polar media, apparent permeability (PAMPA) as well as metabolic stability (with Human Liver Microsomes, HLM) and plasma hydrolysis.

Then the most interesting prodrugs were tested in a cellular assay with human GBM U87 cell line to assess their biological activity as well as the kinetics of uptake and hydrolysis in a cellular setting. As *in vivo* proof of concept, the pharmacokinetics of the most promising pair of drug and prodrug were studied, followed by the analysis of their pharmacological activities in an orthotopic mouse model of GBM.

RESULTS

Synthesis

One aim of this study was to define the most versatile chemical approach for the synthesis of prodrugs starting from different pyrazolo[3,4-*d*]pyrimidines. The synthesis of prodrugs (**1a-8a** and **9a-e**) was performed applying a one-pot, two-step procedure, starting from the appropriate drug

(**1-9**),[5,13,26-29] which by reaction with trisphosgene generated the carbonyl-chloride intermediate on the secondary amine at C4. The displacement of the chlorine using the appropriate alcohol afforded the final products **1a-8a** and **9a-e**, with overall yields ranging from 25 to 85% (Scheme 1 and 2).

Scheme 1. Synthesis of Prodrugs 1a-8a[a]

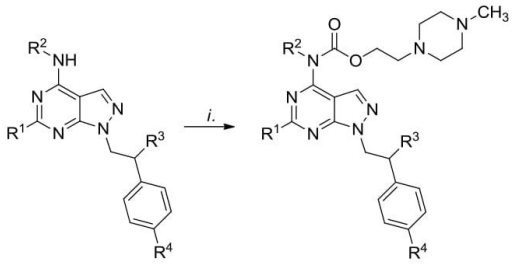

1, 1a: R^1 = H; R^2 = $CH_2C_6H_5$; R^3 = Cl; R^4 = H
2, 2a: R^1 = H; R^2 = $CH_2C_6H_4o$Cl; R^3 = Cl; R^4 = Br
3, 3a: R^1 = SCH_3; R^2 = C_6H_4mCl; R^3 = H; R^4 = H
4, 4a: R^1 = $SCH_2CH_2$4-morpholin; R^2 = C_6H_4mBr; R^3 = Cl; R^4 = H
5, 5a: R^1 = SCH_3; R^2 = $CH_2CH_2C_6H_5$; R^3 = Cl; R^4 = H
6, 6a: R^1 = H; R^2 = C_6H_5; R^3 = Cl; R^4 = Br
7, 7a: R^1 = SCH_3; R^2 = C_6H_4mCl; R^3 = Cl; R^4 = H
8, 8a: R^1 = SCH_2CH_3; R^2 = *n*Bu; R^3 = Cl; R^4 = H

[a]Reagents and Conditions: *i.* triphosgene, $NaHCO_3$, DCM; 3 h, 0 °C to r.t., then 2-(4-methylpiperazin-1-yl)ethanol (**12**) in DCM, r.t. 16 h.

For compounds **1a-8a** the appropriate derivative was reacted with 2-(4-methylpiperazin-1-yl)ethanol (**12**). Alcohol **12** was prepared by nucleophilic substitution of the bromine of 1-bromo-2-ethanol (**10**) with *N*-methylpiperazine (Scheme 3, A). Compounds **1-8** were dissolved in DCM and reacted with triphosgene in the presence of an excess of sodium bicarbonate. The reaction was monitored by TLC and as soon as the starting material disappeared, a solution of the alcohol **12** in DCM was added. The reaction mixture was then stirred at room temperature overnight. Prodrugs **9a-9e** were prepared starting from compound **9**, applying the same synthetic approach but using different alcohols (**12**, **13** and **17-19**) (Scheme 2). Prodrugs **9a-9e** were synthesized in order to have a series of derivatives with increasing steric hindrance close to the carbamate prodrug moiety. Prodrugs **9a-9e** show H, Me, Et, Ph and Bn at the C1 position of the prodrug moiety.

Scheme 2. Synthesis of Prodrugs 9a-e[a]

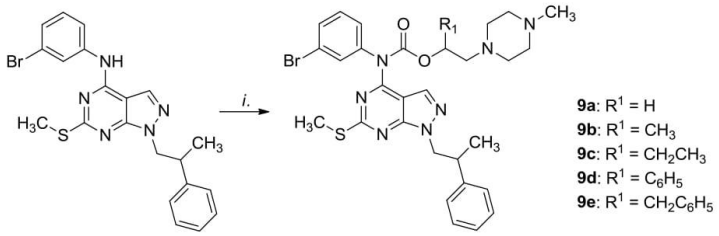

9 **9a-9e**

[a]Reagents and Conditions: *i*. triphosgene, $NaHCO_3$, DCM; 3 h, 0 °C to r.t., then 2-(4-methylpiperazin-1-yl)CH_2CHR^1OH (R^1=H, **12** or R^1=CH_3, **13** or R^1=CH_2CH_3, **17** or R^1=C_6H_5, **18** or R^1=$CH_2C_6H_5$, **19**) in DCM, r.t. 16 h.

Alcohol **13** was synthesized similarly to compound **12** starting from 1-bromo-2-propanol (**11**), whereas alcohols **17** and **18** were prepared from reaction of *N*-methylpiperazine with different epoxides, 1,2-epoxybutane (**14**) and styrene oxide (**15**), respectively.[30,31] Lastly, compound **19** was synthesized starting from 2-benzyloxirane (**15**) using zinc chloride and *N*-methylpiperazine.

Scheme 3. Synthesis of Alcohols 12,13 and 17-19[a]

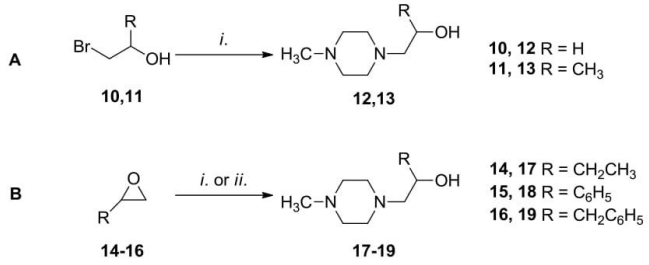

[a]Reagents and Conditions: for compounds **12,13** and **17,18** *i*. *N*-methylpiperazine, K_2CO_3, toluene, 12 h; for compound **19** *ii*. *N*-methylpiperazine, $ZnCl_2$, ACN_{dry}, reflux, 12 h

The synthetic approach here reported was suitable for pyrazolo[3,4-*d*]pyrimidines bearing different chemical features. For instance, the C4 position, which is directly involved in the prodrug-carbamate formation, presented alkyl (**8**), phenyl (**3**, **6**, **7** and **9**), benzyl (**1** and **2**) as well as phenylethyl groups (**5**). In the previously reported synthetic approach triphosgene and sodium

bicarbonate were used to form the carbamic-chloride intermediate that, after isolation, was reacted with 2-(4-methylpiperazin-1-yl)ethanol (**12**) using sodium hydride as base.[22] The new strategy is carried out as a one-pot, two-step procedure, using sodium bicarbonate as the only base. In this way, the time consuming and delicate isolation of the unstable carbamic-chloride intermediate is avoided, with an increase of the resulting yields. In fact, the synthesis of **9a** by the first approach resulted in a yield of 18%, whereas the new synthesis produced a 30% yield of the final prodrug.

***In vitro* ADME**

Several *in vitro* assays were performed to evaluate the ADME properties of the synthesized prodrugs (**1a-8a** and **9a-9e**) and to compare them to their parent drugs (**1-9**). Initially, the stability in several media [phosphate saline buffer (PBS), methanol (MeOH) and human plasma (Plasma)] was studied (Table 1). Next, the aqueous solubility and the apparent permeability (PAMPA) towards gastrointestinal membrane (GI) and blood brain barrier (BBB) were investigated, as well as the stability in the presence of human liver microsomes (HLM) (Table 2).

Table 1. Stability of prodrugs 1a-8a, 9a-9e in phosphate saline buffer (PBS), methanol (MeOH) and human plasma (Plasma)[a]

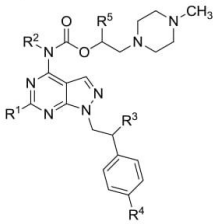

Cpd	R^1	R^2	R^3	R^4	R^5	PBS $t_{1/2}$ (h)	MeOH $t_{1/2}$ (h)	Plasma $t_{1/2}$ (h)
1a	H	$CH_2C_6H_5$	Cl	H	H	>48	>48	64.4
2a	H	$CH_2C_6H_4o$Cl	Cl	Br	H	>48	>48	75.0
3a	SCH_3	C_6H_4mCl	H	H	H	>48	>48	3.13
4a	$SCH_2CH_2$4-morpholino	C_6H_4mBr	Cl	H	H	>48	>48	3.48
5a	SCH_3	$CH_2CH_2C_6H_5$	Cl	H	H	>48	>48	45.2

6a	H	C_6H_5	Cl	Br	H	>48	>48	5.68
7a	SCH_3	C_6H_4mCl	Cl	H	H	>48	>48	3.71
8a	SCH_2CH_3	*n*Bu	Cl	H	H	1.0	2.0	0.46
9a	SCH_3	C_6H_4mBr	CH_3	H	H	>48	>48	3.21
9b	SCH_3	C_6H_4mBr	CH_3	H	CH_3	>48	>48	10.4
9c	SCH_3	C_6H_4mBr	CH_3	H	CH_2CH_3	>48	>48	11.3
9d	SCH_3	C_6H_4mBr	CH_3	H	C_6H_5	<0.25	<0.25	ND[b]
9e	SCH_3	C_6H_4mBr	CH_3	H	$CH_2C_6H_5$	>48	>48	40.0

[a]Determined by UV/LC-MS, $t_{1/2} = ln\ 2/K_{obs}$. Concentration of each compound 500 µM. [b]Not Determined.

Stability in polar media such as methanol and PBS was analyzed by UV/LC-MS, after dissolving the compound in the appropriate media. Resulting half-lives were greater than 48 h for prodrugs **1a-7a**, **9a-c** and **9e** (Table 1). These values indicated the good stability of these compounds, which were thus regarded as chemically stable for the subsequent studies. On the other hand, prodrugs **8a**[17] and **9d**, showed low stability in the polar media tested (Table 1). This high rate of hydrolysis is the reason why these compounds could not be tested for their aqueous solubility, the ability to overcome membranes as well as their metabolic stability. For **9d**, even the plasma hydrolysis could not be analyzed as it demonstrated a half-life less than 15 min in PBS and methanol.

A key property to be evaluated was the rate of plasma hydrolysis. In fact, our prodrugs display an *O*-alkyl-carbamate linker that should undergo *in vivo* hydrolysis in order to release the active compound. Prodrugs **1a-8a** and **9a-9e** were incubated in human plasma at 37 °C, and their disappearance, together with the formation of the respective drugs **1-9**, was monitored by UV/LC-MS (Table 1). Prodrugs with a plasma half-life higher than 40 h were **1a** ($t_{1/2}$ = 64.4 h), **2a** ($t_{1/2}$ = 75.0 h), **5a** ($t_{1/2}$ = 45.2 h) and **9e** ($t_{1/2}$ = 40.0 h). These compounds (**1a**, **2a**, **5a** and **9e**) present a common chemical feature: a phenyl ring spaced by one or two methylene groups from the carbamate group. In fact, prodrugs **1a**, **2a** and **5a** show a benzyl or phenethyl amine in the C4 position of the pyrazolo[3,4-*d*]pyrimidine nucleus, whereas prodrug **9e** has a benzyl group at the

C1 position of the *O*-alkyl-carbamate prodrug moiety. Prodrugs **9b** and **9c**, with a methyl and ethyl group at the C1 position of the *O*-alkyl-carbamate moiety, showed half-lives of 10.4 h and 11.3 h, respectively, whereas compounds **3a**, **4a**, **6a**, **7a** and **9a**[22] displayed plasma half-lives lower than 6 h ($t_{1/2}$ of 3.13 h, 3.48 h, 5.68 h, 3.71 h and 3.21 h, respectively). Also these compounds (**3a**, **4a**, **6a**, **7a** and **9a**) share a common chemical feature: a substituted aniline in the C4 position and a basic *O*-alkyl-carbamate group. For compound **8a**, the plasma half-life confirmed the data obtained by stability assays, highlighting that the contribution of solvent-mediated hydrolysis in the cleavage of this prodrug cannot be ignored. Subsequently, the passive membrane permeability was evaluated performing two different PAMPA assays, one reproducing the GI membrane, the other the BBB (Table 2). Prodrugs **1a**, **2a**, **4a** and **5a** demonstrated an apparent permeability lower than their respective drug (**1**, **2**, **4** and **5**) towards GI membrane and BBB. On the contrary, compounds **3a**, **7a**, and **9a-c** and **9e** showed an improved ability of overcoming these artificial membranes. Pair **6-6a** exhibited a mixed behaviour with prodrug **6a** showing enhanced permeability towards GI membrane but minor towards BBB, in comparison with drug **6**. Prodrug **8a** and **9d**, as previously mentioned, could not be tested due to their limited stability in polar media. To study CYP-metabolism, compounds **1a, 4a** and **9a** were incubated for one hour at 37 °C with a solution of man-pooled HLM. After this time, the percentage of prodrugs and metabolites was determined by HPLC–MS analysis. The percentage of unmodified prodrug recovered after the incubation was 86.4% for compound **1a**, 93.6% for **4a** and 99.9% for **9a**, suggesting that these compounds are not a direct substrate of CYP enzymes (Table 2). The parent drugs were previously reported as metabolic stable (metabolic stability higher than 78.3%). Interestingly, the pattern of metabolites generated from prodrugs was similar to the one obtained from the respective drugs, results that further support the hypothesis that the prodrug linker is not a substrate of CYP-metabolism (see supporting information for further details).

Table 2. Apparent permeability, aqueous solubility and metabolic stability of parent compounds 1-9 and prodrugs 1a-8a, 9a-9e[a]

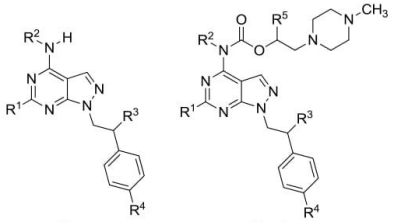

Drug I

Prodrug II

Cpd	R^1	R^2	R^3	R^4	R^5	GI[b] P_{app} (10^{-6} cm·sec^{-1})	BBB[c] P_{app} (10^{-6} cm·sec^{-1})	H_2O Sol. μg·mL^{-1}	Metabolic Stab.[d] %
1	H	$CH_2C_6H_5$	Cl	H	-	11.08	16.5	0.70	78.3
1a	H	$CH_2C_6H_5$	Cl	H	H	6.70	5.01	18.81	86.4
2	H	$CH_2C_6H_4o$Cl	Cl	Br	-	8.78	13.23	<0.01	95.2
2a	H	$CH_2C_6H_4o$Cl	Cl	Br	H	2.38	1.92	1.95	ND[e]
3	SCH_3	C_6H_4mCl	H	H	-	0.25	1.48	0.12	99.0
3a	SCH_3	C_6H_4mCl	H	H	H	4.69	4.30	6.32	ND[e]
4	$SCH_2CH_2$4-morpholino	C_6H_4mBr	Cl	H	-	5.27	7.10	3.70	97.2
4a	$SCH_2CH_2$4-morpholino	C_6H_4mBr	Cl	H	H	2.13	2.91	8.70	93.6
5	SCH_3	$CH_2CH_2C_6H_5$	Cl	H	-	7.40	6.17	0.07	96.2
5a	SCH_3	$CH_2CH_2C_6H_5$	Cl	H	H	0.85	0.01	106.97	ND[e]
6	H	C_6H_5	Cl	Br	-	6.64	13.10	0.06	96.4
6a	H	C_6H_5	Cl	Br	H	9.91	6.97	41.56	ND[e]
7	SCH_3	C_6H_4mCl	Cl	H	-	0.26	3.14	0.13	91.1
7a	SCH_3	C_6H_4mCl	Cl	H	H	4.95	4.14	4.22	ND[e]
8	SCH_2CH_3	*n*Bu	Cl	H	-	5.99	9.99	0.05	91.5
9	SCH_3	C_6H_4mBr	CH_3	H	-	0.01	0.50	0.01	95.1
9a	SCH_3	C_6H_4mBr	CH_3	H	H	2.11	1.89	6.47	99.9
9b	SCH_3	C_6H_4mBr	CH_3	H	CH_3	2.15	2.39	3.40	ND[e]
9c	SCH_3	C_6H_4mBr	CH_3	H	CH_2CH_3	1.45	0.93	1.96	ND[e]
9e	SCH_3	C_6H_4mBr	CH_3	H	$CH_2C_6H_5$	2.32	1.01	0.99	ND[e]

[a]Determined by UV/LC-MS See experimental section for details. [b]Gastro-Intestinal Parallel Artificial Membrane Permeability Assay. [c]Blood Brain Barrier Parallel Artificial Membrane Permeability Assay. [d]Expressed as percentage of unmodified drug. [e]Not Determined.

***In vitro* biological assays**

Parent drugs **1**, **4**, **6** and **9**, were previously reported and studied for their activity against c-Src and c-Abl. [5,13] Herein, a cell-free assay was performed to determine k_i values of selected prodrugs (**4a**, **9a**, **9b** and **9e**) and to monitor the potential inhibitory activity of these compounds before *in vivo* hydrolysis (see supporting info for method details). The results of the enzymatic assays showed that prodrugs were not able to inhibit directly c-Src and c-Abl at the concentrations tested (below 100 µM). These data support the hypothesis that prodrugs have a limited intrinsic inhibitory activity (Table 3).

Table 3. Biological data: enzymatic and cellular assays

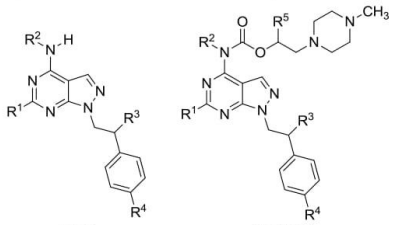

Cpd	R^1	R^2	R^3	R^4	R^5	Src (Ki µM)	Abl (Ki µM)	U87 IC_{50} µM 24h	U87 IC_{50} µM 48h	U87 IC_{50} µM 72h
1	H	$CH_2C_6H_5$	Cl	H	-	3.0	0.37	14.6 ± 1.3	4.9 ± 1.2	2.9 ± 1.1
1a	H	$CH_2C_6H_5$	Cl	H	H	ND[b]	ND[b]	18.6 ± 1.2	15.2 ± 1.1	15.0 ± 1.2
4	$SCH_2CH_2$4-morpholine	C_6H_4mBr	Cl	H	-	0.13	0.12	17.3 ± 1.7	6.8 ± 2.8	1.9 ± 1.2
4a	$SCH_2CH_2$4-morpholine	C_6H_4mBr	Cl	H	H	>100	>100	7.5 ± 1.4	5.2 ± 1.9	1.8 ± 1.8
6	H	C_6H_5	Cl	Br	-	0.06	0.61	25.3 ± 1.8	17.3 ± 1.9	14 ± 1.9
6a	H	C_6H_5	Cl	Br	H	ND[b]	ND[b]	8.2 ± 1.7	5.1 ± 1.5	2.0 ± 1.4
7	SCH_3	C_6H_4mCl	Cl	H	-	0.72	0.6	21.8 ± 1.9	17.2 ± 1.7	12.5 ± 1.7
7a	SCH_3	C_6H_4mCl	Cl	H	H	ND[b]	ND[b]	11.5 ± 1.2	7.9 ± 1.3	2.54 ± 1.3
9	SCH_3	C_6H_4mBr	CH_3	H	-	0.02	1.07	16.2 ± 1.2	2.3 ± 1.3	1.5 ± 1.1
9a	SCH_3	C_6H_4mBr	CH_3	H	H	>100	>100	7.3 ± 1.5	2.2 ± 1.1	1.57 ± 1.2
9b	SCH_3	C_6H_4mBr	CH_3	H	CH_3	>100	>100	7.4 ± 1.9	4.5 ± 1.7	1.8 ± 1.5

9c	SCH_3	C_6H_4*m*Br	CH_3	H	CH_2CH_3	ND[b]	ND[b]	7.7 ± 1.9	6.4 ± 1.4	2.0 ± 1.1
9e	SCH_3	C_6H_4*m*Br	CH_3	H	$CH_2C_6H_5$	>100	>100	6.7 ± 1.8	2.45 ± 1.3	1.69 ± 1.5

GBM U87 cell line. Cells were treated for 24 h, 48 h and 72h with different concentrations of compound (0.1 μM, 1 μM, 5 μM, 10 μM). [a]IC_{50}: the half maximal inhibitory concentration of the effectiveness in reducing the number of viable cells with respect to untreated cells. [b] Not determined.

Cellular assays were performed in the human GBM U87 cell line in order to characterize the cytotoxicity of the prodrugs and their parent active compounds. Cells were treated for 24, 48 and 72 h with increasing concentrations of the compounds (0.1 μM, 1 μM, 5 μM, 10 μM). IC_{50} values were calculated counting viable cells compared to untreated cells (Table 3). At 24 h, prodrugs with an *in vitro* plasma half-life lower than 41 h, namely **4a**, **9a**, **9b** and **9e**, showed an activity higher than their respective drug (Table 3).

At 48 h and 72 h, the same prodrugs (**4a**, **9a**, **9b** and **9e**) demonstrated an activity comparable to the one of their parent drugs (Table 3). On the contrary, prodrug **1a** was less active than drug **1** at 24, 48 and 72 h.

In most cases, prodrugs were more effective than the respective drug at 24 h, although they demonstrated an efficacy comparable to the parent compound at 48 h and 72 h. In order to understand if this effect may be related to an enhanced ability to enter into the cytoplasm, a cellular kinetics assay was performed (Fig. 1). GBM U87 cells were treated with prodrugs **4a**, **9a-b** and **9e** and drugs **4** and **9** at a concentration of 20 μM and the quantity of compound inside the cell was determined by HPLC.

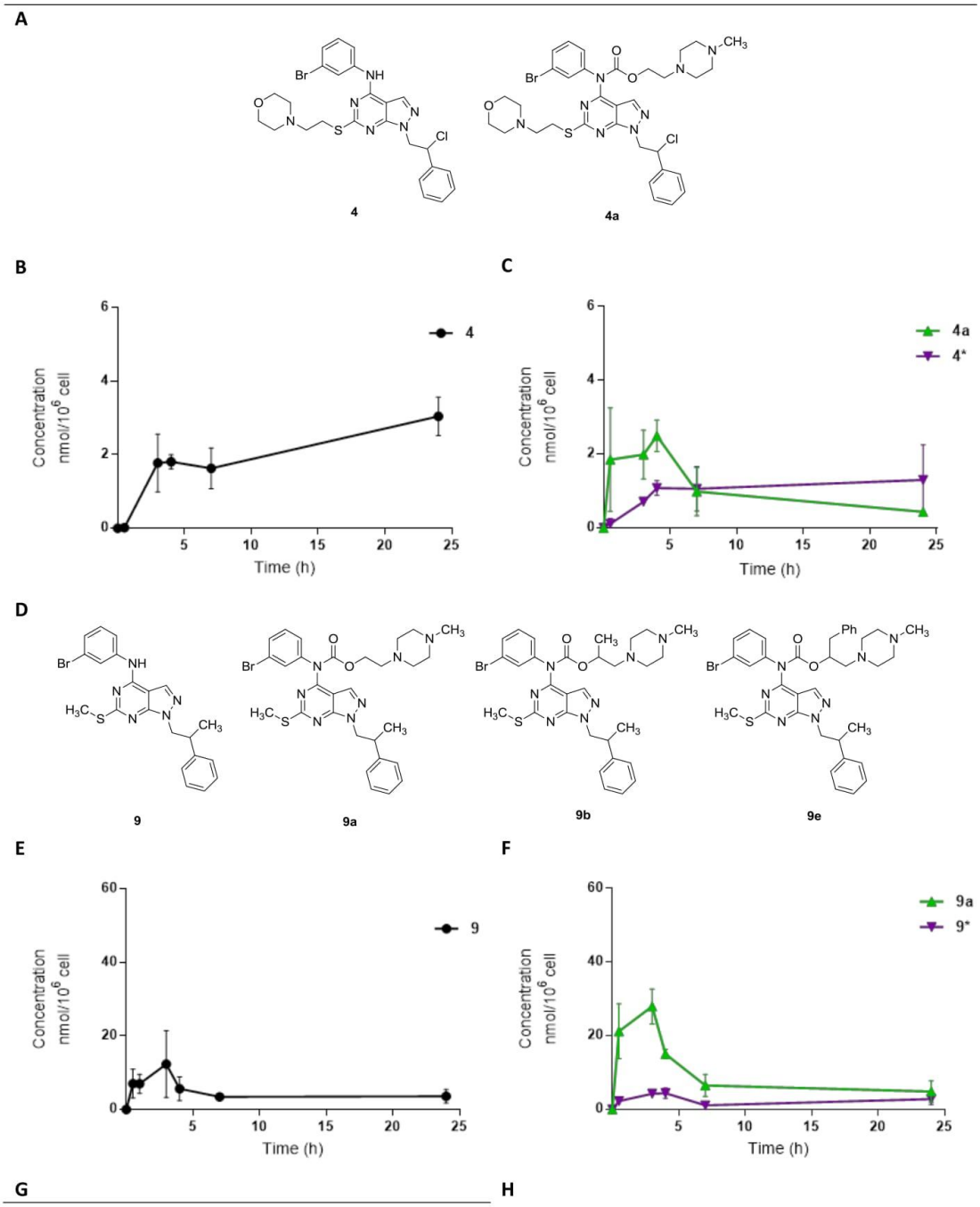
A
4
4a
B
C
Concentration nmol/10^6 cell
Time (h)
4
4a
4*
D
9
9a
9b
9e
E
F
9
9a
9*
G
H

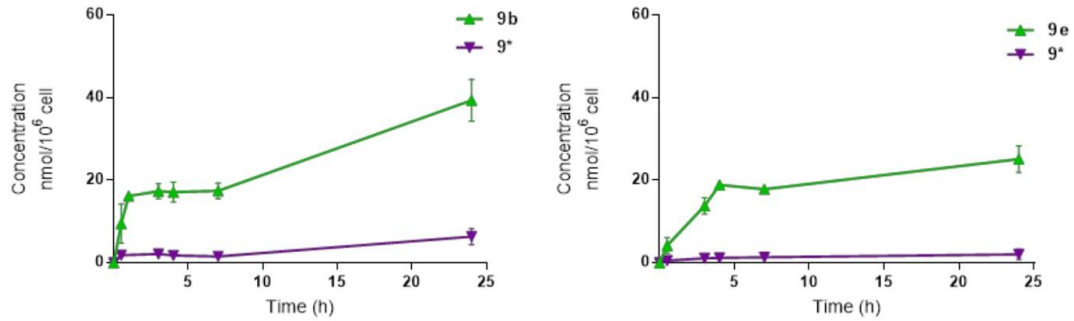

Figure 1. Cellular kinetics of drug/prodrug: 4/4a and 9/9a, 9b, 9e. A) Chemical structures of compound **4** and **4a**. B, C) Time-dependent concentration of drug and prodrugs within cells after treatment with compounds **4** (B) and prodrug **4a** (C). D) Chemical structures of compound **9**, **9a**, **9b** and **9e**. E, F, G, H) Time-dependent concentration of drug and prodrugs within cells after treatment with the following compounds: drug **9** (E), prodrug **9a** (F), prodrug **9b** (G), prodrug **9e** (H).
The curves display the quantity of compound (nanomoles) found within the cells at several time points (0.5, 3.0, 4.0, 7.0, 24.0 h). For prodrugs (**4a** and **9a**, **9b**, **9e**) the green curve shows the quantity of prodrug whereas the purple line indicates quantity of drug released after hydrolysis (**4*** and **9***). Human GBM U87 cells were treated with drugs **4** and **9** and prodrugs **4a**, **9a**, **9b** and **9e** at a concentration of 20 µM for different time periods. Cells were lysed and the quantity of compound within the cytoplasm was determined by HPLC.

Compounds **4** and **9** were selected as representative of two opposite situations, as they are the most and the least hydrophilic drug of the set of pyrazolo[3,4-*d*]pyrimidines studied herein. Cellular kinetics showed that prodrugs were subjected to a faster uptake compared to the respective drugs. Moreover, the quantity of each prodrug within the cytoplasm was higher than the quantity of the corresponding drug. However, the amount of each drug released from its prodrug was comparable to the quantity of drug obtained after treatment with the free drug only. Interestingly, prodrugs with a plasma half-life close to 3 h, namely **4a** and **9a**, showed a similar kinetics curve that depicts the rapid increase of the cytoplasmic concentration of prodrug within the first two hours, followed by a quick decrease in the next five hours (Fig. 1C and 1F, respectively).

Similarly, prodrugs **9b** and **9e**, rapidly accumulated inside the cytoplasm, but their concentrations increased constantly also after 7h (Fig. 1G and 1H). This could be related to the higher stability towards plasma hydrolysis of prodrug **9b** and **9e**, with respect to **4a** and **9a**.

***In vivo* studies: pharmacokinetics and orthotopic xenograft model**

A pharmacokinetic study was performed to further investigate if the preparation of prodrugs is an effective strategy to enhance the pharmacokinetic properties of pyrazolo[3,4-*d*]pyrimidines. Drug **4** and its prodrug **4a** were chosen for this study, based on the promising cellular kinetic (Fig. 1) and physiochemical properties. The mice were divided in two groups, one receiving drug **4** (50 mg/Kg *i.p.* bolus) and the other group receiving prodrug **4a** (50 mg/Kg *i.p.* bolus). Plasma and brain tissue were collected from mice and the concentration of drug **4**, prodrug **4a** and drug **4** released by hydrolysis (from now on called **4***, in this article) was determined using HPLC analysis (Fig. 2). Prodrug **4a** showed a higher plasma concentration and a longer circulation time (Fig. 2B, **4a**) compared to drug **4** (Fig. 2A).

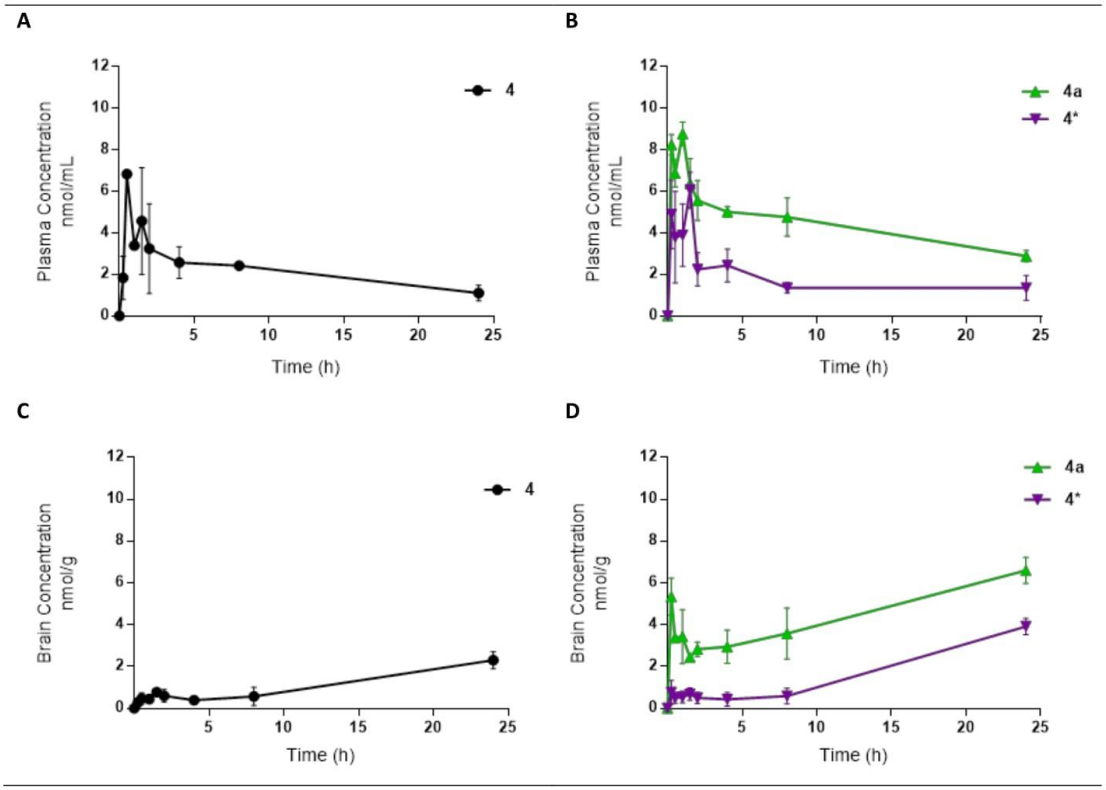

E

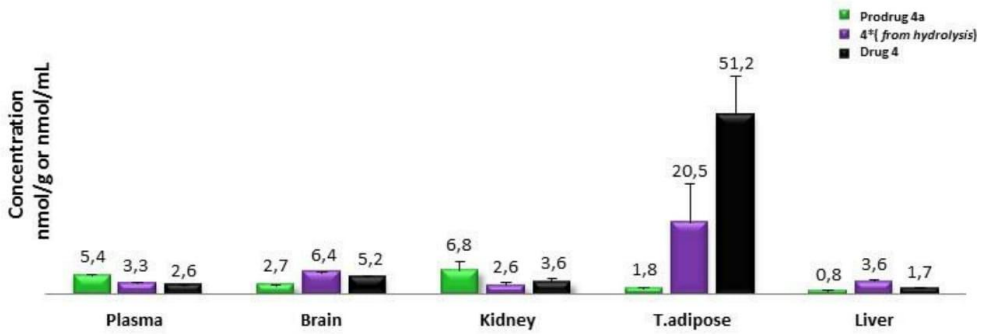

Figure 2. Pharmacokinetics of drug 4 and prodrug 4a.
A) Plasma concentration-time curve of drug **4**. B) Plasma concentration-time curve of prodrug **4a**: the green curve displays the quantity of **4a**, whereas the violet one represents the quantity of drug released from hydrolysis, **4***. C) Brain concentration-time curve of drug **4**. D) Brain concentration-time curve of prodrug **4a**: the green curve displays the quantity of **4a**, whereas the purple represents the quantity of drug released from hydrolysis, **4***. E) Biodistribution of prodrug **4a** and drug **4** at 24 h: the concentration is expressed in nmol/mL for plasma and nmol/g for the other tissues. Concentrations were determined by UV/LC-MS in plasma and brain of mice treated with compounds at a dose of 50 mg/kg (*i.p.* administration).

The resulting $AUC_{0\to\infty}$ of prodrug **4a**, was 3 fold greater than the one obtained with the free drug **4** (Table 4). The concentration of drug **4** released from prodrug **4a** (Fig 2B, **4***), was comparable to the quantity of compound **4** found after administration of free drug **4** (Fig. 2A), however the $AUC_{0\to\infty}$ indicated greater plasma exposure for the drug **4***, released by the hydrolysis of prodrug **4a** (Table 4). Both compounds **4** and **4a** were able to reach the brain, with increasing concentrations during the 24 h (Fig. 2C and 2D). As for the plasma tissue, also in brain a higher concentration of prodrug **4a**, with respect to drug **4**, was obtained (Fig. 2D, **4a**). The resulting pharmacokinetic data are shown in Table 4.

Table 4. Plasma pharmacokinetic parameters[a]

IP Parameters	Drug 4	Prodrug 4a	Drug 4* *(from hydrolysis)*
Dose (mg/kg)	50	50	-
Formulation	solution in DMSO	solution in DMSO	-
C_{max}[b] (nmol/mL)	6.83	8.78	6.07
T_{max}[c] (h)	0.50	1.00	1.50

MRT[d] (h)	19.15	33.34	46.62
AUC[e] 0→∞ (nmol∗h/mL)	79.70	264.80	135.11
AUC[e] 0→24h (nmol∗h/mL)	56.10	136.00	55.14
CL[f] (mL/min)	0.46	0.14	0.27
$\mathbf{t_{1/2}}$[g] (h)	14.82	23.80	33.30

[a]Calculated with PKCALC. [b]C_{max}: maximum concentration observed. [c]T_{max}: time of maximum concentration observed. [d]MRT: mean residence time. [e]AUC: area under the curve. [f]CL: plasma clearance. [g]$t_{1/2}$: plasma half-life. Pharmacokinetic data were evaluated using a one-compartment model.

The antitumor properties of drug **4** and prodrug **4a** were tested in an orthotopic model of GBM. Twenty-one immunodeficient mice received intracranial injection of GBM U87 cells, and were randomly assigned to one of the three experimental groups: vehicle-treated group (control); drug-treated group (receiving 50 mg/Kg of **4**); prodrug-treated group (receiving 50 mg/Kg of **4a**).

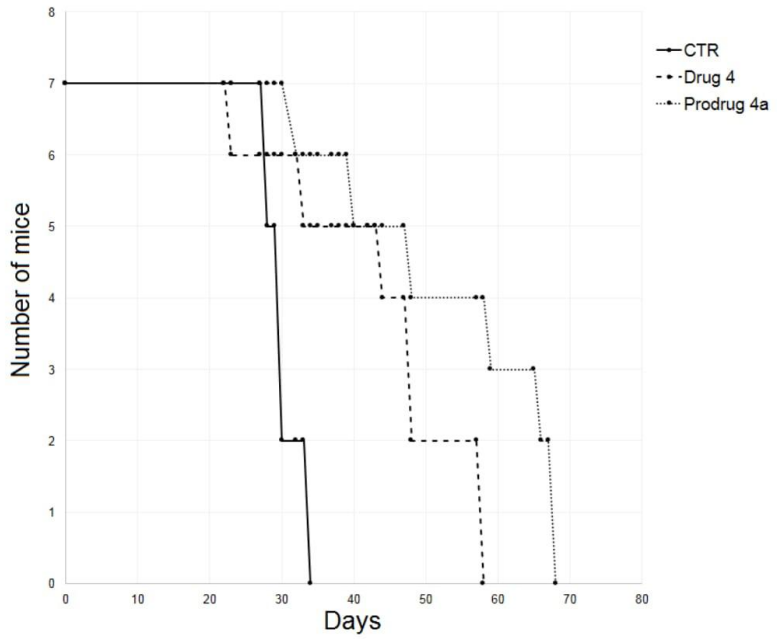

Figure 3. Orthotopic mouse model of GBM: survival curves for mice treated with vehicle (CTR), drug 4 and prodrug 4a.
Each group initially contained 7 mice. Mice received every other day oral administration of methylcellulose vehicle (CTR), 50 mg/kg of compound **4** or 50 mg/kg of prodrug **4a**. Compound **4** and its prodrug **4a** were prepared as suspension in 0.5% methylcellulose solution.

All mice died within 68 days after cell injection, but survival curves demonstrated that mice receiving drug **4** or prodrug **4a** had a longer life expectancy compared with vehicle-treated mice (Fig. 3). In fact, median survival time was 44 days for the mice treated with drug **4**, 49 days for the group that received prodrug **4a** and 30 days for the control group (Table 5). In addition, the survival time data showed a statistically significant difference between the group treated with drug **4** and the group that received prodrug **4a**, with a small but substantial increase in the survival time in the second group.

Table 5. *In vivo* antitumor efficiency: median survival time and statistics

Group	Median survival (days)	95% CI for the median	P (*vs* CTR)	P (*vs* drug 4)
CTR	30	28-34	-	-
Drug 4	44	33-48	0.0114*	-
Prodrug 4a	49	42-59	<0.01*	0.0397

*P<0.05 was considered statistically significant, P according to Logrank test.

DISCUSSION

Compounds **1-9** were selected for this study, among the pyrazolo[3,4-*d*]pyrimidines of our in-house library as they offer a suitable balance between the already reported *in vitro* activity and ADME properties, together with several different chemical features at the N1, C4 and C6 positions.[5,13,26-29] Particularly position C4, which contains the group involved in the formation of the carbamate group, required to link the prodrug moiety to the pyrazolo[3,4-*d*]pyrimidines. To develop an efficient synthesis and demonstrate its versatility, it was therefore important to select derivatives with suitable chemical diversity at C4. The NH-group at the C4 position was chosen as the group to link the prodrug-moiety as it is the easiest group to access chemically and the most shared feature within the pyrazolo[3,4-*d*]pyrimidine library (i.e. it creates crucial bonds within the ATP binding site of the tyrosine kinase).[32] To improve the low aqueous solubility of compounds **1-9**, *N*-methylpiperazine was selected as the 'solubilizing' prodrug group for its characteristic of being protonated at physiological conditions.[33] *N*-methylpiperazine was attached by an *in vivo* hydrolysable ethylcarbamate-linker to the C4 position of the pyrazolo[3,4-*d*]pyrimidine nucleus.[34]

In this study, we first improved the prodrug synthesis previously reported which involved two separate steps and the isolation of the unstable carbamic-chloride intermediate, resulting in medium to low yields of final prodrugs.[22] The new synthesis was instead performed in a one-pot, two-step fashion starting from the appropriate pyrazolo[3,4-*d*]pyrimidine (**1-9**) with the addition of trisphogene and sodium bicarbonate. Once the carbamic-chloride intermediate was formed (1-5h), the appropriate alcohol (**12,13** and **17-19**) was added (Scheme 1). This synthesis provided better yields (i.e. for **9a**) and has proven to be an effective strategy to introduce the prodrug moiety in several pyrazolo[3,4-*d*]pyrimidines bearing different chemical features. For instance, the secondary amino group at C4, which is directly involved in the carbamate group formation, showed alkyl, substituted-phenyl, phenylethyl and benzylic groups. This synthetic approach

further demonstrated its versatility in the synthesis of the final prodrugs **9b-9e**, where alcohols more sterically hindered than **12**, were used (**13** and **17-19**) (Scheme 2). These alcohols (**13** and **17-19**) were used to generate a series of prodrugs with increasing steric hindrance in proximity of the carbamate linker. Alcohols **12,13** and **17-19**, bearing H, Me, Et, Ph and Bn as substituent in position 1, were prepared using different procedures, as described in Scheme 3.

Aqueous solubility, stability in methanol, phosphate buffer and plasma were investigated, as well as metabolic stability (HLM) and permeability (PAMPA). Prodrugs' data regarding solubility, stability and permeability are shown in Table 2 and Table 3, together with the data obtained from their parent drugs, for comparison. The stability of the prodrugs was initially determined by UV/LC−MS in methanol and phosphate buffer (PBS, pH 7.4) to evaluate if the contribution of chemical hydrolysis induced by these polar media was minimal with respect to the rate of hydrolysis measured in subsequent plasma stability test. Prodrugs (**1a-7a**, **9a-c**, **9e**) demonstrated a good stability profile in the polar solutions tested and were consequently regarded as chemically stable for the subsequent evaluation of their susceptibility to enzymatic hydrolysis. On the contrary, the stability of prodrugs **8a** and **9d** was too low to further test these compounds regarding their aqueous solubility, metabolic stability and permeability.

Prodrugs are usually defined as bioreversible derivatives of active drugs and, in this regard, our strategy was to synthesize prodrugs with a carbamate moiety, potentially cleavable by *in vivo* hydrolases.[34] To confirm the hypothesis, all synthesized prodrugs were tested for their stability in human plasma and the rate of hydrolysis was monitored by UV/LC-MS. Results demonstrated that all tested prodrugs were converted into the corresponding active drugs. As the half-lives ranged from 0.46 to 75.0 h, a potential connection between the rate of hydrolysis and the substituent at the C4 position of the pyrazolo[3,4-*d*]pyrimidines was investigated. The analysis showed that compounds with a benzyl or phenylethyl amine at C4 (**1a**, **2a**, **5a** and **9e**) demonstrated a very high

stability, whereas compounds having a C4-aniline group, lead to prodrugs more susceptible to plasma hydrolysis (**3a**, **4a**, **6a**, **7a** and **9a**). Prodrug **8a**, with an *n*-butylamino moiety at C4, was already reported for its low half-life in plasma. Prodrugs **9b-9e**, which show an increasing steric bulk in proximity of the hydrolysable centre, were investigated to further understand if steric hindrance could determine a remarkable difference in the rate of enzymatic hydrolysis. Results demonstrated that the bulkier the substituent R^5 of the linker, the greater the plasma half-life of the prodrug (H<Me<Et<Bn = **9a**<**9b**<**9c**<**9e** = 3.21 h<10.4 h<11.3 h<40.0 h). A possible explanation is that the steric hindrance generated by the substituent close to the centre of hydrolysis, namely the carbamate group, could hurdle the access of plasma hydrolytic enzymes. To understand if metabolism of prodrugs could involve CYP-oxidative pathways, the compounds were incubated with HLM for 1 h and their concentration within the samples was monitored by UV/LC-MS. The percentage of unmodified prodrug was in general very high (86.4% was the lowest value obtained (**1a**)) and the metabolite patterns generated from prodrugs were similar to those obtained from the respective drugs. These data support the hypothesis that prodrugs and prodrug-linkers do not represent a direct substrate of CYP-metabolism. The analysis of thermodynamic solubility demonstrated the enhanced aqueous solubility of each prodrug in comparison to the respective drug, validating the synthesis of prodrugs as a strategy to overcome the poor aqueous solubility of pyrazolo[3,4-*d*]pyrimidines.

Prodrugs are chemically modified version of an active drug and typically, bioconversion (from prodrug to drug) is required for the interaction with the drug's biological target. [24,25] Pyrazolo[3,4-*d*]pyrimidines have been studied for their inhibitory activity towards tyrosine kinases activated in cancer such as c-Abl and c-Src. This activity is related to the interactions that most of these compounds create within the tyrosine kinases ATP-binding site. In order to understand if the herein synthesized prodrugs were able to interact directly with c-Abl and c-Src, a cell-free assay

was set up. As confirmation of the data previously reported regarding **9a**, also prodrugs **4a**, **9b** and **9e** were not able to inhibit these tyrosine kinases at the maximum concentration tested (100 μM). These results seemed to support the hypothesis that prodrugs cannot directly establish interactions within the ATP-binding site (i.e. the prodrug-linker masks the C4 secondary amino group that is required to create favorable bonds).[32]

Theoretically, prodrugs acquire antitumor activity after the hydrolysis-mediated release of the parent drug (hydrolysis of the *O*-alkyl-carbamate linker was demonstrated by plasma hydrolysis studies). Accordingly, a cellular assay with human GBM U87 cells was performed to assess the cytotoxicity of our prodrugs and to compare their activity with the one of their respective drugs. Nearly all the prodrugs tested (**4a**, **6a**, **7a**, **9a-c**, **9e**) were more active than the respective drug at 24 h, a result potentially related to the involvement of different cellular uptake mechanisms for drug and prodrug. The only exception was prodrug **1a** whose high resistance to hydrolysis might justify the different behavior at 24h. The difference in cytotoxicity within each pair of drug and prodrug decreased at 48 h and, consistently with this trend, drug and respective prodrug showed the same values of IC_{50} at 72 h.

The cellular kinetics of the series of 'chemically' modified prodrugs **9a-c**, **9e** and of **4a** were also studied (Fig. 1). The series **9a-c**, **9e** was included to understand the behavior towards hydrolysis and cellular uptake of compounds with increasing hindrance close to the hydrolysable group, whereas prodrug **4a** was selected for this test because of the plasma half-life value obtained, lower than 24 h, and the activity towards U87 cells. Further, since drugs **4** and **9** were the most and the least water soluble, it was interesting to analyze their behavior in cells in comparison to their more soluble prodrugs, namely **4a** and **9a**. Prodrugs showed an improved ability of entering into U87 cells, as demonstrated by the faster uptake and the quantity of prodrug measured into the cytoplasm. These data, together with the cytotoxicity values at 24 h, suggest that prodrug

treatment is associated with an increased availability of the active drug into the cellular compartment where the inhibition of biological target takes place. Nevertheless, the measured concentration of drug released by hydrolysis was comparable to the one obtained by treatment with the active drug; these data might be explained by a higher retention of the drug in cell membrane respect to the prodrug. Noticeably the IC_{50} at 72 h, showed the comparable activity of drugs and respective prodrugs, demonstrating that both drug and prodrug during the 72 h are able to reach the concentration needed to determine an equal cytotoxicity.

To evaluate if the preparation of prodrugs can enhance the pharmacokinetic properties of a poorly water-soluble drug, a proof of concept *in vivo* study was performed (Fig. 2). Drug **4** and prodrug **4a** were selected for this purpose taking into account all the properties previously assessed. First, it was required to select a drug with appropriate solubility to avoid possible issues during the administration of the compound to animals. Drug **4** showed the superior aqueous solubility and a good, although comparable to others, IC_{50} value of 2 μM, at 72 h. Remarkably, in the group of mice treated with prodrug **4a**, the quantity of prodrug measured in plasma was 2 fold higher than the quantity of drug inside the plasma of mice treated with the free drug **4** (Fig. 2A and 2B). The measured plasma concentration and the resulting $AUC_{0\rightarrow 24h}$ of drug **4***, released by hydrolysis of prodrug **4a**, were comparable to those obtained by administration of the free drug **4**. However, it is worth to notice that the $AUC_{0\rightarrow\infty}$ of the drug released form hydrolysis **4*** (value of 135.11 nmol h/mL) was twice as high as the value obtained with the administration of free drug **4** (79.7 nmol h/mL). These data suggests that prodrug **4a**, allows for a slow release of drug **4***, guaranteeing a prolonged overall exposure to the active compound. The pharmacokinetics in the brain compartment were also investigated, as the assessment of the cellular activity of these compounds was performed in human GBM U87 cell line (Fig. 2C and 2D). The concentration of prodrug **4a** quantified into the brain was higher than the quantity of drug **4** measured in the brain

of mice treated only with the free drug (**4**). Moreover, the curve obtained indicates that after 24 h the prodrug still accumulates within the brain, suggesting that the tumor site will have a prolonged exposure to prodrug **4a** and, consequently to hydrolysis, also to active drug **4***.

Finally, in an orthotopic model of GBM, prodrug **4a** was effective in prolonging the survival of mice (Fig. 3). The groups of mice treated with both drug **4** and prodrug **4a** showed a benefit in cancer survival with respect to the vehicle-treated mice. In addition, treatment with prodrug **4a** resulted in a minor but significant increase in median survival time. These results are in agreement with our previous data regarding the antitumor activity of drug **4** in GBM. The increased brain concentration and the improved biological activity, demonstrated *in vivo* after administration of prodrug **4a** with respect to drug **4**, suggest that prodrug **4a** could represent an effective step forward in the development of drug **4**.

In conclusion, in this study we advanced our synthetic strategy to produce prodrugs of a variety of pyrazolo[3,4-*d*]pyrimidines in an easy and versatile fashion. The synthesized prodrugs displayed improved aqueous solubility and good metabolic stability. The hydrolysis of the prodrugs was confirmed in plasma, where the active drugs were released by enzymatic cleavage of the carbamate prodrug-moiety. Cellular kinetics further supported the hydrolysis of prodrugs and showed a quicker uptake process for prodrugs in comparison to their respective drugs. The cytotoxicity at 72 h of the drugs and prodrugs tested were comparable, suggesting the complete release of the active drug. At the end, as *in vivo* proof of concept, the pharmacokinetics and efficacy of the most promising pair of drug/prodrug were studied. In comparison to the parent drug **4**, prodrug **4a** demonstrated an improved pharmacokinetic profile and resulted effective in a pivotal *in vivo* study, prolonging the median survival time of mice with human GBM xenografts. All together these results demonstrate the success of the application of the studied prodrug approach to pyrazolo[3,4-*d*]pyrimidine compounds with the aim of improving their poor water solubility and

their pharmacokinetic properties, determining a positive impact also in their biological efficacy as demonstrated by an *in vivo* model of GBM xenograft.

EXPERIMENTAL SECTION

Synthesis and characterization of compounds

Compounds **1-9** were previously synthesized and published by our group.[5,13,26-29]

All commercially available chemicals were used as purchased from Sigma Aldrich. DCM was dried over sodium hydride. Anhydrous reactions were run under a positive pressure of dry N_2. TLC was carried out using Merck TLC silica gel 60 F_{254}. Chromatographic purifications were performed on columns packed with Merck silica gel 60, 23-400 mesh, for flash technique. ^{1}H NMR and ^{13}C NMR spectra were recorded at 400 MHz on a Bruker Avance DPX400. Chemical shifts are reported relative to tetramethylsilane at 0.00 ppm. Mass spectra (MS) data were obtained using an Agilent 1100 LC/MSD VL system (G1946C) with a 0.4 mL/min flow rate using a binary solvent system of 95/5 = MeOH/H_2O. UV detection was monitored at 254 nm. MS were acquired in positive and negative mode scanning over the mass range 100-1500. The following ion source parameters were used: drying gas flow, 9 mL/min; nebulizer pressure, 40 psi; drying gas temperature, 350 °C.

General procedure for the synthesis of pyrazolo[3,4-d]pyrimidine prodrugs (1a-8a, 9a-e)

$NaHCO_3$ (2.25 mmol, 5.00 eq.) was added to a solution of the appropriate pyrazolo[3,4-*d*]pyrimidine compound (**1-9**) (0.45 mmol, 1.00 eq.) in DCM_{dry} (8 mL). After 5 min of stirring at r.t., the suspension was cooled with an ice-bath, then a solution of triphosgene (0.45 mmol, 1.00 eq.) in DCM_{dry} (8 mL) was added. After 30 min the ice-bath was removed and the reaction mixture was allowed to warm to r.t. and stirred until the spot of the starting material disappeared on TLC (2 h, approximately). A solution of alcohol (**10-14**) (0.90 mmol, 2.00 eq.) in DCM_{dry} (8 mL) was added and the resulting mixture was stirred at r.t. for 16 h. The solvent was evaporated under reduced pressure and the resulting residue was purified by flash chromatography using a mixture of DCM and MeOH as eluent.

2-(4-methylpiperazin-1-yl)ethyl benzyl1-(2-chloro-2-phenylethyl)-1H-pyrazolo[3,4-*d*]pyrimidin-4-ylcarbamate (1a)

Colourless oil. Yield: 79%. ^{1}H-NMR ($CDCl_3$) δ (ppm): 8.65 (s, 1H), 8.26 (s, 1H), 7.39 (d, *J* = 7.6 Hz, 2H), 7.24 (m, 8H), 5.52 (dd, *J* = 6, 8.4 Hz, 1H), 5.35 (s, 2H), 5.02 (dd, *J* = 8.8, 14.4 Hz, 1H), 4.79 (dd, *J* = 6, 14 Hz, 1H), 4.33 (t, *J* = 5.6 Hz, 2H), 2.55 (t, *J* = 5.6 Hz, 2H), 2.40 (m, 8H), 2.24 (s, 3H). ^{13}C-NMR ($CDCl_3$) δ (ppm): 154.7, 154.1, 154.0, 137.7, 135.7, 128.7, 128.5, 128.2, 128.1, 127.1, 127.0, 106.3, 63.9, 60.1, 56.3, 54.8, 53.7, 52.9, 49.9, 45.8. MS (ES) *m/z*: 535 $[M+H]^+$.

2-(4-methylpiperazin-1-yl)ethyl 2-chlorobenzyl1-(2-(4-bromophenyl)-2-chloroethyl)-1H-pyrazolo[3,4-*d*]pyrimidin-4-ylcarbamate (2a)

Colourless oil. Yield: 76% ^{1}H-NMR ($CDCl_3$) δ (ppm): 8.62 (s, 1H), 8.31 (s, 1H), 7.42 (d, *J* = 8.4 Hz, 2H), 7.18 (m, 6H), 5.50 (m, 1H), 5.44 (s, 2H), 4.99 (m, 1H), 4.82 (m, 1H), 4.34 (t, *J* = 5.2 Hz, 2H), 2.54 (t, *J* = 5.6 Hz, 2H), 2.41 (m, 8H), 2.26 (s, 3H). ^{13}C-NMR ($CDCl_3$) δ (ppm): 154.7, 154.6, 154.2, 136.7, 135.8, 135.1, 132.3, 131.7, 129.2, 128.9, 128.0, 127.0, 126.6, 122.8, 106.1, 64.3, 59.0, 56.2, 54.7, 53.4, 52.7, 48.1, 45.6, 29.5. MS (ES) *m/z*: 648 $[M+H]^+$, 670 $[M+Na]^+$.

2-(4-methylpiperazin-1-yl)ethyl 3-chlorophenyl6-(methylthio)-1-phenethyl-1H-pyrazolo[3,4-*d*]pyrimidin-4-ylcarbamate (3a)

Colourless oil. Yield: 75%. ^{1}H-NMR ($CDCl_3$) δ (ppm): 7.93 (s, 1H), 7.35 (d, *J* = 4.8 Hz, 2H), 7.22 (m, 7H), 4.62 (t, *J* = 7.6 Hz, 2H), 4.39 (t, *J* = 5.2 Hz, 2H), 3.22 (t, *J* = 7.6 Hz, 2H), 2.60 (t, *J* = 5.2 Hz, 2H), 2.47 (m, 8H), 2.32 (S, 3H), 2.28 (s, 3H). ^{13}C-NMR ($CDCl_3$) δ (ppm): 168.2, 155.2, 153.7, 153.1, 140.8, 137.8, 134.3, 134.1, 129.6, 129.4, 129.1, 128.7, 128.4, 127.9, 127.0, 126.7, 126.6, 103.2, 64.5, 63.8, 56.2, 54.8, 52.7, 48.3, 48.1, 45.6, 45.5, 35.1. MS (ES) *m/z*: 567 $[M+H]^+$.

2-(4-methylpiperazin-1-yl)ethyl 6-(2-morpholinoethylthio)-1-(2-chloro-2-phenylethyl)-1H-pyrazolo[3,4-*d*]pyrimidin-4-yl3-bromophenylcarbamate (4a)

Colourless oil. Yield: 51%. ^{1}H-NMR ($CDCl_3$) δ (ppm): 7.95 (s, 1H), 7.48 (d, *J* = 8 Hz, 1H), 7.42 (m, 3H), 7.29 (m, 4H), 7.15 (d, *J* = 8.4 Hz, 1H), 5.51 (t, *J* = 6 Hz, 1H), 4.94 (dd, *J* = 8.8, 14 Hz, 1H), 4.71 (dd, *J* = 6, 14 Hz, 1H), 4.35 (t, *J* = 5.2 Hz, 2H), 3.69 (t, *J* = 4.4 Hz, 4H), 3.01 (m, 2H), 2.49 (m, 19H), 2.27 (s, 3H). ^{13}C-NMR ($CDCl_3$) δ (ppm): 168.1, 155.8, 153.9, 153.0, 140.8, 137.7, 135.2, 131.8, 130.9, 130.0, 128.8, 128.5, 127.4, 127.1, 121.9, 103.2, 77.1, 76.8, 76.5, 66.7, 64.5, 59.9, 57.4, 56.2, 54.8, 53.3, 53.2, 52.8, 45.6, 31.7, 30.7, 29.5, 29.1, 27.9. MS (ES) *m/z*: 745 $[M+H]^+$, 767 $[M+Na]^+$.

2-(4-methylpiperazin-1-yl)ethyl 1-(2-chloro-2-phenylethyl)-6-(methylthio)-1H-pyrazolo[3,4-*d*]pyrimidin-4-ylphenethylcarbamate (5a)

Colourless oil. Yield: 71%. ^{1}H-NMR ($CDCl_3$) δ (ppm): 8.06 (s, 1H), 7.41 (d, *J* = 6.4 Hz, 2H), 7.24 (m, 8H), 5.51 (t, *J* = 8 Hz, 1H), 4.93 (dd, *J* = 8, 14 Hz, 1H), 4.78 (dd, *J* = 6.8, 14.4 Hz, 1H), 4.30 (m, 4H), 3.02 (t, *J* = 7.6 Hz, 2H), 2.65 (m, 11H), 2.38 (s, 3H). ^{13}C-NMR ($CDCl_3$) δ (ppm): 168.7, 155.7, 154.1, 138.7, 138.0, 136.1, 129.0, 128.7, 128.5, 127.4, 126.5, 103.7, 63.6, 60.1, 56.4, 54.7, 53.8, 52.3, 48.8, 45.4, 35.1, 29.7, 14.3. MS (ES) *m/z*: 595 $[M+H]^+$.

2-(4-methylpiperazin-1-yl)ethyl 1-(2-(4-bromophenyl)-2-chloroethyl)-1H-pyrazolo[3,4-*d*]pyrimidin-4-ylphenylcarbamate (6a)

Colourless oil. Yield: 25%. ^{1}H-NMR ($CDCl_3$) δ (ppm): 8.61 (s, 1H), 7.77 (s, 1H), 7.42 (m, 4H), 3.76 (m, 5H), 5.48 (t, *J* = 8 Hz, 1H), 4.97 (dd, *J* = 8.4, 14 Hz, 1H), 4.80 (dd, *J* = 6.4, 14 Hz, 1H), 4.36 (t, *J* = 5.6 Hz, 2H), 2.57 (t, *J* = 5.6 Hz, 2H), 2.43 (m, 8H), 2.31 (S, 3H). ^{13}C-NMR ($CDCl_3$) δ (ppm): 155.6, 155.0, 154.7, 153.6, 139.9, 136.8, 135.0, 131.9, 129.1, 128.7, 128.3, 123.1, 106.1, 65.2, 64.8, 59.2, 56.3, 56.2, 54.8, 54.7, 53.6, 53.4, 52.4, 45.5, 30.3, 29.7. MS (ES) *m/z*: 598 $[M+H]^+$, 620 $[M+Na]^+$.

2-(4-methylpiperazin-1-yl)ethyl (1-(2-chloro-2-phenylethyl)-6-(methylthio)-1*H*-pyrazolo[3,4-*d*]pyrimidin-4-yl) 3-chlorophenylcarbamate (7a)

Colourless oil. Yield: 85%. ^{1}H-NMR ($CDCl_3$) δ (ppm): 7.95 (s, 1H), 7.40 (d, *J* = 6.8 Hz, 2H), 7.29 (m, 6H), 7.11 (m, 1H), 5.50 (t, *J* = 7.0 Hz, 1H), 4.93 (dd, *J* = 8.4, 14 Hz, 1H), 4.76 (dd, *J* = 6.4, 14 Hz, 1H),

4.35 (t, *J* = 5.2 Hz, 2H), 2.55 (t, *J* = 5.2 Hz, 2H), 2.41 (m, 8H), 2.27 (s, 3H), 2.26 (s, 3H). ^{13}C-NMR ($CDCl_3$) δ (ppm): 168.6, 155.8, 153.7, 153.1, 140.6, 137.7, 135.2, 134.1, 129.6, 129.0, 128.8, 128.5, 127.9, 127.2, 126.9, 103.0, 64.6, 59.8, 56.2, 54.8, 53.6, 52.8, 45.7, 29.5. MS (ES) *m/z*: 601 $[M+H]^+$.**2-(4-methylpiperazin-1-yl)ethyl butyl1-(2-chloro-2-phenylethyl)-6-(ethylthio)-1H-pyrazolo[3,4-*d*]pyrimidin-4-ylcarbamate (8a)**

Colourless oil. Yield: 39%. ^{1}H-NMR ($CDCl_3$) δ (ppm): 8.08 (s, 1H), 7.39 (d, *J* = 6.8 Hz, 2H), 7.27 (m, 3H), 5.50 (t, *J = 7.6* Hz, 1H), 4.91 (dd, *J* = 8.4, 14.4 Hz, 1H), 4.76 (dd, *J* = 6.4, 14 Hz, 1H), 4.37 (t, *J* = 5.6 Hz, 2H), 4.03 (t, *J* = 7.6 Hz, 2H), 3.17 (q, *J* = 7.2 Hz, 2H), 2.67 (t, *J* = 5.6 Hz, 2H), 2.54 (m, 8H), 2.31 (s, 3H), 1.66 (q, *J* = 7.6 Hz, 2H), 1.43 (t, *J* = 7.2 Hz, 3H), 1.31 (m, 3H), 0.93 (t, *J* = 7.1 Hz, 3H). ^{13}C-NMR ($CDCl_3$) δ (ppm): 168.2, 155.7, 154.4, 154.4, 138.1, 136.1, 128.9, 128.7, 127.4, 104.0, 63.9, 60.1, 56.6, 55.1, 53.8, 53.2, 47.3, 46.0, 30.9, 29.7, 25.4, 20.1, 14.7, 13.9. MS (ES) *m/z*: 561 $[M+H]^+$.

2-(4-methylpiperazin-1-yl)ethyl 3-bromophenyl6-(methylthio)-1-(2-phenylpropyl)-1H-pyrazolo[3,4-*d*]pyrimidin-4-ylcarbamate (9a)

Colourless oil. Yield: 30%.^{1}H-NMR ($CDCl_3$) δ (ppm): 7.88 (s, 1H), 7.49 (d, *J* = 8 Hz, 1H), 7.42 (s, 1H), 7.12 (m, 7H), 4.49 (t, *J* = 7.5 Hz, 2H), 4.35 (t, *J* = 5.2 Hz, 2H), 3.53 (m, 1H), 2.55 (m, 10H), 2.35 (s, 3H), 2.8 (s, 3H)1.41 (s, 3H). ^{13}C-NMR ($CDCl_3$) δ (ppm): 175.5, 168.4, 155.8, 153.9, 153.3, 141.0, 134.5, 132.0, 131.1, 130.2, 128.5, 127.6, 127.2, 126.8, 122.1, 103.2, 64.6, 56.1, 54.0, 53.8, 51.8, 44.5, 39.9, 21.8, 18.8, 14.1. MS (ES) *m/z*: 626 $[M+H]^+$, 648 $[M+Na]^+$.

1-(4-methylpiperazin-1-yl)propan-2-yl 3-bromophenyl6-(methylthio)-1-(2-phenylpropyl)-1H-pyrazolo[3,4-*d*]pyrimidin-4-ylcarbamate (9b)

Colourless oil. Yield: 30%.^{1}H-NMR ($CDCl_3$) δ (ppm): 7.88 (s, 1H), 7.46 (m, 2H), 7.24 (m, 5H), 7.16 (m, 2H); 5.20 (m, 1H), 4.50 (m, 2H), 3.52 (q, J = 7.2 Hz, 1H), 2.45 (m, 10H), 2.33 (s, 3H), 2.28 (s, 3H), 1.22 (m, 6H). ^{13}C-NMR ($CDCl_3$) δ (ppm): 168.1, 155.5, 153.9, 152.9, 143.1, 141.1, 134.29, 131.8,

130.6, 129.8, 128.2, 127.3, 127.0, 126.5, 121.7, 103.15, 71.0, 62.6, 54.8, 53.5, 52.7, 45.4, 39.7, 29.5, 18.5, 17.9. MS (ES) *m/z*: 639 $[M+H]^+$.

1-(4-methylpiperazin-1-yl)butan-2-yl 3-bromophenyl6-(methylthio)-1-(2-phenylpropyl)-1H-pyrazolo[3,4-*d*]pyrimidin-4-ylcarbamate (9c)

Colourless oil. Yield: 40%.^{1}H-NMR ($CDCl_3$) δ (ppm): 7.90 (s, 1H), 7.46 (m, 2H), 7.24 (m, 5H), 7.16 (m, 2H); 5.08 (m, 1H), 4.50 (m, 2H), 3.52 (q, *J* = 6.8 Hz, 1H), 2.50 (m, 12H), 2.29 (s, 3H), 2.27 (s, 3H), 1.23 (s, 3H), 0.88 (m, 3H). ^{13}C-NMR ($CDCl_3$) δ (ppm): 170.2, 155.4, 154.0, 153.2, 143.1, 141.1, 134.4, 131.8, 130.5, 129.7, 128.2, 127.3, 127.0, 126.5, 121.7, 103.4, 75.4, 61.0, 54.9, 53.5, 45.6, 39.7, 29.5, 25.1, 18.5, 13.9, 9.34. MS (ES) *m/z*: 652 $[M+H]^+$.

2-(4-methylpiperazin-1-yl)-1-phenylethyl 3-bromophenyl6-(methylthio)-1-(2-phenylpropyl)-1H-pyrazolo[3,4-*d*]pyrimidin-4-ylcarbamate (9d)

Colourless oil. Yield: 32%.^{1}H-NMR ($CDCl_3$) δ (ppm): 7.74 (s, 1H), 7.54 (d, J = 8 Hz, 1H), 7.46 (s, 1H), 7.21 (m, 12H), 6.00 (d, *J* = 8.8 Hz, 1H); 4.48 (m, 2H), 3.53 (q, *J* = 6.8 Hz, 1H), 2.88 (bs, 6H), 2.72 (m, 7H), 2.31 (s, 3H), 1.25 (s, 3H). ^{13}C-NMR ($CDCl_3$) δ (ppm): 168.4, 155.7, 153.9, 152.8, 143.3, 141.2, 137.6, 134.4, 132.1, 131.1, 130.3, 128.7, 127.4, 127.2, 126.8, 126.3, 122.0, 103.2, 75.4, 63.2, 54.4, 53.8, 51.2, 44.4, 39.9, 29.7, 25.1, 18.7. MS (ES) *m/z*: 652 $[M+H]^+$.

1-(4-methylpiperazin-1-yl)-3-phenylpropan-2-yl 3-bromophenyl-6-(methylthio)-1-(2-phenylpropyl)-1H-pyrazolo[3,4-*d*]pyrimidin-4-ylcarbamate (9e)

Colourless oil. Yield 52% ^{1}H NMR ($CDCl_3$) δ (ppm)= 7.75 (s, 1H), 7.55-7.53 (d, 1H), 7.46 (s, 1H), 7.31-7.13 (m, 12H), 6.01-5.99 (m, 1H), 4.54-4.43 (m, 2H), 3.55-3.50 (m, 1H), 2.88 (m, 6H), 2.78 (m, 2H), 2.72-2.56 (m, 7H), 2.31 (m, 3H), 1.25 (m, 3H). ^{13}C-NMR ($CDCl_3$) δ (ppm): 168.4, 155.7, 153.9, 152.8, 142.4, 141.2, 137.6, 134.4, 132.1, 131.1, 130.3, 128.7, 127.4, 127.2, 126.8, 126.3, 122.0, 103.2, 78.3, 63.2, 54.4, 53.8, 51.2, 44.4, 39.9, 38.4, 29.7, 25.1, 18.7. MS (ES): *m/z*: 714 $[M+H]^+$.

Synthesis of 2-(4-methylpiperazin-1-yl)ethanol (12)[24]

Methylpiperazine (3.54 mL, 31.9 mmol, 1.33 eq.) was dissolved in toluene (11 mL), bromoethanol (1.70 mL, 23.9 mmol, 1.00eq.) was slowly added and the mixture was stirred o.n. at r.t. Then it was filtered and the organic phase was recovered, the solvent removed under reduced pressure to give the desired product. Yield: 80%. White solid. ^{1}H-NMR ($CDCl_3$) δ (ppm): 4.51 (s, 1H); 3.14 (m, 2H); 2.01 (m, 10H); 1.78 (s, 3H). ^{13}C-NMR ($CDCl_3$) δ (ppm): 59.8, 58.0, 54.4, 52.6, 45.5. MS (ES) *m/z*: 145 $[M+H]^+$.

Synthesis of 1-(4-methylpiperazin-1-yl)propan-2-ol (13)[30,31]

Methylpiperazine (55.0 µL, 0.50 mmol, 2.00 eq.) was dissolved in toluene (7 mL), 1-bromo-2-propanol (23.0 µL, 0.25 mmol, 1.00eq.) was slowly added and the mixture was stirred o.n. at r.t. Then it was filtered and the organic phase was recovered, the solvent removed under reduced pressure to give the desired product. Yield: 38%. Colourless oil. ^{1}H-NMR (MeOD) δ (ppm): 4.51 (s, 1H); 3.14 (m, 2H); 2.01 (m, 10H); 1.78 (s, 3H). ^{13}C-NMR (MeOD) δ (ppm): 59.8, 58.0, 54.4, 52.6, 45.5. MS (ES) *m/z*: 159.0 $[M+H]^+$.

Synthesis of 1-(4-methylpiperazin-1-yl)butan-2-ol (17)[30,31]

$ZnCl_2$ (12.4 mg, 0.09 mmol, 0.10 eq.) was added to a solution of methylpiperazine (110 µL, 1.00 mmol, 1.10 eq.) and 1,2-epoxybutane (79.0 µL, 0.91 mmol, 1.00 eq.) in ACN (8 mL); the mixture was stirred under reflux 16h. Then purified by flash chromatography using PE:AcOEt:MeOH:Et_3N = 10:8:1:1 as eluent. Yield: 31%. Colourless oil. ^{1}H-NMR ($CDCl_3$) δ (ppm): 3.65-3.59 (m, 1H), 2.47 (m, 8H), 2.34-2.32 (m, 2H), 2.26 (s, 3H), 1.40-1.35 (m, 1H), 0.96-0.91 (m, 3H). ^{13}C-NMR (MeOD) δ (ppm): 71.5, 61.5, 58.2, 57.6, 46.6, 28.3, 9.5. MS (ES) *m/z*: 173.0 $[M+H]^+$.

Synthesis of 2-(4-methylpiperazin-1-yl)-1-phenylethanol (18)[30,31]

Methylpiperazine (125.04 mg, 1.25 mmol), K_2CO_3 (517.60 mg, 3.74 mmol) and styrene-oxide (95.0 µL, 0.83mmol, 1,00 eq) were dissolved in toluene. The reaction mixture was heated at 130°C for 24h. After water was added, the crude was extracted with DCM (X3) and washed with brine. The

organic layers were collected, dried over with Na_2SO_4 and the solvent was evaporated under reduced pressure. Then purified by flash chromatography using AcOEt:MeOH= 9:1 as eluent. Yield: 61%. Colourless oil ^{1}H-NMR ($CDCl_3$) δ (ppm): 7.36-7.22 (m, 5H), 4.73-4.70 (m, 1H), 3.69-3.65 (m, 1H), 2.76 (m, 2H), 2.53-2.44 (m, 8H), 2.30 (s, 3H). ^{13}C-NMR ($CDCl_3$) δ (ppm): 142.2, 128.3, 127.5, 125.8, 68.8, 66.2, 55.2, 53.0, 46.0. MS (ES) *m/z*: 221.1 $[M+H]^+$.

Synthesis of 1-(4-methylpiperazin-1-yl)-3-phenylpropan-2-ol (19)

$ZnCl_2$ (14.72 mg, 0.10 mmol, 0.10 eq.) was added to a solution of methylpiperazine (180 µL, 1.62 mmol, 1.50 eq.) and 2-benzyloxirane (142.0 µL, 1.08 mmol, 1.00 eq.) in ACN (8 mL); the mixture was stirred under reflux 12h. Then purified by flash chromatography using DCM:MeOH=95:5.as eluent. Yield: 68%. Colourless oil ^{1}H-NMR ($CDCl_3$) δ (ppm): 7.29-7.19 (m, 5H), 4.02-3.96 (m, 1H), 3.25 (m, 1H), 2.79-2.74 (m, 1H), 2.65-2.61 (m, 3H), 2.37-2.25 (m, 8H), 2.22 (s, 3H). ^{13}C-NMR ($CDCl_3$) δ (ppm): 140.1, 128.3, 127.5, 125.8, 71.1, 65.9, 55.2, 53.0, 46.0, 45.8. MS (ESI) *m/z*: 235.0 $[M+H]^+$.

***In vitro* ADME assays**

Solvents, reagents, NADP, NADPH, D-glucose-6-phosphate, glucose-6-phosphate dehydrogenase and L-α-phosphatidylcoline were purchased from Sigma-Aldrich S.r.l. (Milan, Italy). Brain polar lipid extract (porcine) was purchased from Avanti Polar Lipids, INC (Alabama, USA). Human plasma was obtained from volunteers/donors. HLM pooled male donors (20 mg/mL) were purchased from BD Gentest-Biosciences (San Jose, California). Milli-Q water was used (Millipore, Milford, MA, USA).

UV/HPLC-MS method. LC analyses were performed by Agilent 1100 LC/MSD VL system (G1946C) (Agilent Technologies, Palo Alto, CA) constituted by a vacuum solvent degassing unit, a binary high-pressure gradient pump, an 1100 series UV detector and a 1100 MSD model VL benchtop mass spectrometer was used. The Agilent 1100 series mass spectra detection (MSD) single-quadrupole instrument was equipped with the orthogonal spray API-ES (Agilent Technologies, Palo Alto, CA). Nitrogen was used as nebulizing and drying gas. The pressure of the nebulizing gas, the

flow of the drying gas, the capillary voltage, the fragmentor voltage and the vaporization temperature were set at 40 psi, 9 L/min, 3000 V, 70 V and 350 °C, respectively. UV detection was monitored at 280 nm. The LC-ESI-MS determination was performed by operating the MSD in the positive ion mode. Spectra were acquired over the scan range m/z 50-1500 using a step size of 0.1 u. Chromatographic analysis was performed using a Kinetex EVO C18 100A column (150 x 4.6 mm, 5 µm particle size) at room temperature. Analysis was carried out using a gradient elution of acetonitrile (ACN) and water (H_2O): t = 0min ACN 0%, t = 3min ACN 0%, t = 12min ACN 98%, t =18 min ACN 98%. The analysis was performed at flow rate of 0.6 mL/min and injection volume was 20 µL.

Aqueous Solubility. Each solid compound (1 mg) was added to 1 mL of water. Each sample was mixed at 20 °C, in a shaker water bath for 24 h. The resulting suspension was filtered through a 0.45 µm nylon filter (Acrodisc). The concentration of compound in solution was determined by UV/LC-MS (performed in triplicate) by comparison with the appropriate calibration curve that was obtained from samples of the compound dissolved in methanol at different concentrations.

Stability tests in MeOH, PBS and human plasma. Each prodrug was dissolved at r.t. in phosphate buffer (12.5 mM, pH 7.4) or methanol up to a final concentration of 500 µM. Aliquot samples (20 µL) were taken at fixed time points (0.25, 0.50, 0.75, 1.0, 2.0, 3.0, 4.0, 5.0, 6.0, 7.0, 8.0, 24.0 and 48 h) and were analyzed by UV/LC-MS.

Pooled human plasma (1.5 mL, 55.7 µg protein/mL),[35] phosphate buffer (1.4 mL, pH 7.4, 25 mM) and a solution of prodrug in methanol (100 µL, 3.0 mM) were mixed in a test tube that was incubated at 37 °C. At set time points (0.25, 0.50, 1.0, 2.0, 3.0, 4.0 and 24.0 h), samples of 150 µL were taken, mixed with 600 µL of cold acetonitrile and centrifuged at 5000 rpm for 15 min. The supernatant was removed and analyzed by UV/LC-MS to monitor the hydrolysis process of prodrug (method reported above).

Parallel Artificial Membrane Permeability Assay (PAMPA). Each 'donor solution' was prepared from a solution of the appropriate compound (DMSO, 1 mM) diluted with phosphate buffer (pH 7.4, 25.0 mM) up to a final concentration of 500 μM. The donor wells were filled with 150 μL of 'donor solution'. The filters were coated with 5 μL of a solution of phosphatidylcholine (in dodecane 1% (w/v) to determine GI permeability) or 4 μL of brain polar lipid solution (20mg/mL, 16% chloroform, 84% dodecane) prepared from chloroform 10% w/v solution (to determine BBB permeability) and filled with 300 μL of 'acceptor solution' (50% v/v DMSO and phosphate buffer). The sandwich plate was assembled and incubated for 5 h at r.t. under gentle shaking. After the incubation time, the sandwich was disassembled and the amount of compound in both the donor and acceptor wells was measured by UV/LC-MS. Permeability (P_{app}) was calculated according to the following equation[36]

$$P_{app} = -\frac{V_D V_A}{(V_D + V_A)At}\ln(1-r)$$

where V_A is the volume in the acceptor well (cm^3), V_D is the volume in the donor well (cm^3), A is the "effective area" of the membrane (cm^2), t is the incubation time (s) and r the ratio between drug concentration in the acceptor and equilibrium concentration of the drug in the total volume (V_D+V_A). Drug concentration was estimated by using the peak area integration.

Metabolic Stability in HLM (Human Liver Microsomes). The incubation mixture (total volume of 500 μL) was constituted by the following components: HLM (0.2 mg/mL, 5 μL), a NADPH regenerating system (NADPH 0.2 mM, $NADPH^+$ 1 mM, D-glucose-6-phosphate 4 mM, 4 unit/mL glucose-6-phosphate dehydrogenase and $MgCl_2$ 48 mM), 50 μM of each compound in DMSO and phosphate buffer (pH 7.4, 25 mM, up to a final volume of 500 μL). The mixture was incubated at 37 °C for 1 h. The reaction was cooled down and quenched with acetonitrile (1.0 mL). After centrifugation (10^4 rpm, 10 min), the surnatant was taken, dried under nitrogen flow, suspended

in 100 µL of methanol and analyzed by UV/LC-MS to determine the percentage of compound that was not metabolized.

Biological Assays

Cellular assays. GBM U87 cells were plated in a 6-well plate (5×10^4 cells per well) in EMEM with 10% FBS, 2 mM L-glutamine, 10000 units/mL Penicillin/Streptomycin and incubated with compounds (DMSO solution) at increasing concentrations (0.1 µM, 1.0 µM, 10 µM and 50 µM) for 24, 48 and 72 h at 37°C in 5% CO_2 atmosphere. Cells were harvested to determine cell amount and viability by Trypan Blue assay. The half maximal inhibitory concentration (IC_{50}) for each compound was estimated fitting a curve with a nonlinear regression created with all the collected data using GraphPad Prism Software, version 6.0.

Cellular Kinetics. GBM U87 cells were seeded in a 6-well plate (3×10^5 cells per well) in triplicate. After 24 h, cells were treated with compound (20 µM) for different periods (0.5, 3.0, 4.0, 7.0, 24 h). Cells were harvested and counted by Trypan Blue assay, cell counts were used for normalization purposes. All the harvested cells were lysed in 150 µL of deionized water, subjected to 10 cycles of freeze and thaw and then sonicated for 10 minute at 560 W (maximum intensity) in a bath sonicator. Standard compound at 10 µM was added in lysed cells as control. Lysed cells were then centrifuged at 5000 × g for 20 minutes and supernatant was withdrawn and dried by nitrogen flow. Samples were resuspended in 100 µL of methanol and the amount of compound within the cells was evaluated by UV/LC-MS analysis.

***In vivo* PK**

The used animal protocol was reviewed and approved by the animal care and ethics committee of the Università degli Studi di Siena, Italy. Male BALB/C mice (weight 20-30 g) were obtained from Charles River (Milan, Italy). The experiment was performed in triplicate and mice were divided into two groups and treated with drug or prodrug (DMSO solution). The compounds were administered

intraperitoneally (100 µL) at the dose of 50 mg/Kg. At several time points (0.25, 0.50, 1.0, 1.5, 2.0, 4.0, 8.0 and 24.0 h), after drug administration, mice were treated i.p. with heparin (5000 U/Kg) and sacrificed under CO_2. Blood and brain were collected for the following quantitative analysis. The blood was centrifuged at 4000 rpm for 20 minutes to separate the plasma fraction, which was subsequently collected in a test tube. Acetonitrile (1 mL, with internal standard at the concentration of 10 µM) was added to each sample to denature proteins. Samples were centrifuged at 4000 rpm for 20 minutes, the supernatant was recovered, dried under vacuum and analyzed. Brain was homogenized using a glass/glass Potter-Elvehjem tissue homogenizer, in order to extract the compound from the tissue, 7 mL of acetonitrile were added (with internal standard at the concentration of 10 µM). Brain samples were then treated as previously described for blood samples. Each brain and blood sample was solubilized in 100 µL of methanol and analyzed by UV/LC-MS. The quantification of each compound was performed by reference to the appropriate calibration curve. PKCALC[30] was used to determine pharmacokinetic parameters.

***In vivo* orthotopic mouse model**

Male CD1 nude mice (Charles River, Milan, Italy) were maintained under the guidelines established by our Institution (University of L'Aquila), complying with the Italian government regulation for the use of laboratory animals. After anesthetization with 100 mg/kg ketamine, 15 mg/kg xylazine, the surgical zone was swabbed with Betadine solution, the eyes coated with Lacri-lube. The head was fixed in a stereotactic frame (mouse stereotaxics instrument, Stoelting Europe, Dublin, Ireland) and a midline scalp incision was made. A small hole was made at 1.0 mm anterior and 2 mm lateral to the exposed bregma. A sterile 5 µL Hamilton syringe with a 26 gauge needle was inserted at a depth of 3.0 mm from the skull surface and withdrawn by 0.5 mm to inject 3×10^3 U-87 cells in a volume of 3 µL. The injection rate was set up to 1 µL/min. The needle was then completely withdrawn from the brain over the course of 4 min (1.0 mm/min), and the skin was sutured. Just

before treatment initiation (5 days after injection), animals were randomized to treatment groups of 7 mice each. Compound **4** and its prodrug **4a** were prepared as suspension in 0.5% methylcellulose solution. Each mouse received every other day oral administration of methylcellulose vehicle, 50 mg/kg of compound **4** or 50 mg/kg of prodrug **4a**. Mice were euthanized when they displayed neurological signs (e.g. altered gait, tremors/seizures, lethargy) or weight loss of 20% or greater of pre-surgical weight. Data were analyzed through Kaplan-Meier curves considering mean and median survival values (Med Calc software, MedCalc Software bvba, Ostend, Belgium). The statistical significance was evaluated by the Logrank test and P values <0.05 were considered statistically significant.

ACKNOWLEDGEMENT

We would like to thank Beatrice Gorelli for the technical support in the pharmacokinetic study herein presented.

References

1. Schenone, S.; Radi, M.; Musumeci, F.; Brullo, C.; Botta, M. Biologically driven synthesis of pyrazolo[3,4-*d*]pyrimidines as protein kinase inhibitors: an old scaffold as a new tool for medicinal chemistry and chemical biology studies. *Chem. Rev.* **2014**, *114*, 7189-7238.
2. Yeatman, T.J. A renaissance for SRC. *Nat. Rev. Cancer* **2004**, *4*, 470-480.
3. Spreafico, A.; Schenone, S.; Serchi, T.; Orlandini, M.; Angelucci, A.; Magrini, D.; Bernardini, G.; Collodel, G.; Di Stefano, A.; Tintori, C.; Bologna, M.; Manetti, F.; Botta, M.; Santucci, A. Antiproliferative and proapoptotic activities of new pyrazolo[3,4-*d*]pyrimidine derivative Src kinase inhibitors in human osteosarcoma cells. *FASEB J*. **2008**, *22*, 1560-1571.
4. Angelucci, A.; Schenone, S.; Gravina, G. L.; Muzi, P.; Festuccia, C.; Vicentini, C.; Botta, M.; Bologna, M. Pyrazolo[3,4-*d*]pyrimidines c-Src inhibitors reduce epidermal growth factor-induced migration in prostate cancer cells. *Eur. J. Cancer* **2006**, *42*, 2838–2845.
5. Tintori, C.; Fallacara, A.L.; Radi, M.; Zamperini, C.; Dreassi, E.; Crespan, E.; Maga, G.; Schenone, S.; Musumeci, F.; Brullo, C.; Richters, A.; Gasparrini, F.; Angelucci, A.; Festuccia, C.; Delle Monache, S.; Rauh, D.; Botta, M. Combining X-ray crystallography and molecular modeling toward the optimization of pyrazolo[3,4-*d*]pyrimidines as potent c-Src inhibitors active in vivo against Neuroblastoma. *J. Med. Chem.* **2015**, *58*, 347-361.
6. Navarra, M.; Celano, M.; Maiuolo, J.; Schenone, S.; Botta, M.; Angelucci, A.; Bramanti, P.; Russo, D. Antiproliferative and pro-apoptotic effects afforded by novel Src-kinase inhibitors in human neuroblastoma cells. *BMC Cancer* **2010**, *10*, 602-614.
7. Ceccherini, E.; Indovina, P.; Zamperini, C.; Dreassi, E.; Casini, N.; Cutaia, O.; Forte, I.M.; Pentimalli, F.; Esposito, L.; Polito, M.S.; Schenone, S.; Botta, M.; Giordano, A. SRC family kinase inhibition through a new pyrazolo[3,4-*d*]pyrimidine derivative as a feasible approach for glioblastoma treatment. *J. Cell. Biochem.* **2015**, *116*, 856-863.

8. Calgani, A.; Vignaroli, G.; Zamperini, C.; Coniglio F.; Festuccia, C.; Di Cesare, E.; Gravina, G.L.; Mattei, C.; Vitale, F.; Schenone, S.; Botta M.; Angelucci A. Suppression of SRC signaling is effective in reducing synergy between glioblastoma and stromal cells. *Mol Cancer Ther.* **2016** *15*, 1535-1544.

9. Casini, N.; Forte, I.M., Mastrogiovanni, G.; Pentimalli, F.; Angelucci, A.; Festuccia, C.; Tomei, V.; Ceccherini, E.; Di Marzo, D.; Schenone, S.; Botta, M.; Giordano, A.; Indovina, P. SRC family kinase (SFK) inhibition reduces rhabdomyosarcoma cell growth in vitro and in vivo and triggers p38 MAP kinase-mediated differentiation. *Oncotarget* **2015**, *6*, 12421-35.

10. Indovina, P.; Giorgi, F.; Rizzo, V.; Khadang, B.; Schenone, S.; Di Marzo, D.; Forte, I.M.; Tomei, V.; Mattioli, E.; D'Urso, V.; Grilli, B.; Botta, M.; Giordano, A.; Pentimalli, F. New pyrazolo[3,4-*d*]pyrimidine SRC inhibitors induce apoptosis in mesothelioma cell lines through p27 nuclear stabilization. *Oncogene* **2012**, *31*, 929-938.

11. Rossi, A.; Schenone, S.; Angelucci, A.; Cozzi, M.; Caracciolo, V.; Pentimalli, F.; Puca, A.; Pucci, B.; La Montagna, R.; Bologna, M.; Botta, M.; Giordano, A. New pyrazolo-[3,4-*d*]-pyrimidine derivative Src kinase inhibitors lead to cell cycle arrest and tumor growth reduction of human medulloblastoma cells. *FASEB J*. **2010**, *24*, 2881-2892.

12. Morisi, R.; Celano, M.; Tosi, E.; Schenone, S.; Navarra, M.; Ferretti, E.; Costante, G.; Durante, C.; Botta, G.; D'Agostino, M.; Brullo, C.; Filetti, S.; Botta. M.; Russo, D. Growth inhibition of medullary thyroid carcinoma cells by pyrazolo-pyrimidine derivates. *J. Endocrinol. Invest.* **2007**, *30*, RC31-4.

13. Radi, M.; Tintori, C.; Musumeci, F.; Brullo, C.; Zamperini, C.; Dreassi, E.; Fallacara, A. L.; Vignaroli, G.; Crespan, E.; Zanoli, S.; Laurenzana, I.; Filippi, I.; Maga, G.; Schenone, S.; Angelucci, A.; Botta, M. Design, synthesis, and biological evaluation of pyrazolo[3,4-*d*]pyrimidines active in vivo on the Bcr-Abl T315I Mutant. *J. Med. Chem.* **2013**, *56*, 5382-5394.

14. Cozzi, M.; Giorgi, F.; Marcelli, E.; Pentimalli, F.; Forte, I.M.; Schenone, S.; D'Urso, V.; De Falco, G.; Botta, M.; Giordano, A.; Indovina, P. Antitumor activity of new pyrazolo[3,4-*d*]pyrimidine SRC kinase inhibitors in Burkitt lymphoma cell lines and its enhancement by WEE1 inhibition. *Cell Cycle*. **2012**, *11*, 1029-1039.
15. Stupp, R.; Mason, WP.; van den Bent, MJ.; Weller, M.; Fisher, B.; Taphoorn, M.J. *et al.* Radiotherapy plus concomitant and adjuvant temozolomide for glioblastoma. *N. Engl. J. Med.* **2005**, *352*, 987-996.
16. Ahluwalia, M.S.; de Groot, J.; Liu, W.M.; Gladson, C.L. Targeting SRC in glioblastoma tumors and brain metastases: rationale and preclinical studies. *Cancer Lett.* **2010**, *298,* 139-149.
17. Dreassi, E.; Zizzari, A. T.; Mori, M.; Filippi, I.; Belfiore, A.; Naldini, A.; Carraro, F.; Santucci, A.; Schenone, S.; Botta, M. 2-Hydroxypropyl-β-cyclodextrin strongly improves water solubility and anti-proliferative activity of pyrazolo[3,4-*d*]pyrimidines Src-Abl dual inhibitors. *Eur. J. Med. Chem.* **2010**, *45*, 5958–5964.
18. Radi, M.; Evensen, L.; Dreassi, E.; Zamperini, C.; Caporicci, M.; Falchi, F.; Musumeci, F.; Schenone, S.; Lorens, J. B.; Botta, M. A combined targeted/phenotypic approach for the identification of new antiangiogenics agents active on a zebrafish model: from in silico screening to cyclodextrin formulation. *Bioorg. Med. Chem. Lett.* **2012**, *22*, 5579-5583.
19. Kerns, E.H.; Di, L. Pharmaceutical profiling in drug discovery. *Drug Discov. Today* **2003**, *8*, 316-323.
20. Di, L.; Kerns, E. H. Profiling drug-like properties in discovery research. *Curr. Op. Chem. Biol.* **2003**, *7*, 402-408.
21. Lipinski, C. A. Drug-like properties and the causes of poor solubility and poor permeability. *J. Pharm. Tox. Methods* **2000**, *44*, 235-249.

22. Vignaroli, G.; Zamperini, C.;Dreassi, E.;Radi, M.;Angelucci, A.;Sanità, P.;Crespan, E.; Kissova, M.; Maga, G.;Schenone, S.;Musumeci, F.;Botta, M. Pyrazolo[3,4-*d*]pyrimidine prodrugs: strategic optimization of the aqueous solubility of dual Src/Abl inhibitors. *ACS Med. Chem. Lett.* **2013**, *4*, 622-626.

23. Vignaroli, G.; Calandro, P.; Zamperini, C.; Coniglio, F.; Iovenitti, G.; Tavanti, M.; Colecchia, D.; Dreassi, E.; Valoti, M.; Schenone, S.; Chiariello, M.; Botta, M. Improvement of pyrazolo[3,4-*d*]pyrimidines pharmacokinetic properties: nanosystem approaches for drug delivery. *Sci. Rep.* **2016**, *6, 21*.

24. Rautio, J.; Kumpulainen, H.; Heimbach, T.; Oliyai, R.; Oh, D.; Järvinen, T.; Savolainen, J. Prodrugs: design and clinical applications. *Nat. Rev.* **2008**, *7*, 255−270.

25. Huttunen, K. M.; Raunio, H.; Rautio, J. Prodrugs-from serendipity to rational design. *Pharmacol. Rev.* **2011**, *63*, 750−771.

26. Schenone, S.; Bruno, O.; Bondavalli, F.; Ranise, A.; Mosti, L.; Menozzi, G.; Fossa, P.; Donnini, S.; Santoro, A.; Ziche, M.; Manetti, F.; Botta, M. Antiproliferative activity of new 1-aryl-4-amino-1*H*-pyrazolo[3,4-*d*]pyrimidine derivatives toward the human epidermoid carcinoma A431 cell line. *Eur. J. Med. Chem*. **2004**, *39*, 939-946.

27. Manetti, F.; Santucci, A.; Locatelli, G.A.; Maga, G.; Spreafico, A.; Serchi, T.; Orlandini, M.; Bernardini, G.; Caradonna, N.P.; Spallarossa, A.; Brullo, C.; Schenone, S.; Bruno, O.; Ranise, A.; Bondavalli, F.; Hoffmann, O.; Bologna, M.; Angelucci, A.; Botta M. Identification of a novel pyrazolo[3,4-*d*]pyrimidine able to inhibit cell proliferation of a human osteogenic sarcoma in vitro and in a xenograft model in mice. *J. Med. Chem.* **2007**, *50*, 5579-5588.

28. Carraro, F.; Naldini, A.; Pucci, A.; Locatelli, G.A.; Maga, G.; Schenone, S.; Bruno, O.; Ranise, A.; Bondavalli, F.; Brullo, C.; Fossa, P.; Menozzi, G.; Mosti, L.; Modugno, M.; Tintori, C.; Manetti, F.; Botta, M. Pyrazolo[3,4-*d*]pyrimidines as potent antiproliferative and proapoptotic agents

toward A431 and 8701-BC cells in culture via inhibition of c-Src phosphorylation. *J. Med. Chem.* **2006**, *49*, 1549-1561.

29. Radi, M.; Brullo, C.; Crespan, E.; Tintori, C.; Musumeci, F.; Biava, M.; Schenone, S.; Dreassi, E.; Zamperini, C.; Maga, G.; Pagano, D.; Angelucci, A.; Bologna, M.; Botta, M. Identification of potent c-Src inhibitors strongly affecting the proliferation of human neuroblastoma cells. *Bioorg. Med. Chem. Lett.* **2011**, *21*, 5928-5933.
30. Pinney, K.G.; Miranda, M.G.; Dorsey, J.M. Preparation of piperazine or piperidine derivatives as serotonin reuptake inhibitors acting at both the transporter and receptors. U.S. Pat. Appl. Publ. **2012**/0016124.
31. Botta, M.; Angelucci, A.; Dreassi, E.; Schenone, S.; Tintori, C.; Vignaroli, G. Preparation of 4-amino-substituted pyrazolo[3,4-*d*]pyrimidine and pyrrolo[2,3-*d*]pyrimidine derivative as the Src family kinases. WO 2016066755.
32. Tintori, C.; Magnani, M.; Schenone, S.; Botta, M. Docking, 3D QSAR studies and in silico ADME prediction on c-Src tyrosine kinase inhibitors. *Eur. J. Med. Chem.* **2009**, *44,* 990-1000.
33. Bjerrum, J.; Schwarzenbach, G.; Sillen, L. G. Stability constants. Part I: Organic ligands; Chemical Society Special Publication No. 6; The Chemical Society: London, U.K., **1957**.
34. Slatter, J.G.; Schaaf, L.J.; Sams, J.P.; Feenstra, K.L.; Johnson, M.G.; Bombart, P.A.; Cathcart, K.S.; Verbug, M.T.; Pearson, L.K.; Compton, L.D.; Miller, L.L.; Baker, D.S.; Pesheck, C.V.; Lord, R.S. Pharmacokinetics, metabolism, and excretion of irinotecan (CPT-11) following I.V. infusion of [14C]CPT-11 in cancer patients. *Drug Metab. Dispos.* **2000**, *28*, 423−433.
35. Bradford, M.M. A rapid and sensitive method for the quantitation of microgram quantities of protein utilizing the principle of protein-dye binding. *Anal. Biochem.* **1976**, *72*, 248-54.
36. Wohnsland, F.; Faller, B. High-throughput permeability pH profile and high-throughput alkane/water log P with artificial membranes. *J. Med. Chem.* **2001**, *44*, 923-930.

SECTION 4

‘PLASMIN-ACTIVATED PYRAZOLO[3,4-*d*]PYRIMIDINES PRODRUGS: A NEW STRATEGY OF DRUG DELIVERY’

4.1 INTRODUCTION

A persistent problem in cancer chemotherapy is the low therapeutic index of most anticancer drugs. An approach to overcome this problem is to design anticancer "prodrugs" which are inactive until locally activated by some tumor-associated enzyme.[140] Tumors that contain a high level of some specific enzyme could convert the prodrug into the pharmacologically active drug close to the tumor.[141,142] In this purpose, proteases such as plasmin, are known to participate and collaborate in tumor invasion and metastasis and are one of the most useful family of enzymes.

4.1.1 PROTEASES

Proteases are enzymes that perform proteolysis, thus effecting protein catabolism by hydrolysis of peptidic bonds. Proteases are currently classified into six groups:

Serine proteases;

Threonine proteases;

Cysteine proteases;

Aspartate proteases;

Glutamic acid proteases;

Metalloproteases.

4.1.1.1 SERINE PROTEASES

In particular, serine proteases use a serine residue as a nucleophile to attack the carbonyl group of a peptidic bond, which thus is cleaved. On the basis of their structure they can be further divided in two groups:
Chymotrypsin-like serine proteases, then subdivided in chymotrypsin-, trypsin- and elastase-like; Subtilisin-like serine proteases.
The family of trypsin-like serine proteases contains more than 70 members, involved in many physiological and pathological processes.
Although, all of them cleave their substrates after the basic amino acids arginine or lysine and there are big differences in their substrates specificities: in fact, some of them are highly specific towards very few natural substrates, while others can hydrolize a variety of substrates.

4.1.1.2 FUNCTIONS OF PROTEASES

Proteases are thought to play a primary role in the dissolution of the extracellular matrix that is necessary for the passage of migrating cells through tissue barriers in a diversity of biological processes. The migration and invasion of cells in physiological situations, such as embryo morphogenesis, angiogenesis, wound healing and other processes involving tissue destruction and remodelling, is of limited extent and duration and therefore must be subject to strict regulation to initiate, localize, and terminate the proteolytic activity. The same proteolytic enzyme systems are also thought to contribute to the invasive properties and metastatic potential of malignant tumor cells. Among the proteases involved in these processes, plasmin and its generation by plasminogen activators plays a key role.

4.1.2 PLASMIN

The plasmin system is recognized to play a key role in tumor invasion and metastasis by its matrix degradation activity and its involvement in tumor growth factor activation and angiogenesis.[143] In

fact, active plasmin catalyzed the breakdown of extracell matrix proteins and, thus, contributes to migration, invasion and metastasis of tumor cells. In the body plasmin is predominantly present in its inactive pro-enzyme form plasminogen. Active plasmin is formed locally at or near the surface of tumor cells by urokinase-type plasminogen ativators (u-PA) produced by cancer and/or stroma cells.[144] Plasmin activity is kept localized because cell-bound urokinase can activate cell-bound plasminogen into active plasmin, which stay cell-bound. Active urokinase and active plasmin do not occur in the blood circulation because they are rapidly inhibited by PAI and α_2-antiplasmin respectively.
Many tumor cell lines have significantly higher u-PA level than that of their normal counterparts[145] and u-PA was shown to be correlated with invasive behaviour and to be strong prognostic factors for reduced survival and increased relapse in many types of tumors. Thus, plasmin is a very promising enzyme for exploitation in a tumor specific prodrugs approach because the proteolytically active form is localized at the tumor level. Moreover, it is possible to design highly specific substrates for plasmin incorporating short peptides sequences that can be selectively cleaved by plasmin.

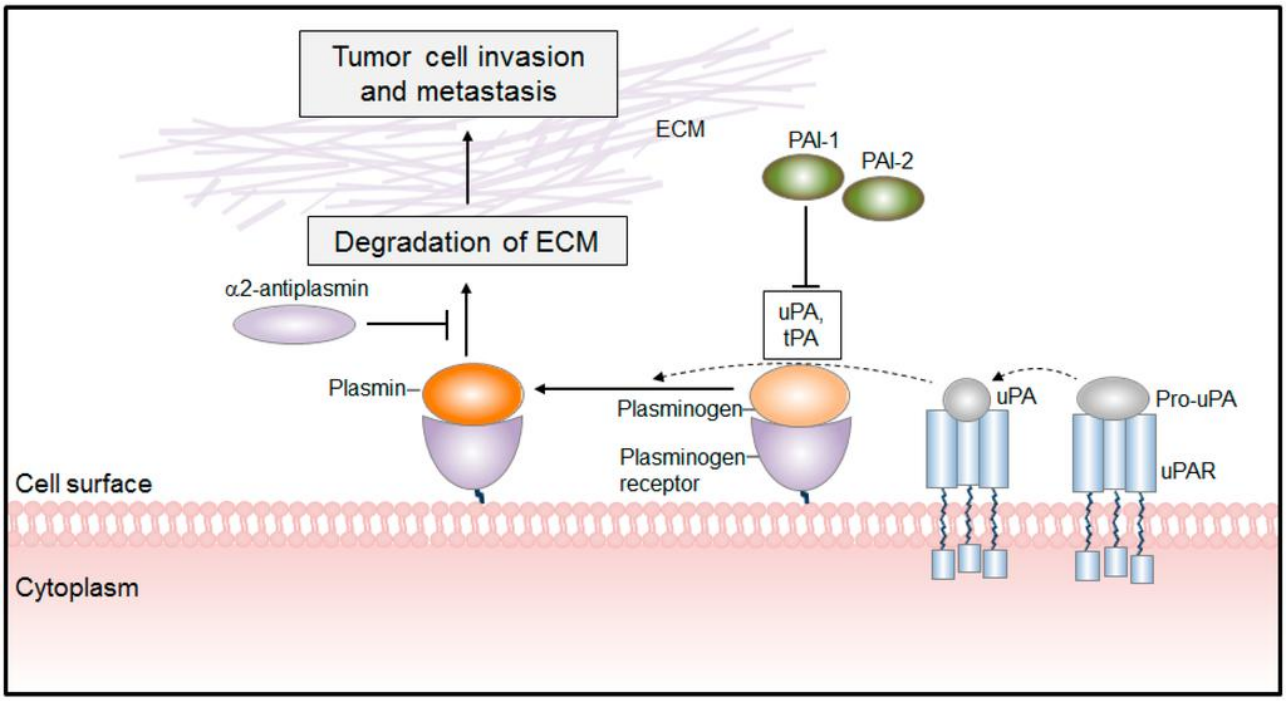

Figure 21: Schematic illustration of the plasminogen activator system

D-Ala-Phe-Lys is the amino acid sequence substrate of plasmin (**D-Ala-Leu-Lys** or **D-Ala-Phe-Lys** play the same role).[146] This protease has high affinity to the different tripeptides due to the presence of a specific reactive site for the proteolytic cleavage of Lys. This strategy, can allow the release of the drug close to tumor cells only, after the interaction with the plasmin protease.[147]
In this context we discovered a prodrugs approach by the inclusion of **D-Ala-Phe-Lys** peptide that acted as driving group for specific target involved in tumor processes.
Moreover, this strategy was also studied to increase the solubility of pyrazolo[3,4-*d*]pyrimidines. This problem, as already discussed, limiting significantly the development of our molecules. Including a peptide portion would be possible to improve also this aspect.

4.2 AIM OF THE PROJECT

SI113 was the selected compound to develop a **plasmin-activated pyrazolo[3,4-*d*]pyrimidines prodrugs**.
In fact as mentioned before, **SI113** showed an interesting activity profile against hepatocellular carcinoma (HCC), where the enzyme plasmin is overexpressed.[139]
First of all the pyrazolo[3,4-*d*]pyrimidine **SI113** and the peptide portion were synthesized.
After several studies, the ester function was chosen to connect the **D-Ala-Phe-Lys tripeptide** (**TP**) with **SI113**.
This hydrolizable group allows the release of the drug close to tumor cells only, after the interaction with the plasmin protease: the sequence is selectively cleaved by proteases at the level of lysine and the parent drug can be selectively generate at the target site, with a decrease of system toxicity.
In order to verify the rate of hydrolysis in human plasma by the esterase and determine the cleavage by plasmin at its active site we have synthesized two kinds of prodrugs.

PROSI113-LKTP, four carbon atoms were introduced as linker (**LK**) between the tripeptide (**TP**) and drug **SI113**. The prodrug synthesized was defined by 5 portions (**Figure 22**):
-D-Ala-Phe-Lys tripeptide (**TP**): amino acid sequence substrate of the enzyme plasmin;

-PLASMIN ACTIVE SITE: this Lys bond is known as active site where the plasmin explains its hydrolytic action;

-LINKER (**LK**): allows the access of plasmin to its active site;

-HYDROLIZABLE GROUP: permits the finally release of the drug by esterase interaction;

-DRUG: to carry out the pharmacological activity.

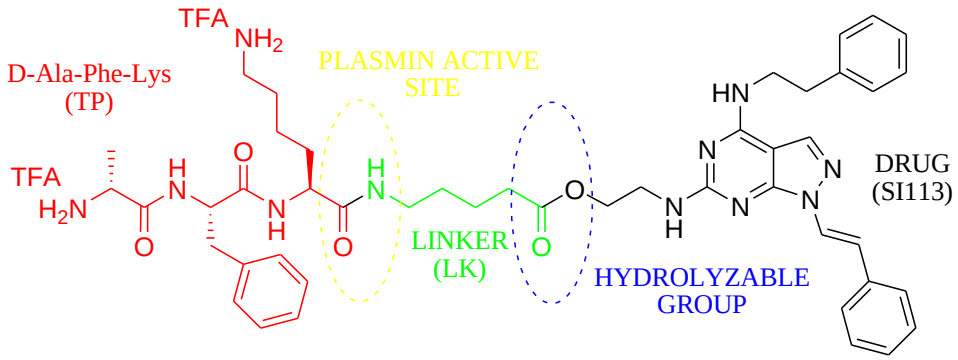

Figure 22: Portions of **PROSI113-LKTP**

PROSI113-TP, D-Ala-Phe-Lys tripeptide (**TP**) is directly connected to **SI113** with an ester group (**Figure 23**).
In this case the hydrolizable group can be cleaved by the plasma esterase, but also represents the plasmin active site where the enzyme explains its hydrolytic action.

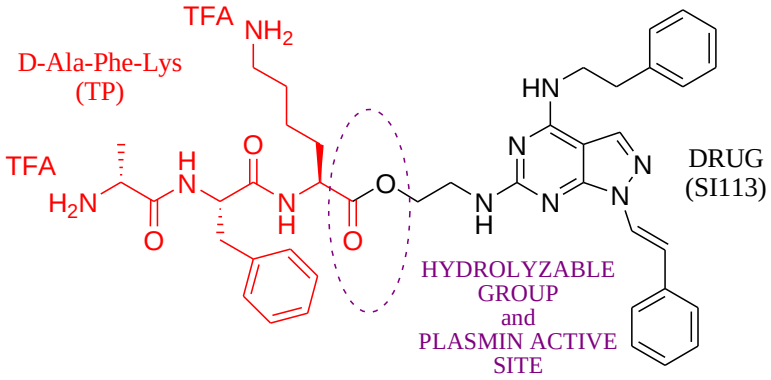

Figure 23: Portions of **PROSI113-TP**

The ADME property of both prodrugs **PROSI113-TP** and **PROSI113-LKTP** (plasma and plasmin half-life, ability to overcome biological membranes, metabolic stability, water solubility) were analyzed in comparison to the drug **SI113**.

Furthermore, the synthesized compounds were tested in a cellular assay with hepatocellular carcinoma HepG2 cell line. *In vitro* cytotoxicity was also determinated by pre-incubation of the cell with plasmin.

Based on obtained results, *in vivo* experiments in xenograft mouse models of hepatocellular carcinoma and in *vivo* studies of pharmacokinetics are ongoing.

4.3 SYNTHETIC STRATEGY

For the preparation of **SI113** we followed the synthetic pathway set up in our laboratories,[148] summarized in **Scheme 1**.

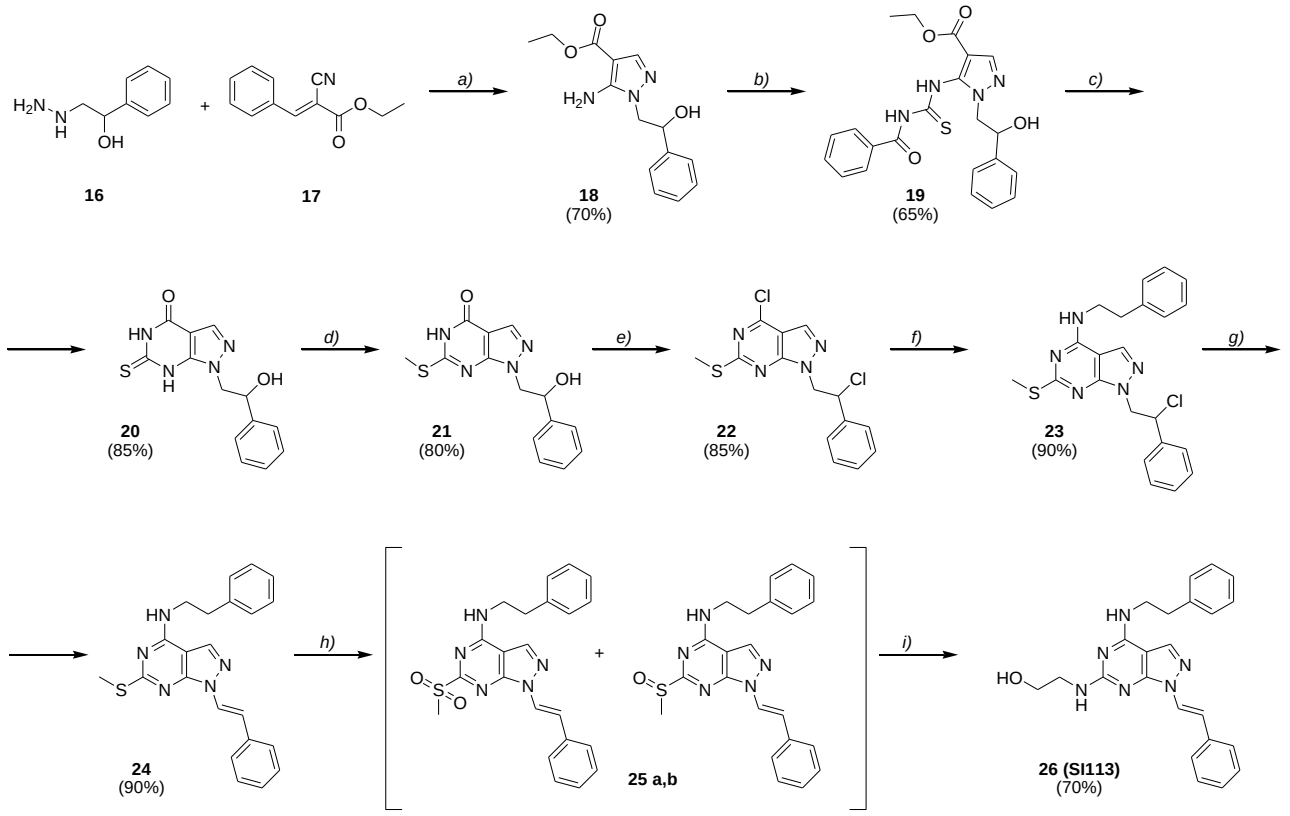

Reagents and conditions: *a)*tol. dry, 80°C, 6h *b)*benzoyl isothiocyanate, THF dry, ref., o.n. *c)*NaOH, 100°C, CH_3COOH *d)*iodomethane, THF dry, ref., 48h *e)*$POCl_3$, DMF dry, $CHCl_3$ dry, ref., 8h *f)*2-phenylethanamine, tol. dry, r.t., 48h *g)*NaOH, 95% EtOH, ref., o.n. *h)*m-CPBA, $CHCl_3$ r.t., 1h *i)*2-aminoethanol, butan-1-ol/DMSO, 90°C, 48h.

Scheme 1: Preparation of **SI113**

The synthetic approach following for the preparation of the tripeptidyl portion is summarized in **Scheme 2**.

H-Lys(Z)-OH methylester hydrochloride, obtain by treatment of H-Lys(Z)-OH with $SOCl_2$ in MeOH, was coupled with Boc-Phe-OH using EDC.HCl/DMAP as activating system. Dipeptide **3** was then N-deprotected with TFA dry affording **4** that was coupled with Boc-D-Ala-OH in the presence, also in this case, of EDC.HCl/DMAP. The carbobenzyloxyl moiety was then cleaved by hydrogenation. In conclusion, the reaction of the tripeptidyl intermediate **6** with Boc_2O and NaOH 5% led to the formation, after pH adjustment to 5, of the desired tripeptide (**TP**) **7**.

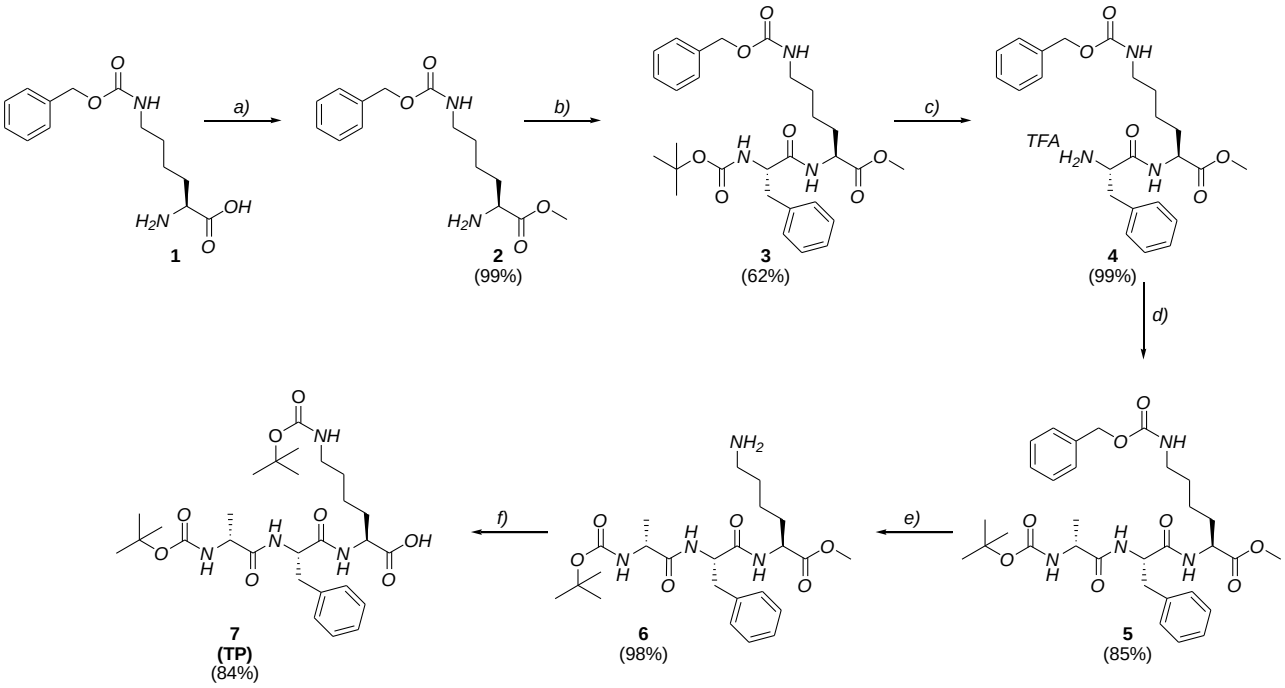

Reagents and conditions: *a)*$SOCl_2$, MeOH, r.t., o.n *b)* Boc-Phe-OH, DMAP, EDC.HCl, CH_2Cl_2 dry, r.t., o.n. *c)*TFA, CH_2Cl_2 dry, r.t., 1h *d)*Boc-D-Ala-OH, DMAP, EDC.HCl, CH_2Cl_2 dry, r.t., o.n. *e)*H_2, Pd/C 10%, MeOH, HCl conc., r.t., 12h *f)*Boc_2O, THF, NaOH 5%, r.t., o.n.

Scheme 2: Preparation of tripeptide portion (**TP**)

The intermediate **10** was synthesized through coupling reaction: the **TP 7** was activated for 30 minutes using EDC.HCl/DMAP, after **SI113** was added and the reaction mixture was stirred at room temperature for 72 hours. Finally the N-deprotection was performed with TFA affording the desired product **PROSI113-TP** (**11**) with 99% yield (**Scheme 3**).

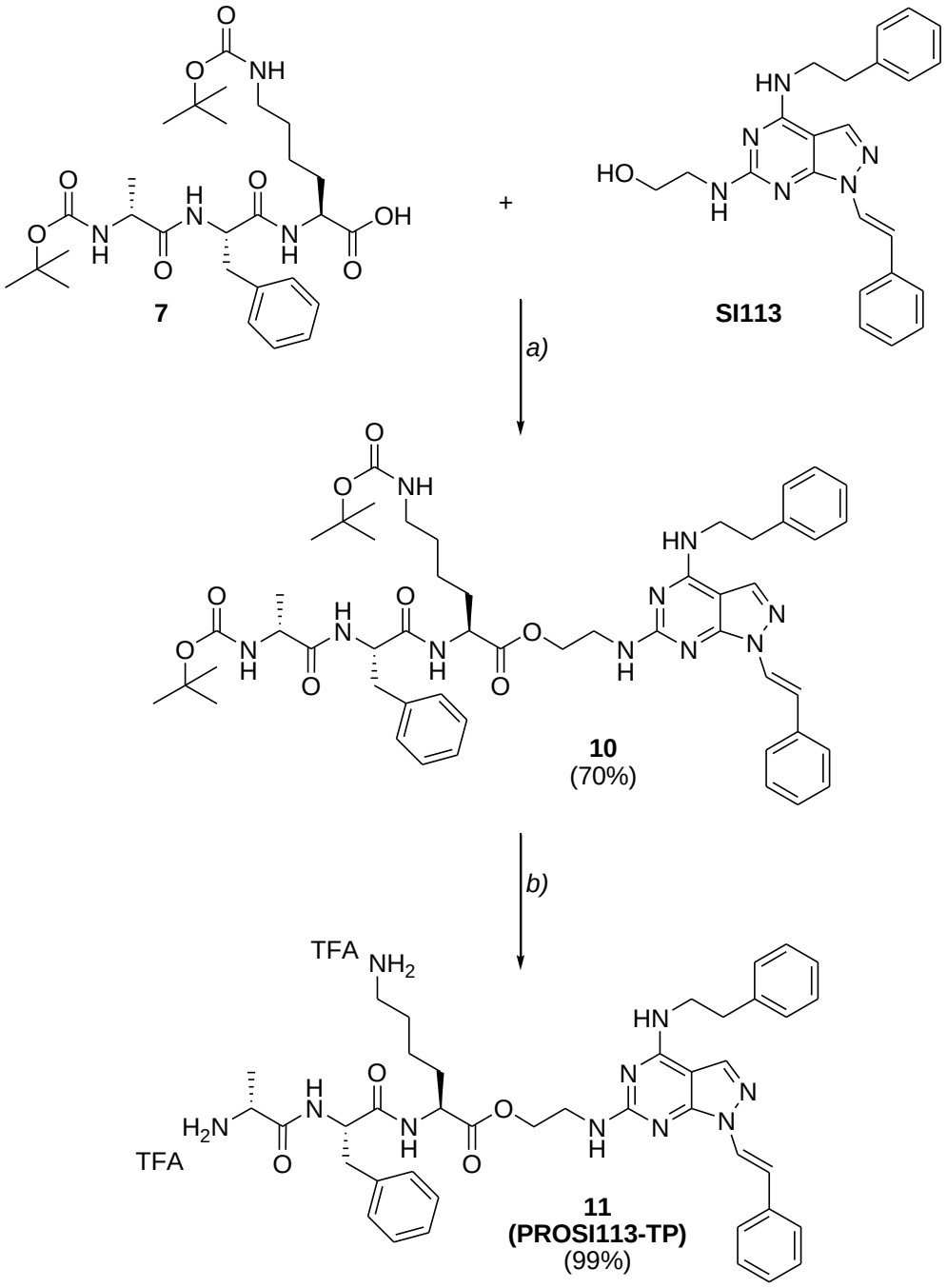

Reagents and conditions: *a)* EDC.HCl, CH_2Cl_2 dry, r.t., o.n. *b)* TFA, CH_2Cl_2 dry, r.t., 3h.

Scheme 3: Preparation of **PROSI113-TP**

The ethyl 5-aminopentanoate hydrochloride (**LK, 9**) was obtained with 99% yield starting from the 5-aminovaleric acid (**8**) and $SOCl_2$ in anhydrous EtOH (**Scheme 4**).

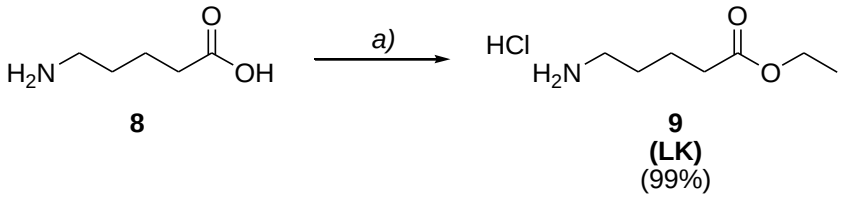

8 **9** **(LK)** (99%)

Reagents and conditions: *a)*$SOCl_2$, EtOH dry, r.t., 12h.

Scheme X: Preparation of linker (**LK)**

Then **LK** (**9**) was coupled with **TP** (**7**) in presence of EDC.HCl/DMAP and subsequently O-deprotected using a solution of 5% NaOH obtaining the derivative **13** (**LKTP**), (**Scheme 5**).

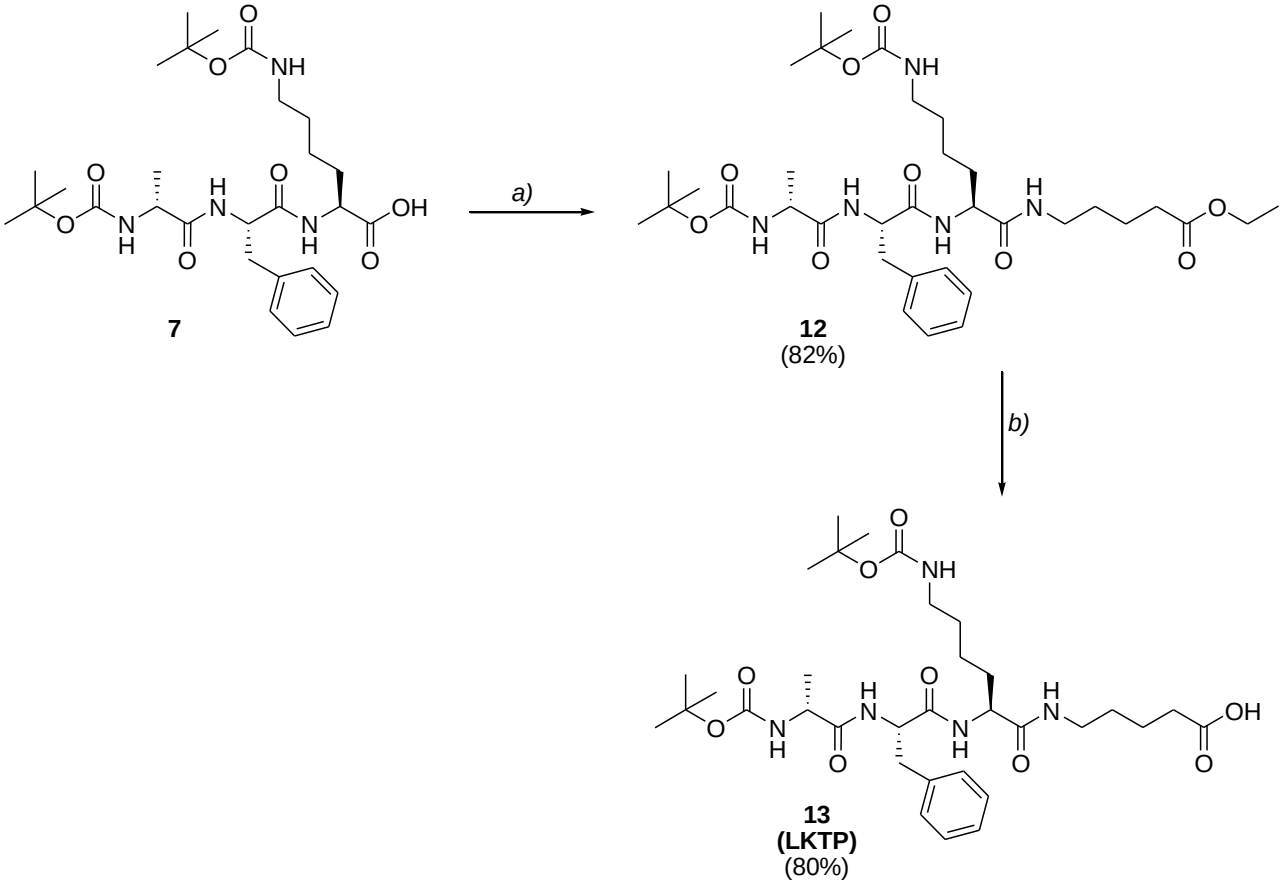

7 **12** (82%) **13** **(LKTP)** (80%)

Reagents and conditions: *a)* LK (9), EDC.HCl, CH_2Cl_2 dry, r.t., o.n. *b)* TFA, CH_2Cl_2 dry, r.t., 3h.

Scheme 5: Preparation of **LKTP**

In order to synthesize **PROSI113-LKTP** the same synthetic approach used for the other prodrug was applied: **LKTP** (**13**) was coupled with **SI113** using EDC.HCl/DMAP as activating system to give the intermediate **14** protected. The latter was then reacted with TFA affording the desired product **PROSI113-LKTP** (**15**) with 99% yield (**Scheme 6**).

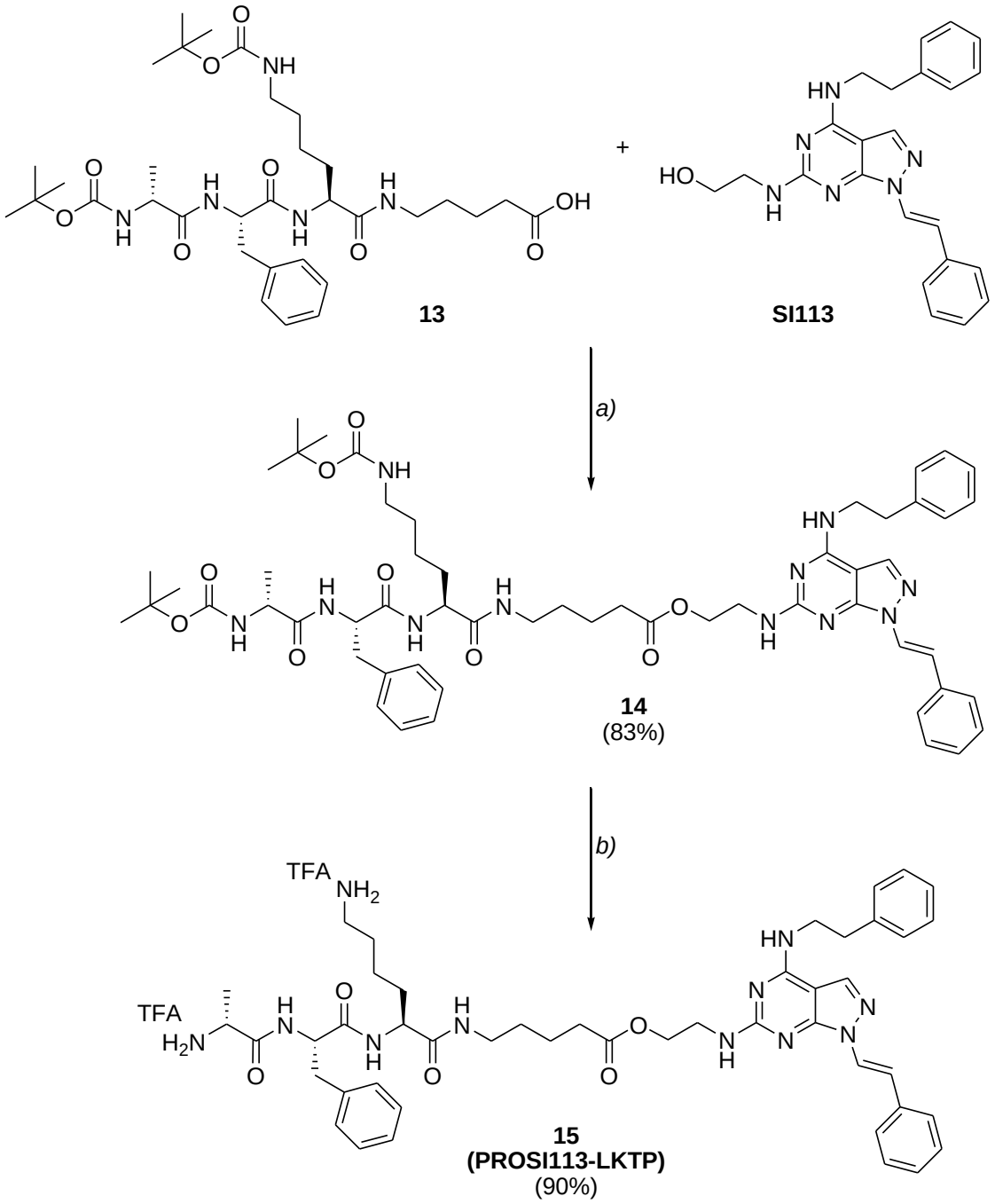

Reagents and conditions: *a)* EDC.HCl, CH_2Cl_2 dry, r.t., o.n. *b)* TFA, CH_2Cl_2 dry, r.t., 3h.

Scheme 6: Preparation of **PROSI113-LKTP**

4.4 *IN VITRO* ADME ASSAYS

Several *in vitro* assays were performed to evaluate the ADME properties of the synthesized prodrugs (**PROSI113-TP** and **PROSI113-LKTP**) and to compare them to their parent drug (**SI113**).
Initially, the stability in several media [Tris-buffer (Tris), methanol (MeOH) and dimethyl sulfoxide (DMSO)] was studied (**Table 2**).
After the rate of hydrolysis in Human Plasma (Plasma) and Human Plasmin (Plasmin) were investigated in order to understand the release ability of the active compound.(**Table 3**) In fact, our prodrugs display an ester group (**PROSI113-TP**) or an ester and an amide group (**PROSI113-LKTP**) that should undergo *in vivo* hydrolysis.
Moreover, the water solubility and the apparent permeability (PAMPA) towards gastrointestinal membrane (GI) were investigated, as well as the stability in the presence of human liver microsomes (HLM) (**Table 4**).

Cpd	Tris $t_{1/2}$ (h)[a]	MeOH $t_{1/2}$ (h)[a]	DMSO $t_{1/2}$ (h)[a]
PROSI113-TP	>48	>48	>48
PROSI113-LKTP	>48	>48	>48

Table 2: Stability of prodrugs in polar media

Stability in polar media such as TRIS-buffer, methanol and dimethyl sulfoxide were analyzed by UV/LC-MS, after dissolving the compound in the appropriate media. Resulting half-lives were greater than 48 h for both prodrugs (**Table 2**).
These were determined in order to evaluate the contribution of chemical hydrolysis by the polar media to the overall rate of hydrolysis in plasma or in plasmin. These values indicated the good stability of these compounds, which were thus regarded as chemically stable for the subsequent studies.

Cpd	PLASMA HYDROLYSIS (%) T1/2 (h)	PLASMIN HYDROLYSIS (%) T1/2 (h)
PROSI113-TP	65	40
	0.3	1.5
PROSI113-LKTP	35	64
	4.3	3.1

Table 3: Stability of prodrugs in Human Plasma and Human Plasmin

In order to verify the ability of **PROSI113-TP** (**11**) and **PROSI113-LKTP** (**15**) to release the corresponding parent drug **SI113**, both prodrugs were incubated at 37 °C in human plasma or plasmin for 24 h (following a procedure described by de Groot).[149] The disappearance of the substrate and the consequent formation of the drug, was monitored by UV/LC-MS (**Table 3**).
The determination proved for **PROSI113-TP** (this compound present only ester as hydrolyzable group), fast conversion in the parent drug in plasma ($T_{1/2}$ = 0.3 h) and lower plasmin hydrolysis at

24 h (40%) while maintaining a good half-life time ($T_{1/2}$ = 1.5 h). This can be explained by an increased affinity for plasma esterases.
Instead, **PROSI113-LKTP** (presents two hydrolyzable sites) showed 35% of hydrolysis in plasma with an half-life value of 4.3 h and 64% of hydrolysis in presence of the plasmin with an half-life of about 4 h. In this case, higher percentage of hydrolysis with plasmin was obtained but the half-life values in plasma and plasmin were comparable. This behaviour may be due to the greater hinderance at the two active site. Both enzymes need more time to carry out its hydrolytic action, justifying the comparable values of $T_{1/2}$ associated with different rates of hydrolysis.

Subsequently thermodynamic solubility was tested in water by adding 1 mL of H_2O to 1 mg of each compound; the resulting mixture was then shaken at ambient temperature for 24 h. The concentration of compounds (**PROSI113-TP**, **PROSI113-LKTP** and **SI113**) was determined by LC−MS-MS, following filtration through a 0.45 μm nylon filter.[150] Both prodrugs, when compared to its parent drug **SI113**, showed an encouraging enhancement of water solubility. In fact, the solubility increased from 0.04 to >1000 μg mL^{-1}(**Table 4**), thus demonstrating that this prodrug approach could be also the correct choice for overcoming the lack of water solubility of these types of compounds.

Regarding to PAMPA GI assay (**Table 4**), as expected by the significant increased hydrophilicity, both prodrug showed a decrease of ability to overcome biological membranes, respect to the parent drug SI113.

To study CYP-metabolism, compounds **SI113**, **PROSI113-TP** and **PROSI113-LKTP** were incubated for one hour at 37 °C with a solution of man-pooled HLM. After this time, the percentage of prodrugs and metabolites was determined by UV/LC-MS. The percentage of unmodified compound recovered after the incubation was ≥95% for each molecule. (**Table 4**)

CPD	Water Solubility (μg/mL)	PAMPA GI (10^{-6} cm^2/sec) MR[a] (%)	Metabolic Stability[b] (%)
SI113	0.4	2.6 (86,2)	≥95%
PROSI113-LKTP	>1000	0.2 (0)	≥95%
PROSI113-TP	>1000	0.2 (0)	≥95%

[a]Membrane Retention (MR) expressed as percentage of compound unable to reach the acceptor compartment. [b]Expressed as percentage of unmodified compound

Table 4: Apparent permeability, water solubility and metabolic stability of parent compound and prodrugs.

4.5 *IN VITRO* BIOLOGICAL ASSAYS

Cellular assays were performed using the hepatocellular carcinoma (HCC) cell line HepG2 cells in order to characterize the cytotoxicity of the prodrugs and their parent active compound. Cells were treated for 24, 48 and 72 h with increasing concentrations of the compounds (0.1 µM, 1 µM, 10 µM, 100 µM). In order to verify if prodrugs could be activated by plasmin, *in vitro* cytotoxicity assays have been also performed in presence of the enzyme. In this case cells were incubated with increasing concentrations of our compounds (0.1 µM, 1 µM, 10 µM, 100 µM).and plasmin (final concentration 15 µg/mL) for 24h h. Finally IC_{50} values were calculated as reported in the experimental section.(**Table 5**).

CPD	HepG2 IC_{50} µM 24h	HepG2 IC_{50} µM 48h	HepG2 IC_{50} µM 72h	HepG2+plasmin IC_{50} µM 24h
SI113	25.63	5.22	3.97	16.55
PROSI113-LKTP	28.49	23.53	23.55	33.70
PROSI113-TP	22.69	16.16	16.53	7.41

Table 5: Cellular assays of **SI113**, **PROSI113-LK** and **PROSI113-LKTP**

As expected, both prodrugs were less active than drug **SI113** at 24, 48 and 72 h.
In presence of the plasmin an improvement of activity for **PROSI113-TP** was obtained (**Table 5**).
Instead, compared to assays performed without plasmin, for **PROSI113-LKTP**, a cytotoxicity of the same order of magnitude was shown. A possible explanation is that the steric hindrance could hurdle the access of hydrolytic enzyme, as also occurred in the previous hydrolysis assays.

4.6 CONCLUSION

In conclusion, in this study we have synthesized and developed two kind of plasmin-activated pyrazolo[3,4-*d*]pyrimidines prodrugs by the inclusion of a small peptide: **PROSI113-TP** and **PROSI113-LKTP**. The analysis of thermodynamic solubility demonstrated the enhanced of water solubility for each prodrugs in comparison to the respective drug **SI113**, validating this approach as an excellent strategy to overcome the poor water solubility of pyrazolo[3,4-*d*]pyrimidines. The synthesized prodrugs also showed a good metabolic stability.
Both prodrugs displayed a decrease of ability to overcome biological membranes, respect to the parent drug. This feature makes them not suitable for oral bolus but this could be overcome by intravenous administration of these compounds.
The ability to release the active compound from each prodrugs was confirmed by the hydrolysis assays in plasmin and by biological evaluation performed after incubation of HepG2 cells in the presence of the same enzyme.
Furthermore, the cellular assays showed a good activity profile on the hepatocellular carcinoma cells.
To further investigate if the preparation of these pyrazolo[3,4-*d*]pyrimidines prodrugs is an effective strategy to enhance the pharmacokinetic properties and to increase selectivity toward cancer overexpressing plasmin, *in vivo* pharmacokinetic studies and orthotopic xenograft model are required. These experiments are currently in progress.
To date, the results obtained, including the remarkable increase of solubility in water of our molecules, make this approach interesting to further investigation.

4.7 EXPERIMENTAL SECTION

4.7.1 CHEMISTRY

All commercially available chemicals were used as purchased from Sigma Aldrich. CH_2Cl_2, was dried over sodium hydride, while MeOH and EtOH where dried over magnesium and iodine as indicator. Anhydrous reactions were run under a positive pressure of dry N_2. TLC was carried out using Merck TLC silica gel 60 F254. Chromatographic purifications were performed on columns packed with Merck silica gel 60, 23-400 mesh, for flash technique. 1H NMR and 13C NMR spectra were recorded at 400 MHz on a Bruker Avance DPX400. Chemical shifts are reported relative to tetramethylsilane at 0.00 ppm. Mass spectra (MS) data were obtained using an Agilent 1100 LC/MSD VL system (G1946C) with a 0.4 mL/min flow rate using a binary solvent system of 95/5 = MeOH/H2O. UV detection was monitored at 254 nm. MS were acquired in positive and negative mode scanning over the mass range 100-1500. The following ion source parameters were used: drying gas flow, 9 mL/min; nebulizer pressure, 40 psi; drying gas temperature, 350 °C. All target compounds possessed a purity of ≥95% verified by UV/LC-MS. LC, analysis were performed by Agilent 1100 LC/MSD VL system (G1946C) (Agilent Technologies, Palo Alto, CA) constituted by a vacuum solvent degassing unit, a binary high-pressure gradient pump, a 1100 series UV detector and a 1100 MSD model VL benchtop mass spectrometer. The Agilent 1100 series mass spectra detection (MSD) single-quadrupole instrument was equipped with the orthogonal spray API-ES (Agilent Technologies, Palo Alto, CA). Nitrogen was used as nebulizing and drying gas. The pressure of the nebulizing gas, the flow of the drying gas, the capillary voltage, the fragmentor voltage and the vaporization temperature were set at 40 psi, 9 L/min, 3000 V, 70 V and 350 °C, respectively. UV detection was monitored at 254 nm. The HPLC-ESI-MS determination was performed by operating the MSD in the positive ion mode. Spectra were acquired over the scan range m/z 105-1500 using a step size of 0.1 u. Chromatographic analysis were performed using a Phenomenex Kinetex C18-100A column (150 x 4.6 mm, 5 μm particle size) at room temperature. Analysis were carried out using gradient elution of a binary solution; (eluent A: ACN, eluent B: Water, both eluents were acidified with formic acid 0.1%). The analysis started with 5% of A (from t = 0 to t = 3 min), then A was increased to 95% (from t = 3 to t = 12 min), then kept at 95% (from t = 12 to t = 20 min) and finally return to 5% of eluent A in 1.0 min. The analysis were performed at a flow rate of 0.6 mL/min with 20 μL as injection volume.

Compound **SI113** was synthesized as previously published by our group.[148]

benzyl (S)-5-(methoxycarbonyl)-5-aminopentylcarbamate hydrochloride (2)
H-Lys(Z)-OH (0.500 g, 0.001786 mol) was suspended in anhydrous MeOH (17 mL). At 0°C, $SOCl_2$ (0.257 mL, 0.003571 mol) was added dropwise and the reaction mixture was stirred overnight at room temperature. The volatiles were then removed under reduced pressure, affording **2** as a white solid without any further purification (0.580 g, Yield: 99%).
1H NMR (400 MHz, MeOD-d4): δ (ppm)= 7.39 (m, 5H), 5.10 (s, 2H), 4.78 (br s, 2H, NH_2 disappears with D_2O), 3.75 (s, 3H), 3.16 (m, 2H), .1.74 (m, 1H), 1.72 (m 1H) 1.68 (m, 2H), 1.56 (m, 2H).
MS (ESI): m/z 295 $[M+H]^+$

(9S,12S)-methyl 12-benzyl-16,16-dimethyl-3,11,14-trioxo-1-phenyl-2,15-dioxa-4,10,13-triazaheptadecane-9-carboxylate (3)
To a solution of **2** (1.178 g, 0.003570 mol) in anhydrous CH_2Cl_2 (35 mL) DMAP (0.740 g, 0.006068 mol), EDC.HCl (1.028 g, 0.005355 mol) and Boc-Phe-OH (0.946 g, 0.003570 mol) were added. The reaction mixture was stirred overnight at room temperature. Then the solvent was

removed under reduced pressure and the crude residue was purified by flash chromatography (AcOEt:PE from 1:2 to 2:1) affording **3** as a white solid (1.196 g, Yield: 62%).
1H-NMR (400 MHz, MeOD-d4): δ (ppm)= 7.31-7.24 (m, 10H), 5.06 (s, 2H), 4.42 (m, 2H), 3.65 (s, 3H), 3.10-3.07 (m, 3H), 2.82-2.76 (m, 1H), 1.80 (m, 1H), 1.68 (m, 1H), 1.48 (m, 2H), 1.33 (s, 9H.), 1,31 (m, 2H).
13C-NMR (100 MHz, MeOD-d4) δ (ppm)= 177.0; 176.5; 161.6; 160.1; 141.2; 133.1; 131.9; 131.6; 131.1; 1030.1; 83.2; 69.9; 59.7; 56.2; 55.2; 44; 41.7; 34.9; 32.8; 31.4; 26.5.

(S)-methyl 2-((S)-2-amino-3-phenylpropanamido)-6-(benzyloxycarbonylamino)hexane-trifluoroacetate (4)
To a solution of **3** (0.127 g, 0.000234 mol) in anhydrous CH_2Cl_2 (2 mL) trifluoroacetic acid (1.5 mL) was added and the reaction mixture was stirred at room temperature for 1h. The volatiles were then removed under reduced pressure and the crude was washed with toluene, affording **4** as a white solid without any further purification (0.130 g, Yield: 99%).
1H-NMR (400 MHz, MeOD-d4) δ (ppm)= 7.37-7.32 (m, 10H), 5.07 (s, 2H), 4.47(m, 1H), 4.17 (m, 1H), 3.69 (s, 3H), 2.30-3.27 (m, 1H), 3.13-3.11 (m, 3H), 1.83 (m, 1H), 1.75 (m, 1H), 1.52 (m, 2H), 1.39 (m, 2H).
MS (ESI): m/z 442 $[M\text{-}TFA+H]^+$

(9S,12S,15R)-methyl 12-benzyl-15,19,19-trimethyl-3,11,14,17-tetraoxo-1-phenyl-2,18-dioxa-4,10,13,16-tetraazaicosane-9-carboxylate (5)
To a solution of **4** (0.525 g, 0.000946 mol) in anhydrous CH_2Cl_2 (9 mL) DMAP (0.231 g, 0.001892 mol) EDC.HCl (0.272 g, 0.001419 mol) and. Boc-D-Ala-OH (20, 0.179 g, 0.000946 mol) were added. The reaction mixture was stirred overnight at room temperature. Then the solvent was removed under reduced pressure and the crude residue was purified by flash chromatography (AcOEt:PE 1:2) affording **5** as a white solid (0.496 g, Yield: 85%).
1H-NMR (400 MHz, MeOD-d4) δ (ppm)= 7.33-7.12 (m, 10H), 5.03 (s, 2H), 4.60 (m, 1H), 4.34 (m, 1H), 3.91 (m, 1H), 3.64 (s, 3H), 3.28 (m, 1H), 3.10-3.08 (m, 2H), 2.89-2.83 (m, 1H), 1.81 (m, 2H), 1.47 (m, 2H), 1.38 (m, 13H (9H+2H+2H)), 1.06 (m, 3H).
13C-NMR (100 MHz, MeOD-d4) δ (ppm)=173.3, 171.1, 156.4, 154.9, 135.8, 128.8, 126.7, 124.34, 77.9, 64.5, 51.3, 49.2, 46.8, 45.9, 29.5, 27.5, 25.9, 21.4, 15.2.
MS (ESI): m/z 613 $[M+H]^+$

(6R,9S,12S)-methyl 16-amino-9-benzyl-2,2,6-trimethyl-4,7,10-trioxo-3-oxa-5,8,11-triazahexadecane-12-carboxylate (6)
To a solution of **5** (1.125 g, 0.001835 mol) in anhydrous MeOH (28 mL) Pd/C 10% (0.195 g, 0.000183 mol) and HCl conc. (2 drops) were added The reaction mixture was stirred under H_2 pressure at room temperature for 12 hours. After filtration over celite and evaporation of the solvent under reduced pressure, the desired **6** was obtained as a white solid without any further purification (0.866 g, Yield: 98%).
1H-NMR (400 MHz, MeOD-d4) δ (ppm)= 7.24-7.17 (m, 5H), 4.55 (m, 1H), 4.41-4.38 (m. 1H), 3.93-3.91 (m, 1H), 3.67 (s, 3H), 3.21 (m, 1H), 2.92-2.89 (m, 3H), 1.89 (m, 1H), 1.79 (m, 1H), 1.66-1.64 (m, 2H), 1.46-1.44 (m, 2H), 1.38 (s, 9H), 1.09 (d, 3H).
MS (ESI): m/z 479 $[M+H]^+$

(6R,9S,12S)-9-benzyl-2,2,6,20,20-pentamethyl-4,7,10,18-tetraoxo-3,19-dioxa-5,8,11,17-tetraazahenicosane-12-carboxylic acid (TP, 7)
To a solution of **6** (1.853 g, 0.003868 mol) in THF (35 mL), NaOH 5% (10 mL) and Boc_2O (1.265 g, 0.005803 mol) were added and the reaction mixture was stirred overnight at room temperature. The solvent was removed under reduced pressure, H_2O (40 mL) was added and the pH value was

adjusted to 5 with HCl 0.1M. The precipitate was recovered by filtration and washed with H_2O, obtaining the desired product **7** without any further purification (1.831 g, Yield: 84%).
1H-NMR (400 MHz, MeOD-d4) δ (ppm)= 7.21-7.14 (m, 5H), 4.66 (m, 1H), 4.36 (m, 1H), 3.96 (m, 1H), 3.27-3.23 (m, 1H), 3.00-2.99 (m, 2H), 2-90-2.84 (m, 1H), 1.86 (m, 1H), 1.75 (m, 1H), 1.39-1.37 (m, 22H (18H+2H+2H)), 1.05 (m, 3H).
13C-NMR (100 MHz, MeOD-d4) δ (ppm)=174.2, 172.0, 171.9, 156.9, 156.1, 137.0, 128.9, 127.8, 126.1, 79.1, 78.3, 53.8, 52.1, 50.2, 39.6, 36.7, 30.6, 28.9, 27.2, 22.7, 16.5.
MS (ESI): m/z 587 $[M+Na]^+$

ethyl 5-aminopentanoate hydrochloride (LK, 9)
$SOCl_2$ (0.280 mL, 0.00384 mol) was added dropwise to anhydrous EtOH (8 mL) while cooling. Subsequently, 5-aminovaleric acid (0.300 g 0.256 mol) was addesd and the reaction mixture was stirred at r.t. for 12h.
The solvent was then removed under reduced pressure and the crude residue was purified by flash chromatography (CH_2Cl_2:MeOH 95:5) affording **9** as a white solid (0.371 g, Yield: 99%).
1H-NMR (400 MHz, MeOD-d4) δ (ppm)= 4.85 (br s, 2H, NH_2 disappears with D_2O), 4.17-4.12 (q, *J* = 7.2 Hz, 2H), 2.96-2.39 (d, *J* = 6.4. Hz, 2H), 2.41-2.39 (d, *J* = 6.4 Hz, 2H), 1.72 (m, 4H), 1.28-1.25 (t, *J* = 7.2 Hz, 2H).
MS (ESI): m/z 146 $[M+H]^+$

(6R,9S,12S)-2-((4-(phenethylamino)-1-((E)-styryl)-1H-pyrazolo[3,4-d]pyrimidin-6-yl)amino)ethyl 9-benzyl-12-(4-((tert-butoxycarbonyl)amino)butyl)-2,2,6-trimethyl-4,7,10-trioxo-3-oxa-5,8,11-triazatridecan-13-oate (10)
A solution of **7** (0.340 g, 0.00060 mol), EDC.HCl (0.115 g 0.00060 mol) and DMAP (0.092 g, 0.00075 mol) in anhydrous CH_2Cl_2 (20 mL) was stirred at room temperature for 30 min. After **SI113** (0.120 g, 0.00030 mol) was added and the reaction mixture was stirred at room temperature for 72 hours. The solvent was then removed under reduced pressure and the crude residue was purified by flash chromatography (CH_2Cl_2:AcOEt from 8:2 to 7:3) affording **10** as a white solid (0.200 g, Yield: 70%).
1H-NMR (400 MHz, acetone-d6) δ (ppm)= 7.93 (m, 2H), 7.59 (m, 1H), 7.43-7.21 (m, 15H), 4.63 (m, 1H), 4.59 (m, 1H), 4.34 (m, 2H), 4.22 (m, 1H), 3.98-3.96 (m, 4H), 3.34 (m, 1H), 3.32 (m, 1H), 3.18 (m, 4H), 1.97 (m, 1H) 1.96 (m, 1H) 1.49-1.31 (m, 22H (18H+2H+2H)), 1.21 (m, 3H).
13C-NMR (100 MHz, Acetone-d6) δ (ppm)= 173.2, 171.6, 171.1, 161.9, 156.8, 155.7, 155.4, 139.5, 137.5, 136.2, 133.7, 129.3, 129.0, 128.8, 128.7, 128.5, 127.9, 126.8, 126.5, 125.8, 125.7, 122.4, 114.23, 96.5, 78.5, 77.5, 63.8, 54.2, 52.5, 50.1, 41.9, 39.8, 37.4, 36.9, 35.3, 30.8, 29.5, 27.7, 22.87, 17.8

(S)-2-((4-(phenethylamino)-1-((E)-styryl)-1H-pyrazolo[3,4-d]pyrimidin-6-yl)amino)ethyl 6-amino-2-((S)-2-((R)-2-aminopropanamido)-3-phenylpropanamido) hexane-di-trifluoroacetate (PRO-SI113-TP, 11)
To a solution of **10** (0.096 g, 0.000009 mol) in anhydrous CH_2Cl_2 (8.0 mL) a trifluoroacetic acid (0.8 mL) was added and the reaction mixture was stirred at room temperature for 3 hours. The volatiles were then evaporated under reduced pressure and the crude was washed with toluene affording **11** (0.101 g, Yield: 99.9%) without any further purification.
1H-NMR (400 MHz, acetone-d6) δ (ppm)= 8.18 (m, 2H), 7.63 (m, 1H), 1.38-7.23 (m 15H), 4.65 (m, 1H), 4.38 (m, 1H), 4.36 (m, 2H), 4.25 (m, 1H), 3.88-3.86 (m, 4H), 3.73 (m, 1H), 3.33 (m, 1H), 3.24 (m,4H), 2.96 (m, 1H), 2.54-2.47 (m, 2H), 1.95 (m, 4H), 1.45(m, 3H).
13C-NMR (100 MHz, Acetone-d6) δ (ppm)= 171.5, 171.2, 169.8, 161.3, 156.6, 138.8, 137.2, 137.1, 135.1, 129.7, 129.0, 128.6, 128.1, 126.2, 121.6, 118.3, 117.7, 115.4, 96.7, 63.0, 54.9, 54.6, 52.1, 48.9, 40.5, 38.7, 37.8, 34.8, 26.5, 16.6.
MS (ESI): m/z 747 $[M+H]^+$, 374 $[M+2H]^{++}$, 249 $[M+3H]^{+++}$

(6R,9S,12S)-ethyl 9-benzyl-12-(4-((tert-butoxycarbonyl)amino)butyl)-2,2,6-trimethyl-4,7,10,13-tetraoxo-3-oxa-5,8,11,14-tetraazanonadecan-19-oate (12)

To a solution of **7** (0.400 g, 0.000710 mol) in anhydrous CH_2Cl_2 (20 mL) DMAP (0.174 g, 0.001420 mol), ethyl 5-aminopentanoate hydrochloride **9** (0.155 g, 0.001065 mol) and EDC.HCl (0.204 g, 0.001065 mol) were added and the reaction mixture was stirred overnight at room temperature. The solvent was then removed under reduced pressure and the crude residue was purified by flash chromatography (CH_2Cl_2:MeOH 95:5) affording **12** as a white solid (0.402 g, Yield: 82%).

1H-NMR (400 MHz, MeOD-d4) δ (ppm)=7.24-7.17 (m, 5H), 4.56 (m, 1H), 4.24 (m, 1H), 4.1-4.04 (q, *J* = 7.2Hz, 2H), 3.95-3.92 (m, 1H), 3.21 (m, 2H), 3.09 (m, 1H), 3.01 (m, 2H), 2.92 (m, 1H), 3.32-2.28 (t, *J* = 6.8 Hz, 2H), 1.89 (m, 1H) 1.83 (m, 1H), 1.71 (m, 2H), 1.59 (m, 2H), 1.47-1.39 (m, 22H (18H+2H+2H)), 1.21-1.18 (t, *J* = 7.2 Hz, 3H), 1.08 (m, 3H).

(6R,9S,12S)-9-benzyl-12-(4-((tert-butoxycarbonyl)amino)butyl)-2,2,6-trimethyl-4,7,10,13-tetraoxo-3-oxa-5,8,11,14-tetraazanonadecan-19-oic acid (13, LKTP)

To a solution of **12** (0.004 g, 0.000140 mol) in THF (10 mL), NaOH 5% was added. The reaction mixture was stirred overnight at room temperature. The solvent was then removed under reduced pressure. After H_2O (8 mL) was added and the pH value was adjusted to 5 with HCl 0.1M. The precipitate was recovered by filtration and washed with H_2O, obtaining the desired product **13** without any further purification (0.003 g, Yield: 80%).

1H-NMR (400 MHz, MeOD-d4) δ (ppm)= 7.24-7.17 (m, 5H), 4.56 (m, 1H), 4.24 (m, 1H), 3.95-3.92 (m, 1H), 3.21 (m, 2H), 3.09 (m, 1H), 3.01 (m, 2H), 2.92 (m, 1H), 3.30-2.26 (t, *J* = 6.8 Hz, 2H), 1.82 (m, 1H) 1.70 (m, 1H), 1.61 (m, 2H), 1.59 (m, 2H), 1.47-1.39 (m, 22H (18H+2H+2H)), 1.08 (m, 3H)

13C-NMR (100 MHz, MeOD-d4) δ (ppm)=175.7, 174.3, 172.4, 171.9, 156.9, 136.9, 128.8, 127.9, 126.3, 79.1, 78.3, 54.6, 53.6, 50.1, 39.6, 38.7, 38.5, 36.3, 32.9, 30.8, 28.9, 28.2, 26.6, 22.9, 21.8, 16.1.

(6R,9S,12S)-2-((4-(phenethylamino)-1-((E)-styryl)-1H-pyrazolo[3,4-d]pyrimidin-6-yl)amino)ethyl 9-benzyl-12-(4-((tert-butoxycarbonyl)amino)butyl)-2,2,6-trimethyl-4,7,10,13-tetraoxo-3-oxa-5,8,11,14-tetraazanonadecan-19-oate (14)

A solution of **13** (0.160 g, 0.00024 mol), EDC.HCl (0.046 g 0.00024 mol) and DMAP (0.036 g, 0.00030 mol) in anhydrous CH_2Cl_2 (20 mL) was stirred at room temperature for 30 min. After **SI113** (0.050 g, 0.00012 mol) was added and the reaction mixture was stirred at room temperature for 72 hours. The solvent was then removed under reduced pressure and the crude residue was purified by flash chromatography (CH_2Cl_2:MeOH 95:5) affording **14** as a white solid (0.105 g, Yield: 83%).

1H-NMR (400 MHz, acetone-d6) δ (ppm)= 7.95 (m, 2H), 7.31, (m, 1H), 7.31-7.18 (m, 15H), 4.72 (m, 1H), 4.39 (m, 1H), 4.31 (m, 2H), 4.10 (m, 1H), 4.76 (m, 4H), 3.29 (m, 1H), 3.27 (m, 1H), 3.19 (m, 4H), 2.30 (m, 2H), 1.59 (m, 2H), 1.49 (m, 2H), 1.47-1.34 (m, 22H (18H+2H+2H)), 1.17 (m, 3H).

13C-NMR (100 MHz, Acetone-d6) δ (ppm)=173.8, 172.8, 171.3, 170.9, 161.9, 156.8, 155.8, 155.7, 139.5, 137.4, 136.2, 133.8, 129.2, 128.7, 128.6, 128.2, 126.6, 126.3, 126.0, 125.8, 125.7, 122.5, 114.3, 96.5, 78.8, 77.5, 62.9, 54.7, 53.3, 50.3, 41.9, 41.5, 40.0, 38.6, 37.0, 35.4, 33.2, 31.4, 29.5, 29.4, 29.3, 28.9, 27.7, 23.1, 21.9.

2-((4-(phenethylamino)-1-((E)-styryl)-1H-pyrazolo[3,4-d]pyrimidin-6-yl)amino)ethyl 5-((S)-6-amino-2-((S)-2-((R)-2-aminopropanamido)-3-phenylpropanamido)hexanamido)pentan-di-trifluoroacetate (PRO-SI113-LKTP, 15)

To a solution of **14** (0.096 g, 0.000009 mol) in anhydrous CH_2Cl_2 (8.0 mL) a trifluoroacetic acid (0.8 mL) was added and the reaction mixture was stirred at room temperature for 3 hours. The

volatiles were then evaporated under reduced pressure and the crude was washed with toluene affording **15** (0.101 g, Yield: 99.9%) without any further purification.
1H-NMR (400 MHz, acetone-d6) δ (ppm)= 8.15 (m, 2H), 7.58 (m, 1H), 7.29-7.13 (m, 15H), 4.76 (m, 1H), 4.38 (m, 1H), 4.27 (m, 2H), 3.90 (m, 1H), 3.76 (m, 4H), 3.22 (m, 1H), 3.12 (m, 1H), 3.04 (m, 4H), 2.45 (m, 2H), 1.72 (m, 3H), 1.58 (m, 3H), 1.55 (m, 4H), 1.24 (m, 3H).
13C-NMR (100 MHz, Acetone-d6) δ (ppm)= 172.9, 171.6, 170.1, 161.2, 156.7, 155.3, 139.6, 138.8, 137.4, 137.3, 137.0, 135.4, 135.0, 133.7, 129.2, 128.1, 128.0, 126.2, 121.8, 118.4, 117.4, 115.5, 62.0, 57.2, 55.3, 54.8, 52.9, 50.8, 48.9, 42.4, 40.7, 38.4, 37.4, 34.9, 33.0, 26.5, 22.3, 17.6.
MS (ESI): m/z 847 $[M+H]^{+}$, 424 $[M+2H]^{++}$, 283 $[M+3H]^{+++}$

4.7.2 *IN VITRO* ADME ASSAYS

Chemicals. All solvents, reagents, NADPH, D-glucose-6-phosphate, glucose-6-phosphate dehydrogenase, L-α-phosphatidylcholine, plasmin from human plasma (lyophilized powder, ≥2.0 units/mg protein) were from Sigma-Aldrich Srl (Milan,Italy). Dodecane was purchased from Fluka (Milan, Italy). HLM pooled male donors (20 mg/mL) were purchased from BD Gentest-Biosciences (San Jose, California)
The human plasma for plasma stability was obtained by volunteers donors. Milli-Q quality water (Millipore, Milford, MA, USA) was used. Hydrophobic filter plates (MultiScreen-IP, Clear Plates, 0.45 μm diameter pore size), 96-well micro-plates, and 96-well UV-transparent microplates were obtained from Millipore (Bedford, MA, USA).

UV/LC-MS methods. LC analyses for water solubility were performer by **LC-MS-MS** system consisted of a Varian apparatus (Varian Inc) including a vacuum solvent degassing unit, two pumps (212-LC), a Triple Quadrupole MSD (Mod. 320-LC) mass spectrometer with ES interface and Varian MS Workstation System Control Vers. 6.9 software. Chromatographic separation was obtained using a Pursuit C18 column (50 x 2.0 mm) (Varian) with 3 μm particle size and gradient elution with a binary solution; (eluent A: ACN, eluent B: Water, both eluents were acidified with formic acid 0.1%). The analysis started with 5% of A (from t = 0 to t = 3 min), then A was increased to 95% (from t = 3 to t = 12 min), then kept at 95% (from t = 12 to t = 20 min) and finally return to 5% of eluent A in 1.0 min. The flow rate was 0.2 mL min^{-1} and injection volume was 5 μL. The instrument operated in positive mode and parameters were: detector 1850 V, drying gas pressure 25.0 psi, desolvation temperature 300.0 °C, nebulizing gas 45.0 psi, needle 5000 V and shield 600 V. Nitrogen was used as nebulizer gas and drying gas. Collision induced dissociation was performed using Argon as the collision gas at a pressure of 1.8 mTorr in the collision cell. The transitions as well as the capillary voltage and the collision energy used are appropriated for each tested compound. Quantification of the single compound was made by comparison with apposite calibration curves realized with standard solutions in methanol.
LC anlyses of PAMPA, Metabolic Stability and Stability Tests (in DMSO, Tris-buffer, Human Plasma and Human Plasmin) were performed by **UV/LC-MS** with an Agilent 1100 LC/MSD VL system (G1946C) (Agilent Technologies, Palo Alto, CA) using a Phenomenex Kinetex C18-100A column (150 x 4.6 mm, 5 μm particle size) at room temperature. Analyses were carried out with the same chromatographic method above reported for purity determination.

Water Solubility. Each solid compound (1 mg) was added to 1 mL of water. Each sample was mixed at 20 °C, in a shaker water bath for 24 h. The resulting suspension was filtered through a 0.45 μm nylon filter (Acrodisc). The concentration of compound in solution was determined by UV/LC-MS (performed in triplicate) by comparison with the appropriate calibration curve that was obtained from samples of the compound dissolved in methanol at different concentrations.

Parallel Artificial Membrane Permeability Assay (PAMPA). Each 'donor solution' was prepared from a solution of the appropriate compound (DMSO, 1 mM) diluted with phosphate buffer (pH 7.4, 25.0 mM) up to a final concentration of 500 μM. The donor wells were filled with 150 μL of 'donor solution'. The filters were coated with 5 μL of a solution of phosphatidylcholine in dodecane 1% (w/v) and filled with 300 μL of 'acceptor solution' (50% v/v DMSO and phosphate buffer). The sandwich plate was assembled and incubated for 5 hours at r.t. under gentle shaking. After the incubation time, the sandwich was disassembled and the amount of compound in both the donor and acceptor wells was measured by UV/LC-MS. Permeability (P_{app}) was calculated according to the following equation:[128]

$$P_{app} = -\frac{V_D V_A}{(V_D + V_A)At}\ln(1-r)$$

where V_A is the volume in the acceptor well (cm^3), V_D is the volume in the donor well (cm^3), A is the "effective area" of the membrane (cm^2), t is the incubation time (s) and r the ratio between drug concentration in the acceptor and equilibrium concentration of the drug in the total volume (V_D+V_A). Drug concentration was estimated by using the peak area integration.

Metabolic Stability in HLM (Human Liver Microsomes). The incubation mixture (total volume of 500 μL) was constituted by the following components: human liver microsomes (0.2 mg/mL, 5 μL), a NADPH regenerating system (NADPH 0.2 mM, $NADPH^+$ 1 mM, D-glucose-6-phosphate 4 mM, 4 unit/mL glucose-6-phosphate dehydrogenase and $MgCl_2$ 48 mM), 50 μM of each compound in DMSO and phosphate buffer (pH 7.4, 25 mM, up to a final volume of 500 μL). The mixture was incubated at 37 °C for 1 h. The reaction was cooled down and quenched with acetonitrile (1.0 mL). After centrifugation (10^4 rpm, 10 min), the surnatant was taken, dried under nitrogen flow, suspended in 100 μL of methanol and analyzed by UV/LC-MS to determine the percentage of compound that was not metabolized.

Stability tests in DMSO, PBS and Tris-buffer. Each prodrug was dissolved at r.t. in DMSO, phosphate buffer (12.5 mM, pH 7.4) or Tris-buffer (100mM, pH 7.4) up to a final concentration of 500 μM. Aliquot samples (20 μL) were taken at fixed time points (0.25, 0.50, 0.75, 1.0, 2.0, 3.0, 4.0, 5.0, 6.0, 7.0, 8.0, 24.0 and 48 h) and were analyzed by UV/LC-MS.

Stability tests in Human Plasma. Pooled human plasma (1.5 mL, 55.7 μg protein/mL),[151] phosphate buffer (1.4 mL, pH 7.4, 25 mM) and a solution of prodrug in DMSO (100 μL, 3.0 mM) were mixed in a test tube that was incubated at 37 °C. At set time points (0.25, 0.50, 1.0, 3.0, 7.0 and 24.0 h), samples of 150 μL were taken, mixed with 600 μL of cold acetonitrile and centrifuged at 5000 rpm for 15 min. The supernatant was removed and analyzed by UV/LC-MS to monitor the hydrolysis process of prodrug.

Stability tests in Human Plasmin.[149] Human plasmin (10 μL, 150 μg/mL), Tris-buffer (970 μL, pH 7.4, 100 mM) and a solution of prdrug in DMSO (20 μL, 7.5 mM) were mixed in a test tube that was incubated at 37 °C. At set time points (0.25, 0.50, 1.0, 3.0, 7.0 and 24.0 h), samples of 50 μL were taken, mixed with 200 μL of cold acetonitrile and centrifuged at 5000 rpm for 15 min. The supernatant was removed and analyzed by UV/LC-MS to monitor the hydrolysis process of prodrug.

4.7.3 *IN VITRO* BIOLOGICAL ASSAYS

In vitro experiments were carried out using the hepatocellular carcinoma (HCC) cell line HepG2. Cells, kindly provided from Prof. Ali O. Gure (Bilkent University, Ankara, Turkey), were cultured in Dulbecco's Modified Eagle's Medium (DMEM) supplemented with 10% FBS, 2 mM L-glutamine and 10000 units/mL Penicillin/Streptomycin at 37 °C in 5% CO_2 atmosphere.
Briefly, 2.5×10^4 HepG2 cells were sedeed in 12-well plates, the day after seeding compounds dissolved in DMSO were added at increasing concentrations (0.1, 1.0, 10 and 100 µM) and incubated for 24, 48 and 72 h at 37 °C in 5% v/v CO_2. In order to verify if prodrugs could be activated by plasmin, *in vitro* cytotoxicity assays have been also performed in presence of the enzyme. First, 24 h after seeding our compounds were added by using serum free DMEM to which plasmin has been added at a final concentration of 15 µg/mL. Then, cells were incubated for 24 h at 37 °C in 5% v/v CO_2.
Cell number and viability were evaluated using Z2 Coulter Counter (Beckman Coulter). IC_{50} (drug concentration that determined the 50% of growth inhibition) was calculated by GraphPad Prism 6.0 software using the best fitting sigmoid curve.

SECTION 5

‘REFERENCES AND ACKNOWLEDGEMENTS’

5.1 REFERENCES

1 Manning G, Whyte D, Martinez R, Hunter T, Sudarsanam S. The protein kinase complement of the human genome. Science. 2002, 29, 81912–81934.

2 Cohen P. Protein kinases the major drug targets of the twenty-first century?. Nat Rev Drug Discov. 2002, 1, 309–315.

3 Bain J, Plater L, Elliott M, Shpiro N, Hastie C, McLauchlan H, Klevernic I, Arthur J, Alessi D, Cohen P. The selectivity of protein kinase inhibitors: a further update. Biochem J. 2007, 408, 297–315.

4. Vieth M, Higgs R.E, Robertson D.H, Shapiro M, Gragg E.A, Hemmerle H. Kinomics-structural biology and chemogenomics of kinase inhibitors and targets. Biochim Biophys Acta. 2004, 1697, 243-257.

5 Bolen J.B, Rosen N, Israel M.A. Increased pp60c-src tyrosyl kinase activity in human neuroblastoma is associated with aminoterminal tyrosine phosphorylation of the src gene product. Proc.Natl.Acad.Sci. 1985, 82, 7275–7279.

6 O'Shaughnessy J, Deseau V, Amini S, Rosen, N, Bolen J.B. Analysis of the c-src gene product structure, abundance, and protein kinase activity in human neuroblastoma and glioblastoma cells. Oncogene Res. 1987, 2, 1–18.

7 Bjelfman C, Hedborg F, Johansson I, NordenskjÖld M, Påhlman S. Expression of the neuronal form of pp60c-src in neuroblastoma in relation to clinical stage and prognosis. Cancer Res. 1990, 50, 6908–6914.

8 Matsunaga T, *et al*. Expression of n-myc and c-src proto-oncogenes correlating to the undifferentiated phenotype and prognosis of primary neuroblastomas. Cancer Res. 1991, 51, 3148–3152.

9 Finlay D, Vuori K. Novel noncatalytic role for caspase-8 in promoting SRC-mediated adhesion and Erk signaling in neuroblastoma cells. Cancer Res. 2007, 67, 11704–11711.

10 Du J, Bernasconi P, Clauser K.R, Mani D.R, Finn S.P, Beroukhim R, Burns M, Julian B, Peng X.P, Hieronymus H, Maglathlin R.L, Lewis T.A, Liau L.M, Nghiemphu P, Mellinghoff I.K, Louis D.N, Loda M, Carr S.A, Kung AL, Golub T.R. Bead-based profiling of tyrosine kinase phosphorylation identifies SRC as a potential target for glioblastoma therapy. Nat.Biotechnol. 2009, 27, 77–83.

11 Chung E.J.1, Sung Y.K, Farooq M, Kim Y, Im S, Tak W.Y, Hwang Y.J, Kim Y.I, Han H.S, Kim J.C, Kim M.K. Gene expression profile analysis in human hepatocellular carcinoma by cDNA microarray. Mol.Cells. 2002, 14, 382–387.

12 Won M, Park K.A, Byun H.S, Kim Y.R, Choi B.L, Hong J.H, Park J, Seok J.H, Lee Y.H, Cho C.H, Song I.S, Kim Y.K, Shen H.M, et al. Protein kinase SGK1 enhances MEK/ERK complex formation through the phosphorylation of ERK2: Implication for the positive regulatory role of SGK1 on the ERK function during liver regeneration. J.Hepatol. 2009, 51, 67–76.

13 Wang X, Bhattacharyya D, Dennewitz M.B, Kalinichenko V.V, Zhou Y, Lepe R, Costa R.H. Rapid hepatocyte nuclear translocation of the Forkhead Box M1B (FoxM1B) transcription factor caused a transient increase in size of regenerating transgenic hepatocytes. Gene.Expr. 2003, 11, 149–62.

14 Van der Geer P, Hunter T., Lindberg R. A. Receptor protein-tyrosine kinases and their signal transduction pathways. Annu.Rev.Cell Biol. 1994, 10, 251-337.

15 Liu X., Pawson T. Biochemistry of the Src protein-tyrosine kinase: regulation by SH2 and SH3 domains. *Recent Prog.Horm.Res. 1994,* **49**, 149-160.

16 Levitzki A, Gazit, A. Tyrosine kinase inhibition: an approach to drug development. Science. 1995, 267, 1782-1788.

17 Marshal, C.J. Specificity of receptor tyrosine kinase signaling: transient versus sustained extracellular signal-regulated kinase activation. Cell. 1995, 80, 179-185.

18 Schlessinger, J. New Roles for Src Kinases in Control of Cell Survival and Angiogenesis. *Cell.* 2000, 100, 293-296.

19 Ruddon R.W. Cancer Biology. Oxford University Press: New York, 1995.

20 Lemmon, M.A, Schlessinger J. Transmembrane signaling by receptor oligomerization. Meth.Mol.Biol. 1998, 84, 49-71.

21 Neet K, Hunter T. Vertebrate non receptor protein-tyrosine kinase families. Genes Cells. 1996, 1, 147-169.

22 Kuriyan J, Cowburn D. Modular peptide recognition domains in eukaryotic signaling. Annu.Rev.Biophys.Biomol.Struct. 1997, 26, 259–288.

23 Robinson D.R, Wu Y.M, Lin S.F. The protein tyrosine kinase family of the human genome. Oncogene. 2000, 19, 5548.

24 Heldin C.H. Protein tyrosine kinase receptor in signal transuduction. Cell. 1995, 80, 213-223.

25 Brown M.T,Cooper J.A. Regulation, substrates and functions of src. Biochim.Biophys.Acta. 1287, 121-149.

26 Thomas S.M, Brugge J.S. Cellular functions by Src family kinases. Annu Rev Cell Dev.Biol. 1997, 13, 513-609.

27 Abram C.L, Courteneidge S.A. Src family tyrosine kinases and growth factor signalling. Exp.Cell Res. 2000, 254, 1-13.

28 Martin G.S. The hunting of the Src. Nat.Rev.Mol.Cell Biol. 2001, 2, 467-475.

29 Sawyer T, Boyce B, Dalgarno D, Iuliucci B. Src inhibitors: genomics to therapeutics. J.Expert Opin.Investig.Drugs. 2001, 10, 1327-1344.

30 Shah Y.M, Rowan B.G. The Src kinase pathway promotes tamoxifen agonist action in Ishikawa endometrial cells through phosphorylation-dependent stabilization of estrogen receptor (alpha) promoter interaction and elevated steroid receptor coactivator 1 activity. Mol.Endocrinol. 2005, 19, 732-748.

31 Pengetnze Y, Steed M, Roby K.F, Terranova P.F, Taylor C.C. Src tyrosine kinase promotes survival and resistance to chemotherapeutics in a mouse ovarian cancer cell line. Biochem.Biophys.Res.Commun. 2005, 309, 377-383.

32 Schindler T, Bornmann W, Pellicena P, Miller W.T, Clarkson B, Kuriyan A. Structural mechanism for STI-571 inhibition of abelson tyrosine kinase. J. Science. 2000, 289, 1938-1942.

33 Summy J.M, Gallick G.E. Src family kinases in tumor progression and metastasis. Cancer Metastasis Rev.2003, 22, 337-358.

34 Kaplan K.B, Bibbins K.B, Swedlow J.R, Arnaud M, Morgan D.O, Varmus H.E. Association of the amino-terminal half of c-Src with focal adhesions alters their properties and is regulated by phosphorylation of tyrosine 527. EMBO J. 1994, 13, 4745-4756.

35 Mohn H, LeCabec V, Fischer S, Maridonneau-Parini I. The src-family protein-tyrosine kinase p5ghck iS located on the secretory granules in human neutrophils and translocates towards the phagosome during cell activation Biochem.J. 1995, 309, 657-665.

36 Matsuda D, Nakayama Y, Horimoto S, Kuga T, Ikeda, K, Kasahara K, Yamaguchi N. Involvement of Golgi-associated Lyn tyrosine kinase in the translocation of annexin II to the endoplasmic reticulum under oxidative stress. Exp.Cell Res. 2006, 312, 1205-1217.

37 Salvi M, Brunati A.M, Bordin L, La Rocca N, Clari G, Toninello A. Characterization and location of Src dependent tyrosine phosphorylation in rat brain mitochondria. Biochim.Bioph.Acta. 2002, 1589, 181-195.

38 David-Pfeuty T, Nouvian-Dooghe Y.J. Immunolocalization of the cellular *src* protein in interphase and mitotic NIH *c-src*overexpresser cells Cell Biol. 1990, 111, 3097-3116.

39 Chong Y.P, Mulhern T.D, Cheng H.C. C-terminal Src kinase (CSK) and CSK-homologous kinase (CHK) endogenous negative regulators of Src-family protein kinases. Growth Factors. 2005, 23, 233-244.

40 Kmiecik T.E, Shalloway D. Activation and suppression of pp60c-src transforming ability by mutation of its primary sites of tyrosine phosphorylation. Cell. 1987, 49, 65-73.

41 Hu Y, Swerdolw S, Duffy T.M, Weinmann R., Lee F.Y, Li S. Targeting multiple kinase pathways in leukemic progenitors and stem cells is essential for improved treatment of Ph+ leukemia in mice. Proc.Natl.Acad.Sci. 2006, 103, 16870-16875.

42 Li S. Src kinase signaling in leukaemia. Int.J.Biochem.Cell Biol. 2007, 39, 1483-1488.

43 Taagepera S, McDonald D, Loeb J.E, Whitaker L.L, McElroy A.K, Wang J.Y, Hope T.J. Nuclear-cytoplasmic shuttling of C-ABL tyrosine kinase. PNAS. 1998, 95, 7457-7462.

44 Wen S.T, Jackson P.K, Van Etten R.A. The cytostatic function of c-Abl is controlled by multiple nuclear localization signals and requires the p53 and Rb tumor suppressor gene products. EMBO J. 1996, 15, 1583-1595.

45 Wang J.Y.J. Abl tyrosine kinase in signal transduction and cell-cycle regulation. Curr.Opin.Genet.Dev. 1993, 3, 35-43.

46 Van Etten R.A. Cycling, stressed-out and nervous: cellular functions of c-Abl. Trends Cell Biol. 1999, 9, 179-186.

47 Mayer B.J, Baltimore D. Mutagenic analysis of the roles of SH2 and SH3 domains in regulation of the Abl tyrosine kinase. Mol.Cell.Biol. 1994, 14, 2883-2894.

48 Mayer B.J, Jackson P.K, Van Etten R.A, Baltimore D. Point mutations in the abl SH2 domain coordinately impair phosphotyrosine binding in vitro and transforming activity *in vivo*. Mol.Cell Biol. 1992, 12, 609-618.

49 Pluk H, Dorey K, Superti-Furga G. Autoinhibition of c-Abl. Cell. 2002, 108, 247-259.

50 Barila D, Superti-Furga G. An intramolecular SH-3 domain interaction regulates c-Abl sctivity Nat.Genet. 1998, 18, 280-282.

51 Hantschel O, Nagar B, Guettler S, Kretzschmar J, Dorey K, Kuriyan J, Superti-Furga G. A myristoyl/phosphotyrosine switch regulates c-Abl. Cell. 2003, 112, 845-857.

52 Dorey K, Engen J.R, Kretzschmar J, Wilm M, Neubauer G, Schindler T, Superti-Furga G. Phosphorylation and structure-based functional studies reveal a positive and a negative role for the activation loop of the c-Abl tyrosine kinase. Oncogene. 2001, 20, 8075-8084.

53 Plattner R, Kadlec L, DeMali K.A, Kazlauskas A, Pendergast A.M. c-Abl is activated by growth factors and Src family kinases and has a role in the cellular response to PDGF. Genes Dev. 1999, 13, 2400-2411.

54 Furstoss O, Dorey K, Simon V, Barila D, Superti-Furga G, Roche S. c-Abl is an effector of Src for growth factor-induced c-myc expression and DNA synthesis. EMBO J. 2002, 21, 514-524.

55 Tanis K.Q, Veach D, Duewel H.S, Bornmann W.G, Koleske A.J. Two distinct phosphorylation pathways have additive effects on Abl family kinase activation. Mol.Cell Biol. 2003, 23, 3884-3896.

56 Bruhn M.A, Pearson R.B, Hannan R.D, Sheppard K.E. Second AKT: the rise of SGK in cancer signalling. Growth Factors. 2010, 28, 394–408.

57 Hong F, Larrea M.D, Doughty C, Kwiatkowski D.J, Squillace R, Slingerland J.M. mTOR-raptor binds and activates SGK1 to regulate p27 phosphorylation. Mol Cell. 2008, 30, 701-711.

58 Lang F, Cohen P. Regulation and physiological roles of serum- and glucocorticoid-induced protein kinase isoforms. Sci STKE 2001, 2001:re17.

59 Faletti C.J, Perrotti N, Taylor S.I, Blazer-Yost B.L. Sgk: an essential convergence point for peptide and steroid hormone regulation of ENaC-mediated Na+ transport. Am.J.Physiol.Cell Physiol. 2002, 282, 494–500.

60 Perrotti N, He R.A, Phillips S.A, Haft C.R, Taylor S.I. Activation of serum- and glucocorticoid-induced protein kinase (Sgk) by cyclic AMP and insulin. J.Biol.Chem. 2001, 276, 9406–9412.

61 Menniti M, Iuliano R, Föller M, Sopjani M, Alesutan I, Mariggiò S, Nofziger C, Perri A.M, Amato R, Blazer-Yost B, Corda D, Lang F, Perrotti N. 60kDa lysophospholipase, a new Sgk1 molecular partner involved in the regulation of ENaC. Cell.Physiol.Biochem. 2010, 26, 587–596.

62 Boito R, Menniti M, Amato R, Palmieri C, Marinaro C, Iuliano R, Tripodi G, Cusi D, Fuiano G, Perrotti N. RFX-1, a putative alpha Adducin interacting protein in a human kidney library. FEBS Lett. 2005, 579, 6439–6443.

63 Amato R, Menniti M, Agosti V, Boito R, Costa N, Bond H.M, Barbieri V, Tagliaferri P, Venuta S, Perrotti N. IL-2 signals through Sgk1 and inhibits proliferation and apoptosis in kidney cancer cells. J.Mol.Med. 2007, 85, 707–721.

64 Sommer E.M, Dry H, Cross D, Guichard S, Davies B.R, Alessi D.R. Elevated SGK1 predicts resistance of breast cancer cells to Akt inhibitors. Biochem J. 2013, 452, 499–508.

65 Zheng G, Jia X, Peng C, Deng Y, Yin J, Zhang Z, Li N, Deng M, Liu X, Liu H, Lu M, Wang C, Gu Y, He Z. The miR-491-3p/mTORC2/FOXO1 regulatory loop modulates chemosensitivity in human tongue cancer. Oncotarget. 2015, 6, 6931–6943.

66 Stringer-Reasor E.M, Baker G.M, Skor M.N, Kocherginsky M, Lengyel E, Fleming G.F, Conzen S.D. Glucocorticoid receptor activation inhibits chemotherapy-induced cell death in high-grade serous ovarian carcinoma. Gynecol Oncol. 2015, 138, 656–662.

67 Isikbay M, Otto K, Kregel S, Kach J, Cai Y, Vander Griend D.J, Conzen S.D, Szmulewitz R.Z. Glucocorticoid receptor activity contributes to resistance to androgen-targeted therapy in prostate cancer. Horm.Cancer. 2014, 5, 72–89.

68 Abbruzzese C, Mattarocci S, Pizzuti L, Mileo A.M, Visca P, Antoniani B, Alessandrini G, Facciolo F, Amato R, D'Antona L, Rinaldi M, Felsani A, Perrotti N, *et al*. Determination of SGK1 mRNA in non-small cell lung cancer samples underlines high expression in squamous cell carcinomas. J.Exp.Clin.Cancer Res. 2012, 31, 4.

69 Chung E.J, Sung Y.K, Farooq M, Kim Y, Im S, Tak W.Y, Hwang Y.J, Kim Y.I, Han H.S, Kim J.C, Kim M.K. Gene expression profile analysis in human hepatocellular carcinoma by cDNA microarray. Mol.Cells. 2002, 14, 382–387.

70 Won M, Park K.A, Byun H.S, Kim Y.R, Choi B.L, Hong J.H, Park J, Seok J.H, Lee Y.H, Cho C.H, Song I.S, Kim Y.K, Shen H.M, *et al*. Protein kinase SGK1 enhances MEK/ERK complex formation through the phosphorylation of ERK2: Implication for the positive regulatory role of SGK1 on the ERK function during liver regeneration. J.Hepatol. 2009, 51, 67–76.

71 Wang X, Bhattacharyya D, Dennewitz M.B, Kalinichenko V.V, Zhou Y, Lepe R, Costa R.H. Rapid hepatocyte nuclear translocation of the Forkhead Box M1B (FoxM1B) transcription factor

caused a transient increase in size of regenerating transgenic hepatocytes. Gene Expr. 2003, 11, 149–162.

72 Nasir O, Wang K, Föller M, Gu S, Bhandaru M, Ackermann T.F, Boini K.M, Mack A, Klingel K, Amato R, Perrotti N, Kuhl D, Behrens J, *et al*. Relative resistance of SGK1 knockout mice against chemical carcinogenesis. IUBMB Life. 2009, 61, 768–776.

73 Amato R, D'Antona L, Porciatti G, Agosti V, Menniti M, Rinaldo C, Costa N, Bellacchio E, Mattarocci S, Fuiano G, Soddu S, Paggi M.G, *et al*. Sgk1 activates MDM2-dependent p53 degradation and affects cell proliferation, survival, and differentiation. J.Mol.Med. 2009, 87, 1221–1239.

74 Amato R, Scumaci D, D'Antona L, Iuliano R, Menniti M, Di Sanzo M, Faniello M.C, Colao E, Malatesta P, Zingone A, Agosti V, Costanzo F.S, Mileo A.M, *et al*. Sgk1 enhances RANBP1 transcript levels and decreases taxol sensitivity in RKO colon carcinoma cells. Oncogene. 2013, 32, 4572–4578.

75 Menniti M, Iuliano R, Amato R, Boito R, Corea M, Le PI, Gulletta E, Fuiano G, Perrotti N. Serum and glucocorticoid-regulated kinase Sgk1 inhibits insulin-dependent activation of phosphomannomutase 2 in transfected COS-7 cells. Am.J.Physiol.Cell Physiol. 2005, 288, C148-C155.

76 Christiansen M.N, Chik J, Lee L, Anugraham M, Abrahams J.L, Packer N.H. Cell surface protein glycosylation in cancer. Proteomics. 2014, 14, 525-546.

77 Holst S, Stavenhagen K, Balog C.I, Koeleman C.A, McDonnell L.M, Mayboroda O.A, Verhoeven A, Mesker W.E, Tollenaar R.A, Deelder A.M, Wuhrer M. Investigations on aberrant glycosylation of glycosphingolipids in colorectal cancer tissues using liquid chromatography and matrix-assisted laser desorption time-of-flight mass spectrometry (MALDI-TOF-MS). Mol Cell Proteomics. 2013, 12, 3081-3093.

78 Leve F, Marcondes T.G, Bastos L.G, Rabello S.V, Tanaka M.N, Morgado-Diaz J.A. Lysophosphatidic acid induces a migratory phenotype through a crosstalk between RhoA-Rock and Src-FAK signalling in colon cancer cells. Eur J Pharmacol. 2011, 671, 7-17.

79 Zhang H, Bialkowska A, Rusovici R, Chanchevalap S, Shim H, Katz J.P, Yang V.W, Yun C.C. Lysophosphatidic acid facilitates proliferation of colon cancer cells via induction of Kruppel-like factor 5. J Biol Chem. 2007, 282, 15541-15549.

80 Lang F, Perrotti N, Stournaras C. Colorectal carcinoma cells--regulation of survival and growth by SGK1. Int J Biochem Cell Biol. 2010, 42, 1571-1575.

81 Lang F, Voelkl J. Therapeutic potential of serum and glucocorticoid inducible kinase inhibition. Expert Opin Investig Drugs. 2013, 22, 701-714.

82 Towhid S.T, Liu G.L, Ackermann T.F, Beier N, Scholz W, Fuchss T, Toulany M, Rodemann H.P, Lang F. Inhibition of colonic tumor growth by the selective SGK inhibitor EMD638683. Cell Physiol Biochem. 2013, 32, 838-848.

83 Bruhn M.A, Pearson R.B, Hannan R.D, Sheppard K.E. AKT-independent PI3-K signaling in cancer - emerging role for SGK3. Cancer Manag Res. 2013, 5, 281-292.

84 Skor M.N, Wonder E.L, Kocherginsky M, Goyal A, Hall B.A, Cai Y, Conzen S.D. Glucocorticoid receptor antagonism as a novel therapy for triple-negative breast cancer. Clin.Cancer Res. 2013, 19, 6163-6172.

85 Zhao B, Lehr R, Smallwood A.M, *et al*. Crystal structure of the kinase domain of serum and glucocorticoid-regulated kinase 1 in complex with AMP–PNP.Protein Science : A Publication of the Protein Society. 2007, 16, 2761-2769.

86 Arora A, Scholar E.M. Role of tyrosine kinase inhibitors in cancer therapy. J.Pharm.Exp.Ther. 2005, 315, 971−979.

87 Schenone S, Bruno O, Bondavalli F, Ranise A, Mosti L, Menozzi G, Fossa P, Manetti F, Morbidelli L, Trincavelli L, Mataini C, Lucacchini A. Synthesis of 1-(2-chloro-2-phenylethyl)-6-methylthio-1H-pyrazolo 3,4-d pyrimidines 4-amino substituted and their biological evaluation. Eur.J.Med.Chem. 2004, 39, 153-160.

88 Carraro F, Pucci A, Naldini A, Schenone S, Bruno O, Ranise A, Bondavalli F, Brullo C, Foss P, Menozzi G, Mosti L, Manetti F, Botta M. Pyrazolo [3,4-*d*]pyrimidines endowed with antiproliferative activity on ductal infiltrating carcinoma cells. J.Med.Chem. 2004, 47, 1595-1598.

89 Hanke J.H, Gardner J.P, Dow R.L, Changelian P.S, Brissette W.H, Weringer E.J, Pollok B.A, Connelly P.A. Discovery of a Novel, Potent, and Src Family-selective Tyrosine Kinase Inhibitor. J.Biol.Chem. 1996, 271, 695-701.

90 Manetti F, Santucci A, Locatelli G.A, Maga G, Sperafico A, *et al*. Identification of a Novel Pyrazolo[3,4-d]pyrimidine Able To Inhibit Cell Proliferation of a Human Osteogenic Sarcoma in Vitro and in a Xenograft Model in Mice. *J.Med.Chem.* 2007, 50, 5579–5588.

91 Sperafico A, Schenone S, Serchi T, Orlandini M, Angelucci A, Magrini D, Bernardini G, Collodel G, Di Stefano A, Tintori C, Bologna M, Fabrizio M, Botta M, Santucci A. Antiproliferative and proapoptotic activities of new pyrazolo[3,4-*d*]pyrimidine derivative Src kinase inhibitors in human osteosarcoma cells. FASEB J. 2008, 22, 1560-1571.

92 Manetti F, Pucci A, Magnani M, locatelli G.A, Brullo C, Naldini A, Schenone S, Maga G, carraro F, Botta M. Inhibition of Bcr-Abl Phosphorylation and Induction of Apoptosis by Pyrazolo[3,4-*d*]pyrimidines in Human Leukemia Cells. Chem.Med.Chem. 2007, 2, 343-353

93 Schenone S, Brullo C, Bruno O, Bondavalli F, Mosti L, Maga G, Crespan E, Carraro F, Manetti F, Tintori C, Botta M. Synthesis, biological evaluation and docking studies of 4-amino substituted 1*H*-pyrazolo[3,4-*d*]pyrimidines. Eur.J.Med.Chem. 2008, 43, 2665-2676.

94 Rowley J.D. Letter: a new consistent chromosomal abnormality in chronic myelogenous leukemia identified by quinacrine fluorescence and Giemsa staining. Nature. 1973, 243, 290–293.

95 Sawyers C.L. Chronic myeloid leukemia. N.Engl.J. Med. 1999, 340, 1330-1340.

96 Lugo T.G, Pendergast A.M, Muller A.J, Witte O.N. Tyrosine kinase activity and transformation potency of Bcr-Abl oncogene products. Science. 1990, 247, 1079-1082.

97 Wilson M.B, Schreiner S.J, Choi H.J, Kamens J, Smithgall T.E. Selective pyrrolo-pyrimidine inhibitors reveal a necessary role for Src family kinases in Bcr-Abl signal transduction and oncogenesis. Oncogene. 2002, 21, 8075-8088.

98 Santucci M.A, Corradi V, Mancini M, Manetti F, Radi M, Schenone S, Botta M. C6-Unsubstituted Pyrazolo[3,4-*d*]pyrimidines Are Dual Src/Abl Inhibitors Effective against Imatinib Mesylate Resistant Chronic Myeloid Leukemia Cell Lines. Chem.Med.Chem. 2009, 4, 118-126.

99 Navarra M, Celano M, Maiuolo J, Schenone S, Botta M, Angelucci A, Bramanti P, Russo D. Antiproliferative and pro-apoptotic effects afforded by novel Src-kinase inhibitors in human neuroblastoma cells. BMC Cancer 2010, 10, 602-614.

100 Radi M, *et al*. Identification of potent c-Src inhibitors strongly affecting the proliferation of human neuroblastoma cells. Bioorg.Med.Chem.Lett. 2011, 21, 5928–5933.

101 Tintori C, Fallacara A.L, Radi M, Zamperini C, Dreassi E, Crespan E, Maga G, Schenone S, Musumeci F, Brullo C, Richters A, Gasparrini F, Angelucci A, Festuccia C, Delle Monache S, Rauh D, Botta M. Combining X-ray crystallography and molecular modeling toward the optimization of pyrazolo[3,4-d]pyrimidines as potent c-Src inhibitors active in vivo against Neuroblastoma. J.Med.Chem. 2015, 58, 347-361.

102 Ceccherini E, Indovina P, Zamperini C, Dreassi E, Casini N, Cutaia O, Forte I.M, Pentimalli F, Esposito L, Polito M.S, Schenone S, Botta M, Giordano A. SRC family kinase inhibition through a new pyrazolo[3,4-*d*]pyrimidine derivative as a feasible approach for glioblastoma treatment. J.Cell.Biochem. 2015, 116, 856-863.

103 Calgani A, Vignaroli G, Zamperini C, Coniglio F, Festuccia C, Di Cesare E, Gravina G.L, Mattei C, Vitale F, Schenone S, Botta M, Angelucci A. Suppression of SRC signaling is effective in reducing synergy between glioblastoma and stromal cells. Mol.Cancer Ther. 2016, 15, 1535-1544.

104 Ortuso F, Amato R, Artese A, D'Antona L, Costa G, Talarico C, Gigliotti F, Bianco C, Trapasso F, Schenone S, Musumeci F, Botta L, Perrotti N, Alcaro S. In Silico Identification and Biological Evaluation of Novel Selective Serum/Glucocorticoid-Inducible Kinase 1 Inhibitors Based on the Pyrazolo-Pyrimidine Scaffold. J.Chem.Inf.Model. 2014, 54, 1828-1832.

105 D'Antona L, Amato R, Talarico C, Ortuso F, Menniti M, Dattilo V, Iuliano R, Gigliotti F, Artese A, Costa G, Schenone S, Musumeci F, Abbruzzese C, Botta L,Trapasso F, Alcaro S, Paggi MG, Perrotti N. SI113, a Specific Inhibitor of the Sgk1 Kinase Activity that Counteracts Cancer Cell Proliferation. Cell.Physiol.Biochem. 2015, 35,2006–2018.

106 Talarico C, *et al*. Preclinical model in HCC: the SGK1 kinase inhibitor SI113 blocks tumor progression *in vitro* and *in vivo* and synergizes with radiotherapy. Oncotarget. 2015, 6, 37511-37525.

107 Reimer D, Eastman S, Flowers C, Boey A, Redelmeier T, Ouyang C. 2005. Liposome formulations for sparingly soluble compounds: liposome technology offers many advantages for formulation of sparingly soluble compounds. In Pharmaceutical Formulation and Quality. Retrieved from http://www.pharmaquality.com/mag/08092005/pfq_08092005_FO2.htmL.

108 Atrooz O.M. Effects of alkylresorcinolic lipids obtained from acetonic extract of Jordanian wheat grains on liposome properties. Int.J.Biol.Chem. 2011, 5, 314-321.

109 Shehata T, Ogawara K, Higaki K, Kimura T. Prolongation of residence time of liposome by surface-modification with mixture of hydrophilic polymers. Int.J.Pharm. 2008, 359, 272-279.

110 Johnston M.J, Semple S.C, Klimuk S.K, Ansell S, Maurer N, Cullis P.R. Characterization of the drug retention and pharmacokinetic properties of liposomal nanoparticles containing dihydrosphingomyelin. Biochim.Biophys.Acta. 2007, 1768, 1121-1127.

111 Hofheinz R.D, Gnad-Vogt S.U, Beyer U, Hochhaus A. Liposomal encapsulated anti-cancer drugs. Anticancer Drugs. 2005, 16, 691-707.

112 Omri A, Suntres Z.E, Shek P.N. Enhanced activity of liposomal polymyxin B against Pseudomonas aeruginosa in a rat model of lung infection. Biochem.Pharmacol. 2002, 64, 1407-1413.

113 Schiffelers R.M, Storm G, Bakker-Woudenberg I.A. Host factors influencing the preferential localization of sterically stabilized liposomes in Klebsiella pneumoniae-infected rat lung tissue. Pharm.Res. 2001, 18,780-787.

114 Stano P, Bufali S, Pisano C, Bucci F, Barbarino M, Santaniello M, Carminati P, Luisi P.L. Novel camptothecin analogue (gimatecan)-containing liposomes prepared by the ethanol injection method. J.Liposome Res. 2004, 14, 87-109.

115 Hemanthkumar M, Spandana V. Liposomal encapsulation technology a novel drug delivery system designed for ayurvedic drug preparation. IRJP. 2011, 2, 4-7.

116 Maria Laura I, Franco D, Cattel L. Stealth liposomes: review of the basic science, rationale, and clinical applications, existing and potential. Int.J.Nanomedicine. 2006, 1, 297-315.

117 Amarnath S, Sharma U.S. Liposomes in drug delivery: progress and limitations. Int.J.Pharm. 1997, 154, 123-140.

118 Shaheen S.M, Shakil Ahmed F.R, Hossen M.N, Ahmed M, Amran M.S, Ul-Islam M.A. Liposome as a carrier for advanced drug delivery. Pak.J.Biol.Sci. 2006, 9, 1181-1191.

119 Riaz M. Liposome preparation method. Pak.J.Pharm.Sci. 1996, 9, 65-77.

120 Babai I, Samira S, Barenholz Y, Zakay-Rones Z, Kedar E. A novel influenza subunit vaccine composed of liposome-encapsulated haemagglutinin/ neuraminidase and IL-2 or GM-CSF. I. Vaccine characterization and efficacy studies in mice. Vaccine. 1999, 17,1223-1238.

121 Peters T. Serum albumin. Adv.Protein Chem. 1985, 37, 161–245.

122 Carter D.C, He X.M, Munson S.H, Twigg P.D, Gernert K.M, Broom M.B, Miller T.Y. Three-dimensional structure of human serum albumin. Science. 1989, 244, 1195–1198.

123 Carter D.C, Ho J.X. Structure of serum albumin. Adv.Protein Chem. 1994, 45, 153–203.

124 Fasano M, Curry S, Terreno E, Galliano M, Fanali G, Narciso P, Notari S, Ascenzi P. The extraordinary ligand binding properties of human serum albumin. IUBMB Life. 2005, 57, 787–796.

125 Bertucci C, Domenici E. Reversible and covalent binding of drugs to human serum albumin: methodological approaches and physiological relevance. Curr.Med.Chem. 2009, 9, 1463–1481.

126 Patil G.V. Biopolymer albumin for diagnosis and in drug delivery. Drug Dev.Res. 2003, 58, 219–247.

127 Arshady R. Preparation of microspheres and microcapsules by interfacial polycondensation techniques. Microcapsul. 1989, 6, 13–28.

128 Wohnsland F, Faller B. High-throughput permeability pH profile and high-throughput alkane/water log P with artificial membranes. J.Med.Chem. 2001, 44, 923-930.

129 Sugano K, Hamada H, Machida M, Ushio H. High throughput prediction of oral absorption: improvement of the composition of the lipid solution used in parallel artificial membrane permeation assay. J.Biomol.Screen. 2001, 6, 189-196.

130 Schenone S, Radi M, Musumeci F, Brullo C, Botta M. Biologically driven synthesis of pyrazolo[3,4-*d*]pyrimidines as protein kinase inhibitors: an old scaffold as a new tool for medicinal chemistry and chemical biology studies. Chem.Rev. 2014, 114, 7189-7238

131 Angelucci A, Schenone S, Gravina G.L, Muzi P, Festuccia C, Vicentini C, Botta M, Bologna M. Pyrazolo[3,4-*d*]pyrimidines c-Src inhibitors reduce epidermal growth factor-induced migration in prostate cancer cells. Eur.J.Cancer. 2006, 42, 2838–2845.

132 Casini N, Forte I.M, Mastrogiovanni G, Pentimalli F, Angelucci A, Festuccia C, Tomei V, Ceccherini E, Di Marzo D, Schenone S, Botta M, Giordano A, Indovina P. SRC family kinase (SFK) inhibition reduces rhabdomyosarcoma cell growth in vitro and in vivo and triggers p38 MAP kinase-mediated differentiation. Oncotarget. 2015, 6, 12421-35.

133 Indovina P, Giorgi F, Rizzo V, Khadang B, Schenone S, Di Marzo D, Forte I.M, Tomei V, Mattioli E, D'Urso V, Grilli B, Botta M, Giordano A, Pentimalli F. New pyrazolo[3,4-*d*]pyrimidine SRC inhibitors induce apoptosis in mesothelioma cell lines through p27 nuclear stabilization. Oncogene. 2012, 31, 929-938.

134 Rossi A, Schenone S, Angelucci A, Cozzi M, Caracciolo V, Pentimalli F, Puca A, Pucci B, La Montagna R, Bologna M, Botta M, Giordano A. New pyrazolo-[3,4-*d*]-pyrimidine derivative Src kinase inhibitors lead to cell cycle arrest and tumor growth reduction of human medulloblastoma cells. FASEB J. 2010, 24, 2881-2892.

135 Morisi R, Celano M, Tosi E, Schenone S, Navarra M, Ferretti E, Costante G, Durante C, Botta G, D'Agostino M, Brullo C, Filetti S, Botta M, Russo D. Growth inhibition of medullary thyroid carcinoma cells by pyrazolo-pyrimidine derivates. *J.Endocrinol.Invest.* **2007**, *30*, 31-34.

136 Radi M, Tintori C, Musumeci F, Brullo C, Zamperini C, Dreassi E, Fallacara A.L, Vignaroli G, Crespan, E, Zanoli S, Laurenzana I, Filippi I, Maga G, Schenone S, Angelucci A, Botta M. Design, synthesis, and biological evaluation of pyrazolo[3,4-d]pyrimidines active in vivo on the Bcr-Abl T315I Mutant. J.Med.Chem. 2013, 56, 5382-5394.

137 Cozzi M, Giorgi F, Marcelli E, Pentimalli F, Forte I.M, Schenone S, D'Urso V, De Falco G, Botta M, Giordano A, Indovina P. Antitumor activity of new pyrazolo[3,4-d]pyrimidine SRC

kinase inhibitors in Burkitt lymphoma cell lines and its enhancement by WEE1 inhibition. Cell Cycle. 2012, 11, 1029-1039.

138 Vignaroli G, Calandro P, Zamperini C, Coniglio F, Iovenitti G, Tavanti M, Colecchia D, Dreassi E, Valoti M, Schenone S, Chiariello M, Botta M. Improvement of pyrazolo[3,4-d] pyrimidines pharmacokinetic properties: nanosystem approaches for drug delivery. Sci.Rep. 2016, 22,6, 2150.

139 Karen E, Schoedel M.D, Valerie Zajac Tyner B.S, Tae-Hyoung K, George K, Michalopoulos M.D, Mars W.M. HGF, MET, and Matrix-Related Proteases in Hepatocellular Carcinoma, Fibrolamellar Variant, Cirrhotic and Normal Liver. Mod.Pathol. 2003, 16, 14–21.

140 Skwarczynski M, Hayashi Y, Kiso Y. Paclitaxel prodrugs:toward smarterdelivery of anticancer agents. J.Med.Chem. 2012, 49, 7253-7269.

141 Stella V.J, Himmelstein K.J. Prodrugs and site-specific drug delivery. J.Med.Chem. 1980, 23, 1275-1282.

142 Trouet A, Passioukov A,.Van derpoorten K, Fernandez A.M, Abarca- Quinones J, Baurain R, Lobl T.J, Oliyai C, Shochat D, Dubois V. Extracellularly Tumor-activated Prodrugs for the Selective Chemotherapy of Cancer: Application to Doxorubicin and Preliminary *in Vitro* and *in Vivo* Studies. Cancer Res. 2001, 61, 2843-2846.

143 Rening U, Magdolen V, Wilhem O, Fischer K, Lutz V, Graeff H, Schmitt M. Multifunctional potential of the plasminogen activation system in tumor invasion and metastasis. Int.J.Oncol. 1998, 13, 893-906.

144 Hewitt R, Dano K. Stromal cell expression of components of matrixdegradating protease systems in human cancer. Enzyme Protein. 1996, 49, 163- 173.

145 Quax P.H.A, Leeuwen R.T.J, Verspaget H.W, Verheijn J.H. Protein andmessenger RNA levels of plasminogen activators and inhibitors analyzed in 22 human tumor cell lines. Cancer Res. 1990, 50, 1488-1494.

146 Devy L, De Groot F.M, Noel A. Plasmin-activatede doxorubicin prodrugs containing a spacer reduce tumor growth and angiogenesis without systemic toxicity. FASEB J. 2004, 18, 565-567.

147 Agnieszka M, Midura K. Low molecular peptides as potential inibithors of plasmin. Acta Poloniae Pharmaceutica n Drug Research. 2007, 64, 355-358.

148 Radi M, Dreassi E, Brullo C, Crespan E, Tintori C, Bernardo V, Valoti M, Zamperini C, Daigl H, Musumeci F, Carraro F, Naldini A, Filippi I, Maga G, Schenone S, Botta M. Design, Synthesis, Biological Activity, and ADME Properties of Pyrazolo[3,4-*d*]pyrimidines Active in Hypoxic Human Leukemia Cells: A Lead Optimization Study. J.Med.Chem. 2011, 54, 2610–2626.

149 de Groot F.M, van Berkom L.W.A, Scheeren H.W. Synthesis and biological evaluation of 2'-carbamate-linked and 2'-carbonate-linked prodrugs of paclitaxel: selective activation, by the tumor-associated protease plasmin. J.Med.Chem. 2000, 43, 3093-3102.

150 Avdeef A. High-throughput Measurements of Solubility Profiles. In Pharmacokinetic Optimization in Drug Research: Biological, Physicochemical, and Computational Strategies. Wiley: Lausanne, Switzerland. 2001, 305−325.

151 Bradford M.M. A rapid and sensitive method for the quantitation of microgram quantities of protein utilizing the principle of protein-dye binding. Anal.Biochem. 1976, 72, 248-254.

5.2 ACKNOWLEDGEMENTS

First of all, I would like to extend my gratitude to my supervisor Prof. Elena Dreassi and to my co-supervisor Prof. Maurizio Botta for their wise guidance and many helpful suggestions during these three years Ph.D. research.

I'm grateful to my two mentors: Dr.Claudio Zamperini the'analytical mentor'and Dr.Annalaura Brai the'chemical mentor'. I never thank you enough for the endless teachings, support in difficult times and the friendship demonstrated.

I would also thank our research group, in particular Federica Coniglio, 'traveling companion' from the first year of University, Alessio Molinari irreplaceable 'neighbor hood' and colleague; not less Anna Lucia Fallacara, Arianna Mancini, Lucia Falsitta, Nastasja Palombi,Pierpaolo Calandro, Chiara Dasso, Riccardo Martini, Stefania Ronzini, Matteo Borgini, Matteo Tavanti, Laura Friggeri and Marika Tiberi.
We've shared joy and sorrow of the lab.

Furthermore, I would like to thank my family, my friends, in particular Marta, Greta and Stefano.

Finally, I dedicate a special thanks to my mom Antonella and to my boyfriend Andrea, as well as the 'best accomplices of life' that could I have. I thank them for their patience, comprehension and for being always by my side.